The Multiple Roles of Cold-Inducible RBM3 in Neural Stem Cells After Hypoxia-Ischemia Injury

Inauguraldissertation

zur

Erlangung der Würde eines Doktors der Philosophie

vorgelegt der

Philosophisch-Naturwissenschaftlichen Fakultät

der Universität Basel

von

Jingyi Yan

V. R. CHINA

Basel, 2020

Genehmigt von der Philosophisch-Naturwissenschaftlichen Fakultät

auf Antrag von:

Prof. Dr. Sven Wellmann

Prof. Dr. Marek Basler

Prof. Dr. Francisco Campos

Basel, den 18. Februar 2020

Prof. Dr. Martin Spiess

Dekan der Philosophisch Naturwissenschaftlichen Fakultät

Contents

Abstract

Hypoxia-ischemia (HI) inflicts devastating brain injury across all age groups. In clinical practice, therapeutic hypothermia (32–34 °C) has proved a potent tool for alleviating neurological deficit in infants with hypoxia-ischemia encephalopathy and in adults with acute brain injury. Previous reports from our group and others have shown RNA-binding motif protein 3 (RBM3) to be neuroprotective under various stressful conditions through diverse cellular and molecular mechanisms. In the first part of this thesis, we used RBM3 mutant mice to find out how RBM3 promotes ischemia-induced neurogenesis and how it regulates cell proliferation during hypoxia. We showed how RBM3 stimulates neuronal differentiation and inhibits HI-induced apoptosis in the two areas of persistent adult neurogenesis, the subventricular zone (SVZ) and subgranular zone (SGZ), while promoting neural stem/progenitor cell (NSC) proliferation after HI injury only in the SGZ. RBM3 interacts with IGF2 mRNA binding protein 2 (IMP2), elevates its expression and thereby stimulates IGF2 release in SGZ- but not SVZ-NSCs. In summary, we describe niche-dependent regulation of neurogenesis after adult HI injury via the novel RBM3–IMP2–IGF2 signaling pathway. In the second part we analyze the effect of hypoxia on the expression of multifunctional RBM3 and how this protein in turn regulates cell proliferation and death. Our findings identify RBM3 as a potential target for maintaining NSC proliferation capacity during hypoxia, which can be important in NSC-based therapies of acute brain injury and chronic neurodegenerative disease. We devote the third part to ascertaining the functions of RBM3 and IMP2 in neuroblastoma proliferation and differentiation.

Chapter 1. Introduction

1.1 Introduction

Hypoxia-ischemia inflicts devastating brain injury across all age groups. In clinical practice, therapeutic hypothermia (32–34 °C) has proved a potent tool for alleviating neurological deficit in infants with hypoxia-ischemia encephalopathy (HIE) [1] and in adults with acute brain injury [2]. Previous reports from our group and others have shown RNA-binding motif protein 3 (RBM3) to be neuroprotective under various stressful conditions through diverse cellular and molecular mechanisms [3]. In this thesis, we used RBM3 mutant mice to examine the function of RBM3 in neural stem cells (NSCs) in response to HI.

1.2 Hypoxia-ischemia

Birth asphyxia is the leading cause of neonatal HIE and one of the most common causes of neonatal morbidity and mortality [4, 5]. A second common severe threat to the neonatal brain is perinatal arterial ischemic stroke producing a significant morbidity and long-term neurologic sequelae, including neurodevelopmental disabilities, cerebral palsy, epilepsy, behavioral disorders, and impaired vision and language function [6-9]. In older children and adults, out-of-hospital cardiac arrest is the main cause of global HI brain injury and subsequent morbidity and mortality [10].

The cascade of damaging events involved in the pathogenesis of cerebral HI follows chronological order (Table 1). The time immediately after HI onset (a few minutes to hours) represents the acute phase when the decrease in cerebral blood flow disrupts ionic homeostasis, leading to increased intracellular calcium and release of excitatory neurotransmitters. Intracellular edema may occur when sodium and chloride flood the postsynaptic cells. Accumulating intracellular calcium is sequestered by the mitochondria, which causes mitochondrial and DNA damage. Further cytoplasmic calcium accumulation creates mitochondrial dysfunction and activates lipases, proteases, and endonucleases, inducing ATP depletion and reactive oxygen species (ROS) production, and priming apoptotic pathways [2, 11].

The acute phase is followed by the subacute phase occurring hours to days later, characterized by a variety of processes secondary to the initial HI event, such as delayed cell death (apoptosis) in the less severely injured areas (collectively known as the penumbra). Necrotic debris

stimulates immune response and activate proteases. In addition, neuro-inflammation by neutrophils, monocytes and microglia, and the inflammatory response itself lead to further ROS generation. Although many subacute events could be considered damaging in themselves, some of the factors generated may be important in setting the stage for processes of recovery and repair, such as neurogenesis and angiogenesis [12, 13].

The final or chronic phase starts weeks to months later, characterized by multiple restorative processes, including cell genesis, synaptogenesis, and remodeling. Some areas recover function, including necrotic debris removal, reconnection of lost circuits, neurovascular regeneration, and the proliferation, differentiation and maturation of stem cells [2].

Table 1. The events involved in the pathogenesis of cerebral ischemia are classified by their active time.

Acute phase (minutes–hours)	Subacute phase (hours–days)	Chronic phase (weeks–months)
• Blood flow decrease • Ionic homeostasis disturbance • Intracellular calcium increase • Glutamate release increase and excitotoxicity • Cytotoxic oedema • Membrane, mitochondrial and DNA damage • Misfolding of proteins and enzyme dysfunction • Necrosis	• Apoptosis • Inflammation by neutrophils, monocytes and microglia • Cytokine production • Proteolytic enzyme activation • Vasogenic edema and intracranial pressure increase • Reactive oxygen species production • Stimulation of neurogenesis and angiogenesis	• Necrotic debris removal • Stem cell proliferation, differentiation and maturation • Angiogenesis • Gliosis • Reconnection of lost circuits • Neurovascular remodelling and functional recovery

Endogenous neurogenic response has been reported to influence the course of recovery in both short- and long-term experimental stroke [14, 15]. Both neurogenesis and angiogenesis are involved in mobilizing NSCs from the stem cell niche after stroke and inducing them to generate amplifying progenitors that migrate to, and differentiate in, the lesioned areas. NSC niches are intimately associated with local microvascular terminals and this interplay appears to be finely regulated through oxygen tension and diffusible molecules secreted by NSCs and endothelial cells [16-19]. Daadi *et al* showed that human embryonic stem cells, transplanted 24 h after ischemia in neonatal rodent forebrain, induced axonal sprouting and increased the effectiveness of endogenous recovery mechanisms [20]. Endogenous NSC proliferation and migration within the ischemic brain are key spontaneous regenerative processes [21, 22]. But because spontaneous regeneration does not suffice to repair the damage, further stimulation of endogenous neurogenesis is required, alongside the introduction of exogeneous neurogenesis using transplanted stem cells.

1.3 Therapeutic hypothermia

Therapeutic hypothermia – the lowering of body temperature to 32~34°C (mild hypothermia) – has been extensively studied and provides the most potent neuroprotective strategy in acute ischemic stroke [23-25], postanoxic encephalopathy after cardiac arrest [26], perinatal HIE [27], and traumatic brain injury [28, 29]. Mild hypothermia significantly reduces the risk of death and disability from birth asphyxia [4, 30]. Current studies demonstrate that during ischemia and reperfusion hypothermia activates numerous pathways simultaneously via several mechanisms that improve neurological outcome after global HI in acute patients [31-34]. Another advantage of therapeutic hypothermia over other neuroprotective agents is the ability to reduce damage beyond the neuron to include the entire neurovascular unit [33, 34]. It is also a neuroprotective treatment that has been introduced into clinical practice and has proven efficacy in patients with hypoxic brain injury after cardiac arrest [4, 26].

The protective mechanisms of hypothermia affect the ischemic cascade across several pathways (Figure 1). Thus hypothermia: 1) decreases brain oxygen consumption and glucose metabolism and reduces blood flow [35]; 2) conserves high-energy phosphate compounds such as ATP and maintains ion gradients and tissue pH during post-stroke calcium influx and rising

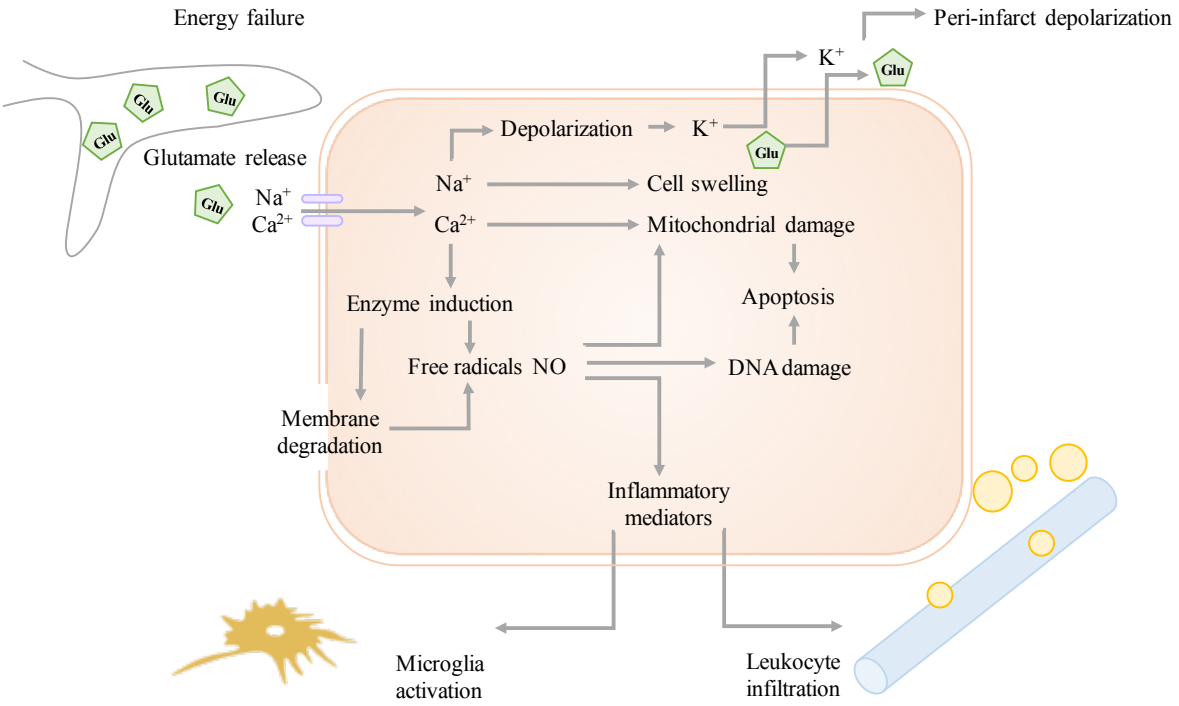

Figure 1. Proposed neuroprotective mechanisms of hypothermia
Adapted from U Dirnagl et al. 1999.

extracellular glutamate levels [36]; 3) reduces neuroinflammatory response and disrupts apoptotic pathways; 4) regulates stress-induced gene expression [35, 37]; 5) induces the expression, activation and release of several neurotrophic factors [38, 39]; and 6) reduces free radical generation and minimizes edema formation [2, 40, 41].

In rat hippocampus, mild hypothermia significantly alters gene expression after traumatic brain injury and reduces the number of AMPA and NMDA receptors expressed on hippocampal neurons after global ischemia; some studies have associated this downregulation with reduced infarct size [42, 43]. Although the full effects of hypothermia in brain injury repair are still unclear and conclusions are controversial, current research suggests that cooling has a protective role under special conditions [44], either by promoting stem cell proliferation and differentiation or by increasing growth factor signaling [45, 46].

Although patients can now be rendered hypothermic rapidly and safely, there are side effects to consider. Cooling can disrupt blood pressure control and induce arrhythmia. Fluid loss may lead to dehydration, electrolyte imbalance, and other complications [41]. Therefore, unraveling the cellular and molecular mechanisms of the neuroprotection conferred by cold inducible factors in cooling may help to provide solutions for better and wider application of therapeutic hypothermia, such as developing targeted and combination treatments.

1.4 Neurogenesis

The concept of neurogenesis goes back to Altman and Das who in 1965 suggested that new neurons generate not only in the developing organism but also in adult brain and that endogenous neurogenesis repairs the brain after injury [47]. In mammals, neurogenesis occurs throughout life in three niches where NSCs reside lifelong [48]. These regions include the SGZ of the hippocampal dentate gyrus (DG) [49], the SVZ of the lateral ventricles in the cerebrum [50-52], and the external germinal layer (EGL) in the cerebellum [53]. The EGL disappears once cerebellar development is completed, by 3 weeks postnatally in rodents [54] and by 2 years of age in humans [55]. Thus, only the two cerebrum niches, the SVZ and SGZ, persist until adulthood. The key characters of NSCs are pluripotency and self-renewal (Figure 2). Virtually all the body's stem cells are located in specific niches, a functional microenvironment

determining how stem cells participate in tissue generation, maintenance and repair under physiological or pathological challenges [56].

NSCs generate neurons, astrocytes, and oligodendrocytes in a regional and developmental stage-appropriate manner throughout life. Neurons newly generated in the SVZ actively migrate to the olfactory bulb via a highly specialized route, the rostral migratory stream (RMS) [57]. Adult SVZ NSCs are glial fibrillary acidic protein (GFAP)-positive radial glia-like cells [58]. Their long extensions contact blood vessels through specialized end-feet [59]. They also extend an apical process with a primary cilium through the ependymal cell layer to contact the cerebrospinal fluid (CSF) [60]. In the SGZ, NSCs also resemble astrocytes and extend a single radial process towards the molecular layer. The SGZ generates only one type of neuron, primary excitatory neurons, which contribute to memory and learning. In contrast to the SVZ, neurogenesis in the DG is almost unaffected by CSF constituents. For example, intra-cerebroventricular infusion of exogenous epidermal growth factor (EGF) and fibroblast growth factor 2 (FGF2) expands the SVZ precursor population but has no effect in the more distant hippocampus [61]. A feature of adult neurogenesis is its dynamic regulation by various physiological, pathological and pharmacological stimuli, such as exercise, antidepressants, aging, epilepsy, and stroke [62], via underlying mechanisms and target pathways that remain to be identified. Whether NSC subtypes are differentially regulated or which signaling cascades affect quiescent NSCs and their progeny are still open questions.

In neural stem cell niches, the oxygen concentration is estimated at 2.5-3% [63, 64]. Oxygen tension is a crucial environmental cue for NSC proliferation and differentiation [63]. NSCs maintain contact with ependymal cells and the basal lamina of endothelial cells (a component of the surrounding blood vasculature). They are also in contact with ventricular CSF [65]. This anatomical co-localization indicates that ependymal cells, endothelial cells and the choroid plexus (the source of CSF) are involved in the niche signals for postnatal and adult neurogenesis. It is hypothesized that differential oxygen tensions are important properties of NSC niches and are involved in distinct cellular processes: quiescence, proliferation and differentiation [63]. Intriguingly, neurogenesis is stimulated in response to hypoxia-ischemia injury in several rodent models [63]. Stroke-damaged adult rat brain even attempts to repair itself by producing new neurons in areas where neurogenesis does not normally occur [66-68].

Since neurogenesis is an important aspect of brain damage therapy, these observations are also relevant to the clinical use of hypothermia in perinatal hypoxia-ischemia cerebral injury. Kanagawa *et al* showed that a hypothermic environment reduces neurogenesis in the neonatal rat [69]. Mild hypothermia has no long-term impact on postischemic neurogenesis in rats [70]. Lasarzik *et al* suggest that postischemic neurogenesis is induced by intraischemic events that are most likely unaffected by hypothermia [70, 71]. Therefore, more knowledge is needed about the mechanisms of stroke-induced neurogenesis and how they may be affected by therapeutic hypothermia.

1.5 RBM3

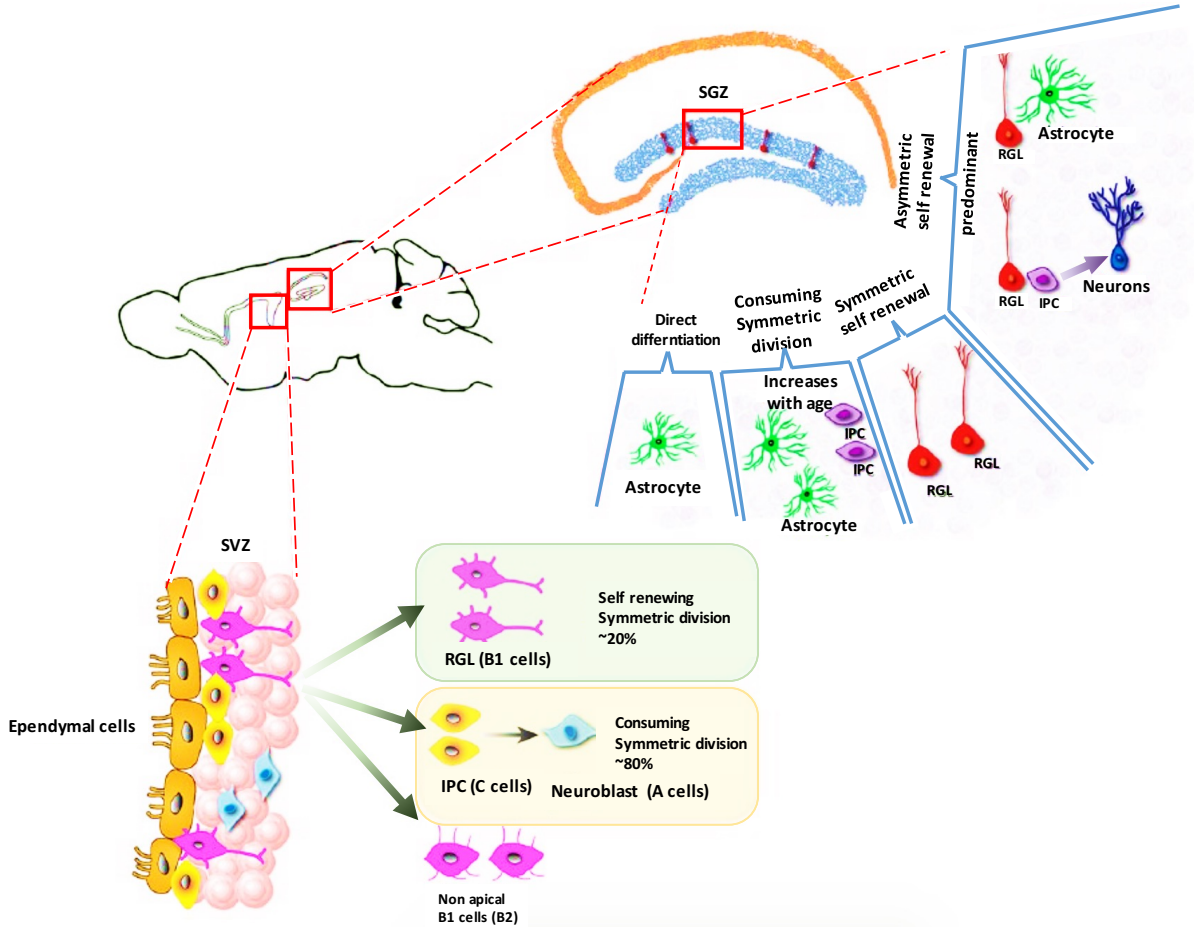

Figure 2. Fate potential of adult neural stem cells in SGZ and SVZ
Ming and Song, Neuron, 2011

RBM3, a glycine-rich RNA-binding protein (RBP), is an important cold inducible protein that responds to environmental stimuli such as hypothermia, ischemia, and hypoxia [72, 73]. RBM3 binds to RNA via its RNA recognition motif (RRM), altering secondary RNA structure and impairing the access of mRNA initiation factor to the ribosome subunit [74]. RBM3 is

expressed widely in brain at an early developmental age, peaking at around 15 days post-birth in the cerebellum and olfactory bulb. High levels are also observed in the cortex, hippocampus, superior and inferior colliculi, and areas that contain proliferating and migrating cells, such as the SVZ and RMS. In developing and adult brain, RBM3 levels decrease markedly [75-77] but still can be detected in the SVZ and cerebellar EGL (Figure 3). RBM3 enhances global translation, protects against apoptosis, and promotes cellular proliferation, all of which functions are compatible with a role for mRNA-BP in neuronal proliferation and differentiation [75]. In addition, RBM3 is related to changes in the expression of different RNAs during the circadian rhythm of body temperature [78] and regulates the expression of temperature-sensitive miRNAs [79]. Neurons have recently been identified as a major source of increased RBM3/β-klotho levels in developing brain, suggesting that RBM3/β-klotho upregulation is critical for CNS maturation [77].

The high level of RBM3 expression in neuron precursors and young neurons in the SVZ and RMS suggests a pivotal role in NSC proliferation and brain development [3, 75]. Our group

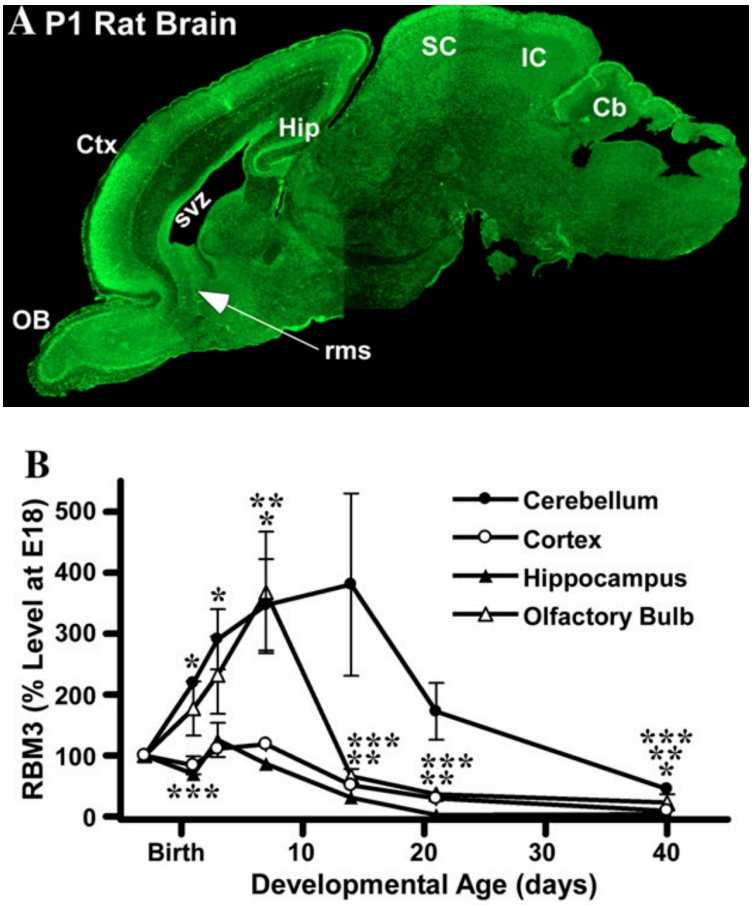

Figure 3. RBM3 is expressed widely in brain and developmentally regulated in brain.
J Pilotte et al. 2008

has shown RBM3 to be neuroprotective under various stressful conditions through diverse cellular and molecular mechanisms, such as maintaining synapse plasticity via reticulon-3, suppressing poly (ADP-ribose) polymerase (PARP) cleavage, and inhibiting endoplasmic reticular stress-induced apoptosis [3, 80-82]. We have also established that hypothermia maintains NSC numbers and elevates RBM3 levels in brain disorders. Taken together, such findings are a strong incentive to identify the precise role of cold inducible RBM3 in neurogenesis after hypoxia-ischemia brain injury.

1.6 IMPs

The insulin-like growth factor-2 (IGF2) mRNA-binding protein (IMP) family has three members: IMP1, IMP2, IMP3 (Figure 4). In mammals, the domain order and spacing structure of the three proteins are highly similar with two RNA recognition motifs in the N-terminal regions and four hnRNP K homology (KH) domains in the C-terminal region [83]. An important characteristic of IMPs in mice is high expression during the zygote to embryo stages [84], peaking at E12.5, in brain, limb buds, and muscle, and in the epithelia of many organs. In most adult organs, IMP1 and IMP3 are expressed at levels negligible compared to those in the embryo [85]. Indeed, IMP1 expression is almost completely abolished in the adult, although modest expression has been observed in the brain, lung and spleen of 16-week-old male mice [86]. IMP3 has been detected in the lung, spleen, kidney, and gut of male adult mice. Thus the pattern of IMP1 and IMP3 expression resembles that of oncofetal proteins, being virtually absent in adult organs but markedly upregulated in various tumors and tumor-derived cells [86-88]. Conversely, IMP2 is expressed in most adult tissue except pancreas [87-89]. IMPs are important proteins in subcellular mRNA sorting and the spatial control of key mRNA translation. They inhibit mRNA decay, enhance or inhibit RNA translation, and regulate IGF2 expression as well as a number of transcripts in neurons, including RNA location [86]. IMPs are present in various cancers and have different functions. For example, there is *in-vitro* evidence that IMP1 promotes cell movement but a role in cancer metastasis has yet to be confirmed *in vivo* [86]. In contrast, IMP3 could be an important biomarker in systemic malignancies of diverse origin [90, 91], while IMP2 is expressed in several tumor-derived and transformed cell types, appears to have multiple functions in cancers [86], and maintains cell stemness in pathological conditions. NSCs tend to differentiate into glial cells when IMP2

expression is silenced [92], while clonogenicity is impaired in glioblastoma stem cells with a deleted IMP2 gene [93].

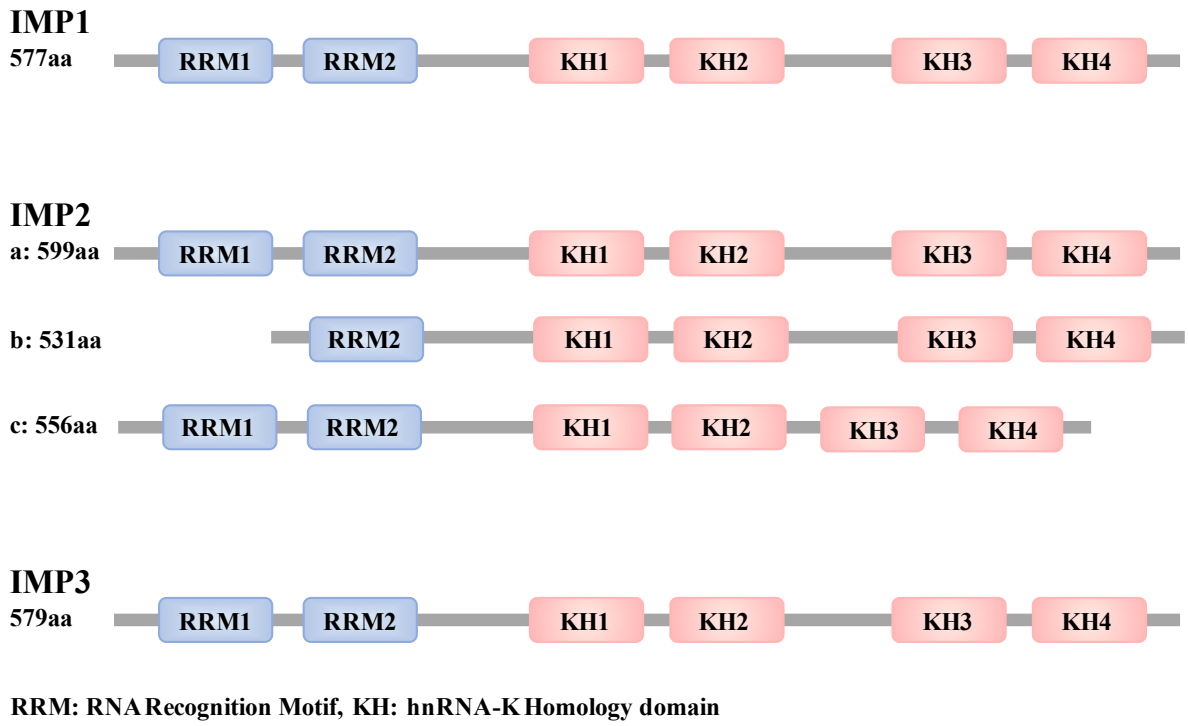

Figure 4. Domain structure of human IMPs famly.
Adapted from J. L. Bell et al. 2013

1.7 Thesis scope

Given RBM3 involvement in neuroprotection and its abundance in NSCs the main objective of this thesis was to characterize its role in the NSC response to HI.

In the first part of this thesis, we used NSCs isolated from the SVZ and SGZ of RBM3-mutant mice to compare RBM3 function in neurogenesis in response to HI versus controls. Our data indicate that RMB3 promotes post-HI neurogenesis in the DG but not the SVZ. Proposing RBM3–IMP2 interaction as the underlying mechanism, in *Nature Communications* we described niche-dependent regulation of neurogenesis after adult HI injury via a novel RBM3–IMP2–IGF2 signaling pathway.

In the second part, we analyzed the effect of hypoxia on RBM3 expression and asked how RBM3 in turn regulates cell proliferation and death in hypoxia. We used a C17.2 mouse neural stem cell line and primary mouse NSCs from both the forebrain of postnatal day 0 (P0) mice and the SGZ of adult RBM3-mutant and control mice. Our results demonstrated that RBM3 expression is highly sensitive to neural cell hypoxia and that hypoxia causes arrest in G0/G1

phase. Our findings, published in *Frontiers in Cell and Developmental Biology*, identify RBM3 as a potential target for maintaining NSC proliferation capacity in hypoxia, which can be important in NSC-based therapies of acute brain injury and chronic neurodegenerative disease.

The third and final part of this thesis addresses the question: "If RBM3 and its downstream target IMP2 are involved in cell proliferation and differentiation, does the RBM3–IMP2–IGF2 signaling pathway play a modulating role in neuroblastoma development?" Many studies have found RBM3 to promote cell proliferation and survival but have failed to explain the favorable prognosis in cancers with high RBM3 expression. Thus other mechanisms are most likely involved in modulating RBM3 action. Our hypothesis is that variations in RBM3 downstream signaling may play a role. In fact, in contrast to IMP1 and IMP3, there are at least three isoforms of IMP2 with varying functions in cancers. The third part of my work, yet to be published, describes the functions of RBM3 and in particular IMP2 in neuroblastoma proliferation, differentiation and development.

1.8 References

1. Committee on, F., et al., Hypothermia and neonatal encephalopathy. Pediatrics, 2014. **133**(6): p. 1146-50.

2. Yenari, M.A. and H.S. Han, Neuroprotective mechanisms of hypothermia in brain ischaemia. Nat Rev Neurosci, 2012. **13**(4): p. 267-78.

3. Chip, S., et al., The RNA-binding protein RBM3 is involved in hypothermia induced neuroprotection. Neurobiol Dis, 2011. **43**(2): p. 388-96.

4. Hypothermia after Cardiac Arrest Study, G., Mild therapeutic hypothermia to improve the neurologic outcome after cardiac arrest. N Engl J Med, 2002. **346**(8): p. 549-56.

5. Lawn, J.E., et al., 4 million neonatal deaths: when? Where? Why? Lancet, 2005. **365**(9462): p. 891-900.

6. Lynch, J.K. and K.B. Nelson, Epidemiology of perinatal stroke. Curr Opin Pediatr, 2001. **13**(6): p. 499-505.

7. Nelson, K.B. and J.K. Lynch, *Stroke in newborn infants.* Lancet Neurol, 2004. **3**(3): p. 150-8.

8. Nelson, K.B., Perinatal ischemic stroke. Stroke, 2007. **38**(2 Suppl): p. 742-5.

9. Raju, T.N., et al., Ischemic perinatal stroke: summary of a workshop sponsored by the National Institute of Child Health and Human Development and the National Institute of Neurological Disorders and Stroke. Pediatrics, 2007. **120**(3): p. 609-16.

10. Heinz, U.E. and J.D. Rollnik, Outcome and prognosis of hypoxic brain damage patients undergoing neurological early rehabilitation. BMC Res Notes, 2015. **8**: p. 243.

11. Chamorro, A., et al., Neuroprotection in acute stroke: targeting excitotoxicity, oxidative and nitrosative stress, and inflammation. Lancet Neurol, 2016. **15**(8): p. 869-881.

12. Font, M.A., A. Arboix, and J. Krupinski, Angiogenesis, neurogenesis and neuroplasticity in ischemic stroke. Curr Cardiol Rev, 2010. **6**(3): p. 238-44.

13. Gopurappilly, R., et al., Stem cells in stroke repair: current success and future prospects. CNS Neurol Disord Drug Targets, 2011. **10**(6): p. 741-56.

14. Jin, K., et al., Transgenic ablation of doublecortin-expressing cells suppresses adult neurogenesis and worsens stroke outcome in mice. Proc Natl Acad Sci U S A, 2010. **107**(17): p. 7993-8.

15. Wang, X., et al., Conditional depletion of neurogenesis inhibits long-term recovery after experimental stroke in mice. PLoS One, 2012. **7**(6): p. e38932.

16. Kim, H., et al., Paracrine and autocrine functions of brain-derived neurotrophic factor (BDNF) and nerve growth factor (NGF) in brain-derived endothelial cells. J Biol Chem, 2004. **279**(32): p. 33538-46.

17. Li, Q., et al., Modeling the neurovascular niche: VEGF- and BDNF-mediated cross-talk between neural stem cells and endothelial cells: an in vitro study. J Neurosci Res, 2006. **84**(8): p. 1656-68.

18. Li, Q., et al., Modeling the neurovascular niche: murine strain differences mimic the range of responses to chronic hypoxia in the premature newborn. J Neurosci Res, 2008. **86**(6): p. 1227-42.

19. Shen, Q., et al., Adult SVZ stem cells lie in a vascular niche: a quantitative analysis of niche cell-cell interactions. Cell Stem Cell, 2008. **3**(3): p. 289-300.

20. Daadi, M.M., et al., Human neural stem cell grafts modify microglial response and enhance axonal sprouting in neonatal hypoxic-ischemic brain injury. Stroke, 2010. **41**(3): p. 516-23.

21. Thored, P., et al., Persistent production of neurons from adult brain stem cells during recovery after stroke. Stem Cells, 2006. **24**(3): p. 739-47.

22. Kokaia, Z. and O. Lindvall, Stem cell repair of striatal ischemia. Prog Brain Res, 2012. **201**: p. 35-53.

23. Schwab, S., et al., Feasibility and safety of moderate hypothermia after massive hemispheric infarction. Stroke, 2001. **32**(9): p. 2033-5.

24. De Georgia, M.A., et al., Cooling for Acute Ischemic Brain Damage (COOL AID): a feasibility trial of endovascular cooling. Neurology, 2004. **63**(2): p. 312-7.

25. Lyden, P.D., et al., Therapeutic hypothermia for acute stroke. Int J Stroke, 2006. **1**(1): p. 9-19.

26. Bernard, S.A., et al., Treatment of comatose survivors of out-of-hospital cardiac arrest with induced hypothermia. N Engl J Med, 2002. **346**(8): p. 557-63.

27. Jacobs, S., et al., Cooling for newborns with hypoxic ischaemic encephalopathy. Cochrane Database Syst Rev, 2007(4): p. CD003311.

28. Hutchison, J.S., et al., Hypothermia therapy for cardiac arrest in pediatric patients. Pediatr Clin North Am, 2008. **55**(3): p. 529-44, ix.

29. Peterson, K., S. Carson, and N. Carney, Hypothermia treatment for traumatic brain injury: a systematic review and meta-analysis. J Neurotrauma, 2008. **25**(1): p. 62-71.

30. Shankaran, S., et al., Whole-body hypothermia for neonates with hypoxic-ischemic encephalopathy. N Engl J Med, 2005. **353**(15): p. 1574-84.

31. Globus, M.Y., et al., Glutamate release and free radical production following brain injury: effects of posttraumatic hypothermia. J Neurochem, 1995. **65**(4): p. 1704-11.

32. Globus, M.Y., et al., Detection of free radical activity during transient global ischemia and recirculation: effects of intraischemic brain temperature modulation. J Neurochem, 1995. **65**(3): p. 1250-6.

33. Zhao, H., G.K. Steinberg, and R.M. Sapolsky, General versus specific actions of mild-moderate hypothermia in attenuating cerebral ischemic damage. J Cereb Blood Flow Metab, 2007. **27**(12): p. 1879-94.

34. Lampe, J.W. and L.B. Becker, State of the art in therapeutic hypothermia. Annu Rev Med, 2011. **62**: p. 79-93.

35. Shackelford, R.T. and S.A. Hegedus, Factors affecting cerebral blood flow--experimental review: sympathectomy, hypothermia, CO2 inhalation and pavarine. Ann Surg, 1966. **163**(5): p. 771-7.

36. Lee, J.M., G.J. Zipfel, and D.W. Choi, The changing landscape of ischaemic brain injury mechanisms. Nature, 1999. **399**(6738 Suppl): p. A7-14.

37. Terao, Y., et al., Hypothermia enhances heat-shock protein 70 production in ischemic brains. Neuroreport, 2009. **20**(8): p. 745-9.

38. D'Cruz, B.J., et al., Hypothermic reperfusion after cardiac arrest augments brain-derived neurotrophic factor activation. J Cereb Blood Flow Metab, 2002. **22**(7): p. 843-51.

39. Schmidt, K.M., et al., Regional changes in glial cell line-derived neurotrophic factor after cardiac arrest and hypothermia in rats. Neurosci Lett, 2004. **368**(2): p. 135-9.

40. Dirnagl, U., C. Iadecola, and M.A. Moskowitz, Pathobiology of ischaemic stroke: an integrated view. Trends Neurosci, 1999. **22**(9): p. 391-7.

41. Wu, T.C. and J.C. Grotta, Hypothermia for acute ischaemic stroke. Lancet Neurol, 2013. **12**(3): p. 275-84.

42. Friedman, L.K., et al., Intraischemic but not postischemic hypothermia prevents non-selective hippocampal downregulation of AMPA and NMDA receptor gene expression after global ischemia. Brain Res Mol Brain Res, 2001. **86**(1-2): p. 34-47.

43. Li, J., S. Benashski, and L.D. McCullough, Post-stroke hypothermia provides neuroprotection through inhibition of AMP-activated protein kinase. J Neurotrauma, 2011. **28**(7): p. 1281-8.

44. Douglas-Escobar, M. and M.D. Weiss, Hypoxic-ischemic encephalopathy: a review for the clinician. JAMA Pediatr, 2015. **169**(4): p. 397-403.

45. VanHook, A.M., Hypothermia-induced neuroprotection. Sci Signal, 2017. **10**(470).

46. Wassink, G., et al., A working model for hypothermic neuroprotection. J Physiol, 2018. **596**(23): p. 5641-5654.

47. Altman, J. and G.D. Das, Autoradiographic and histological evidence of postnatal hippocampal neurogenesis in rats. J Comp Neurol, 1965. **124**(3): p. 319-35.

48. Elder, G.A., R. De Gasperi, and M.A. Gama Sosa, Research update: neurogenesis in adult brain and neuropsychiatric disorders. Mt Sinai J Med, 2006. **73**(7): p. 931-40.

49. Djavadian, R.L., Serotonin and neurogenesis in the hippocampal dentate gyrus of adult mammals. Acta Neurobiol Exp (Wars), 2004. **64**(2): p. 189-200.

50. Alvarez-Buylla, A. and C. Lois, Neuronal stem cells in the brain of adult vertebrates. Stem Cells, 1995. **13**(3): p. 263-72.

51. Alvarez-Buylla, A. and J.M. Garcia-Verdugo, *Neurogenesis in adult subventricular zone.* J Neurosci, 2002. **22**(3): p. 629-34.

52. Lledo, P.M., M. Alonso, and M.S. Grubb, Adult neurogenesis and functional plasticity in neuronal circuits. Nat Rev Neurosci, 2006. **7**(3): p. 179-93.

53. Hatten, M.E. and N. Heintz, Mechanisms of neural patterning and specification in the developing cerebellum. Annu Rev Neurosci, 1995. **18**: p. 385-408.

54. Miale, I.L. and R.L. Sidman, An autoradiographic analysis of histogenesis in the mouse cerebellum. Exp Neurol, 1961. **4**: p. 277-96.

55. Marzban, H., et al., Cellular commitment in the developing cerebellum. Front Cell Neurosci, 2014. **8**: p. 450.

56. Scadden, D.T., The stem-cell niche as an entity of action. Nature, 2006. **441**(7097): p. 1075-9.

57. Lois, C. and A. Alvarez-Buylla, Long-distance neuronal migration in the adult mammalian brain. Science, 1994. **264**(5162): p. 1145-8.

58. Doetsch, F., et al., Subventricular zone astrocytes are neural stem cells in the adult mammalian brain. Cell, 1999. **97**(6): p. 703-16.

59. Tavazoie, M., et al., A specialized vascular niche for adult neural stem cells. Cell Stem Cell, 2008. **3**(3): p. 279-88.

60. Mirzadeh, Z., et al., Neural stem cells confer unique pinwheel architecture to the ventricular surface in neurogenic regions of the adult brain. Cell Stem Cell, 2008. **3**(3): p. 265-78.

61. Kuhn, H.G., et al., Epidermal growth factor and fibroblast growth factor-2 have different effects on neural progenitors in the adult rat brain. J Neurosci, 1997. **17**(15): p. 5820-9.

62. Ming, G.L. and H. Song, Adult neurogenesis in the mammalian brain: significant answers and significant questions. Neuron, 2011. **70**(4): p. 687-702.

63. Panchision, D.M., The role of oxygen in regulating neural stem cells in development and disease. J Cell Physiol, 2009. **220**(3): p. 562-8.

64. Santilli, G., et al., Mild hypoxia enhances proliferation and multipotency of human neural stem cells. PLoS One, 2010. **5**(1): p. e8575.

65. Alvarez-Buylla, A. and D.A. Lim, For the long run: maintaining germinal niches in the adult brain. Neuron, 2004. **41**(5): p. 683-6.

66. Arvidsson, A., et al., Neuronal replacement from endogenous precursors in the adult brain after stroke. Nat Med, 2002. **8**(9): p. 963-70.

67. Parent, J.M., et al., Rat forebrain neurogenesis and striatal neuron replacement after focal stroke. Ann Neurol, 2002. **52**(6): p. 802-13.

68. Lindvall, O. and Z. Kokaia, Neurogenesis following Stroke Affecting the Adult Brain. Cold Spring Harb Perspect Biol, 2015. **7**(11).

69. Kanagawa, T., et al., A decrease of cell proliferation by hypothermia in the hippocampus of the neonatal rat. Brain Res, 2006. **1111**(1): p. 36-40.

70. Lasarzik, I., et al., Mild hypothermia has no long-term impact on postischemic neurogenesis in rats. Anesth Analg, 2009. **109**(5): p. 1632-9.

71. Lasarzik, I., et al., Assessment of postischemic neurogenesis in rats with cerebral ischemia and propofol anesthesia. Anesthesiology, 2009. **110**(3): p. 529-37.

72. Yang, H., J.N. Rao, and J.Y. Wang, Posttranscriptional Regulation of Intestinal Epithelial Tight Junction Barrier by RNA-binding Proteins and microRNAs. Tissue Barriers, 2014. **2**(1): p. e28320.

73. Zhu, X., C. Buhrer, and S. Wellmann, Cold-inducible proteins CIRP and RBM3, a unique couple with activities far beyond the cold. Cell Mol Life Sci, 2016. **73**(20): p. 3839-59.

74. Chappell, S.A. and V.P. Mauro, The internal ribosome entry site (IRES) contained within the RNA-binding motif protein 3 (Rbm3) mRNA is composed of functionally distinct elements. J Biol Chem, 2003. **278**(36): p. 33793-800.

75. Pilotte, J., et al., Developmentally regulated expression of the cold-inducible RNA-binding motif protein 3 in euthermic rat brain. Brain Res, 2009. **1258**: p. 12-24.

76. Nishino, J., et al., A network of heterochronic genes including Imp1 regulates temporal changes in stem cell properties. Elife, 2013. **2**: p. e00924.

77. Jackson, T.C., et al., Robust RBM3 and beta-klotho expression in developing neurons in the human brain. J Cereb Blood Flow Metab, 2019. **39**(12): p. 2355-2367.

78. Liu, Y., et al., Cold-induced RNA-binding proteins regulate circadian gene expression by controlling alternative polyadenylation. Sci Rep, 2013. **3**: p. 2054.

79. Wong, J.J., et al., RBM3 regulates temperature sensitive miR-142-5p and miR-143 (thermomiRs), which target immune genes and control fever. Nucleic Acids Res, 2016. **44**(6): p. 2888-97.

80. Peretti, D., et al., RBM3 mediates structural plasticity and protective effects of cooling in neurodegeneration. Nature, 2015. **518**(7538): p. 236-9.

81. Zhu, X., et al., Cold-inducible RBM3 inhibits PERK phosphorylation through cooperation with NF90 to protect cells from endoplasmic reticulum stress. FASEB J, 2016. **30**(2): p. 624-34.

82. Bastide, A., et al., RTN3 Is a Novel Cold-Induced Protein and Mediates Neuroprotective Effects of RBM3. Curr Biol, 2017. **27**(5): p. 638-650.

83. Nielsen, F.C., J. Nielsen, and J. Christiansen, A family of IGF-II mRNA binding proteins (IMP) involved in RNA trafficking. Scand J Clin Lab Invest Suppl, 2001. **234**: p. 93-9.

84. Hansen, T.V., et al., Dwarfism and impaired gut development in insulin-like growth factor II mRNA-binding protein 1-deficient mice. Mol Cell Biol, 2004. **24**(10): p. 4448-64.

85. Hammer, N.A., et al., Expression of IGF-II mRNA-binding proteins (IMPs) in gonads and testicular cancer. Reproduction, 2005. **130**(2): p. 203-12.

86. Bell, J.L., et al., Insulin-like growth factor 2 mRNA-binding proteins (IGF2BPs): post-transcriptional drivers of cancer progression? Cell Mol Life Sci, 2013. **70**(15): p. 2657-75.

87. Yaniv, K. and J.K. Yisraeli, The involvement of a conserved family of RNA binding proteins in embryonic development and carcinogenesis. Gene, 2002. **287**(1-2): p. 49-54.

88. Yisraeli, J.K., VICKZ proteins: a multi-talented family of regulatory RNA-binding proteins. Biol Cell, 2005. **97**(1): p. 87-96.

89. Christiansen, J., et al., IGF2 mRNA-binding protein 2: biological function and putative role in type 2 diabetes. J Mol Endocrinol, 2009. **43**(5): p. 187-95.

90. Kapoor, S., IMP3: a new and important biomarker of systemic malignancies. Clin Cancer Res, 2008. **14**(17): p. 5640; author reply 5640-1.

91. Findeis-Hosey, J.J. and H. Xu, The use of insulin like-growth factor II messenger RNA binding protein-3 in diagnostic pathology. Hum Pathol, 2011. **42**(3): p. 303-14.

92. Fujii, Y., Y. Kishi, and Y. Gotoh, IMP2 regulates differentiation potentials of mouse neocortical neural precursor cells. Genes Cells, 2013. **18**(2): p. 79-89.

93. Degrauwe, N., et al., The RNA Binding Protein IMP2 Preserves Glioblastoma Stem Cells by Preventing let-7 Target Gene Silencing. Cell Rep, 2016. 15(8): p. 1634-47.

Chapter 2. Results

2.1 Research Article I

RBM3 promotes neurogenesis in a niche-dependent manner via IMP2-IGF2 signaling pathway after hypoxic-ischemic brain injury

Xinzhou Zhu, *[#1] Jingyi Yan, [#1] Catherine Bregere,[2,3] Andrea Zelmer,[1] Tessa Goerne,[1] Josef P. Kapfhammer,[2] Raphael Guzman,[2,3] and Sven Wellmann *[#1,4]

1. University Children's Hospital Basel (UKBB), University of Basel, Basel, 4056 Switzerland
2. Department of Biomedicine, University of Basel, Basel, 4056 Switzerland
3. Department of Neurosurgery, University Hospital Basel, Basel, 4031 Switzerland
4. University Children's Hospital Regensburg (KUNO), University of Regensburg, Regensburg, 93053 Germany

* Corresponding author.

# Contributed equally.

Nature Communications volume 10, Article number: 3983 (2019)

doi:10.1038/s41467-019-11870-x

Contribution statement: I performed most of the experiments and analyzed the data.

nature COMMUNICATIONS

ARTICLE

https://doi.org/10.1038/s41467-019-11870-x OPEN

RBM3 promotes neurogenesis in a niche-dependent manner via IMP2-IGF2 signaling pathway after hypoxic-ischemic brain injury

Xinzhou Zhu[1,5,6], Jingyi Yan[1,5], Catherine Bregere[2,3], Andrea Zelmer[1], Tessa Goerne[1], Josef P. Kapfhammer[2], Raphael Guzman[2,3] & Sven Wellmann[1,4,6]

Hypoxic ischemia (HI) is an acute brain threat across all age groups. Therapeutic hypothermia ameliorates resulting injury in neonates but its side effects prevent routine use in adults. Hypothermia up-regulates a small protein subset that includes RNA-binding motif protein 3 (RBM3), which is neuroprotective under stressful conditions. Here we show how RBM3 stimulates neuronal differentiation and inhibits HI-induced apoptosis in the two areas of persistent adult neurogenesis, the subventricular zone (SVZ) and the subgranular zone (SGZ), while promoting neural stem/progenitor cell (NSPC) proliferation after HI injury only in the SGZ. RBM3 interacts with *IGF2* mRNA binding protein 2 (IMP2), elevates its expression and thereby stimulates IGF2 release in SGZ but not SVZ-NSPCs. In summary, we describe niche-dependent regulation of neurogenesis after adult HI injury via the novel RBM3-IMP2-IGF2 signaling pathway.

[1] University Children's Hospital Basel (UKBB), University of Basel, Basel 4056, Switzerland. [2] Department of Biomedicine, University of Basel, Basel 4056, Switzerland. [3] Department of Neurosurgery, University Hospital Basel, Basel 4031, Switzerland. [4] University Children's Hospital Regensburg (KUNO), University of Regensburg, Regensburg 93053, Germany. [5] These authors contributed equally: Xinzhou Zhu, Jingyi Yan. [6] These authors jointly supervised this work: Xinzhou Zhu, Sven Wellmann. Correspondence and requests for materials should be addressed to X.Z. (email: xinzhou.zhu@unibas.ch) or to S.W. (email: sven.wellmann@ukbb.ch)

The brain is the organ most vulnerable to oxygen and energy deprivation. Hypoxic ischemia (HI) inflicts devastating brain injury across all age groups. Birth asphyxia is the leading cause of neonatal encephalopathy and lifelong neurologic sequelae[1]. In older children and adults, out-of-hospital cardiac arrest is the main cause of global HI brain injury and subsequent morbidity and mortality[2].

Mild hypothermia (32–34 °C) significantly reduces the risk of death and disability from birth asphyxia[1,3], but has side effects that complicate its use in adults after brain injury[4,5]. Unraveling the cellular and molecular mechanisms of the neuroprotection conferred by hypothermia may therefore help the development of targeted treatment.

As well as slowing the cellular metabolic rate, mild hypothermia induces a subset of stress-response proteins in mammals, including RNA-binding motif protein 3 (RBM3)[6]. Previous reports from our group and others showed RBM3 to be neuroprotective under various stressful conditions through diverse cellular and molecular mechanisms, such as maintaining synapse plasticity via reticulon-3 (RTN3), suppressing poly (ADP-ribose) polymerase (PARP) cleavage, and inhibiting endoplasmic reticular (ER) stress-induced apoptosis[7–10].

Rodent studies have shown that RBM3 is highly expressed in proliferating and differentiating brain regions such as the subventricular zone (SVZ), the rostral migratory stream (RMS), and the subgranular zone (SGZ) of the dentate gyrus (DG) in both neonates and adults[9,11]. Notably, RBM3 colocalizes with neural stem cell marker nestin[11] and neuroblast marker doublecortin (Dcx)[9], indicating its role in maintaining neural stem/progenitor cell (NSPC) self-renewal and neurogenesis.

In adults, the SVZ and SGZ are the only two well-characterized neurogenic niches not only in rodents but also in humans[12–14]. NSPC proliferation and neurogenesis are stimulated in both niches after ischemic injury in order to aid post-ischemic recovery[15]. However, it remains uncertain whether hypothermia promotes neuroregeneration after HI injury, as different cooling settings and injury models produce conflicting conclusions[16]. We focused exclusively on the effects of RBM3 on NSPC proliferation and neurogenesis in the SVZ and SGZ niches after HI injury in vitro and in vivo.

Results

RBM3 stimulates NSPC proliferation in SGZ but not in SVZ. As observed in other studies, RBM3 knockout (KO) mice do not exhibit an obvious phenotype under physiological conditions[17]. However, under pathological conditions such as neurodegenerative disease, RBM3 acts as a stress-response protein, significantly influencing neural survival and function[7]. In studying its role in adult neurogenesis we found no difference in brain weight between adult RBM3 KO and wild-type (WT) mice raised under normal conditions (Supplementary Fig. 1a). Nor did we detect structural abnormalities in the brains or any difference in the SVZ and DG volumes of KO compared to WT mice (Supplementary Fig. 1b).

Previously we and others had identified RBM3 in adult NSPCs and neuroblasts[9,11]. The present study confirmed its expression in sex determining region Y-box 2 (Sox2)+ NSPCs and Dcx + neuroblasts in both the SVZ and SGZ in vivo (Supplementary Fig. 1c, d). We monitored basal NSPC proliferation by injecting adult mice intraperitoneally with bromodeoxyuridine (BrdU) every other day for 7 days before sacrifice. The total number and density of proliferating (BrdU+ Sox2+) NSPCs in KO mice was similar to that in WT mice in both the SVZ and SGZ niches (Supplementary Fig. 1e, f). Further analysis by neurosphere assay revealed that the number and size of primary and secondary neurospheres isolated from KO mice resembled those in WT mice, regardless of origin (Supplementary Fig. 1g, h). Thus our data indicate that neurogenic potential appears unimpaired in adult RBM3-deficient mice under physiological growing conditions.

Next, we applied an acute brain HI model to adult RBM3 WT and KO mice to determine whether RBM3 depletion affects NSPC proliferation and neurogenesis under pathological conditions. After permanent ligation of the right common carotid artery, the animals were subjected to 8% hypoxia for 20 min, followed by recovery for 7 days with repeated BrdU pulsing (Fig. 1a). We used equation (1) in Methods to estimate infarction volume. Infarction volume was significantly greater in KO than in WT brains (Supplementary Fig. 2a). Regardless of more neuronal loss in KO mice, the volumes of both SVZ and DG did not differ between ipsilateral and contralateral sides in WT and KO mice (Supplementary Fig. 2b). Equation (2) in Methods was used for stereological cell quantification. After 7 days recovery from HI, total BrdU+ cell density in the SVZ and DG were both increased in the ipsilateral side of WT and KO mice compared to contralateral side, but no difference was observed between WT and KO mice (Supplementary Fig. 2c, d). Simultaneously, large quantities of reactive (glial fibrillary acidic protein [GFAP]+) astrocytes and (ionized calcium-binding adapter molecule 1 [Iba1]+) microglia were induced in the SVZ and surrounding areas such as striatum and corpus callosum, as well as in the ipsilateral hippocampus adjacent to the ischemic core, in both WT and KO brains after HI injury (Supplementary Fig. 3a, b). We saw evidence of oligodendrocyte transcription factor 2 (Olig2)+ oligodendrocyte precursor cell stimulation in the ipsilateral corpus callosum and DG of WT mice but not KO mice (Supplementary Fig. 3c). We observed more terminal deoxynucleotidyl transferase dUTP nick end labeling (TUNEL)+ apoptotic cells in the ischemic cores in ipsilateral cortex and striatum in KO brains than in WT brains (Supplementary Fig. 3d). The total number and density of newborn (BrdU+ Sox2+) NSPCs were barely affected in the SVZ of WT and KO mice (Fig. 1b). Strikingly, whereas there was a significant increase of BrdU+ Sox2+ NSPCs in the HI ipsilateral SGZ of WT mice compared to HI contralateral and sham animals, in KO littermates, BrdU+ Sox2+ NSPCs were not induced in the SGZ (Fig. 1c). Albeit we found some BrdU+ cells in the SGZ of KO mice, many of them were Sox2-negative cells, indicating discrepancies between neurogenic niches in RBM3 effect on NSPC proliferation.

To characterize the role of RBM3 in NSPC proliferation in vitro, we isolated and cultured nestin+ Sox2+ NSPCs from the SVZ and SGZ of RBM3 WT and KO mice (Supplementary Fig. 4a). Cultured NSPCs were challenged with oxygen-glucose deprivation (OGD), an in vitro model of HI, before being reoxygenated for 24 h in BrdU-containing complete medium (Fig. 1d). NSPC proliferation from the SVZ was virtually similar after OGD between WT and KO cultures. In contrast, NSPC proliferation from the SGZ was dramatically elevated in WT cultures but reduced in KO cultures (Fig. 1e, f), consistent with the in vivo findings (Fig. 1b, c). In addition, we treated NSPCs after OGD with mock stress or hypothermia for 3 h (Fig. 1d), thereby enhancing RBM3 expression (Supplementary Fig. 4b). Overall, hypothermia inhibited cell proliferation, but more so in KO than in WT SGZ-NSPCs (Fig. 1f). We detected no difference in RBM3-depleted SVZ-NSPCs (Fig. 1e). Furthermore, when we overexpressed recombinant RBM3 in SVZ- and SGZ-NSPCs after OGD (Supplementary Fig. 4c), only the SGZ-NSPCs proliferated at a higher rate than in a mock vector group (Fig. 1g, h).

Taken together, our data suggest that while RBM3 does not affect basal NSPC proliferation under normal growing conditions, after HI injury it stimulates the proliferation of SGZ-NSPCs but not SVZ-NSPCs in vivo and in vitro.

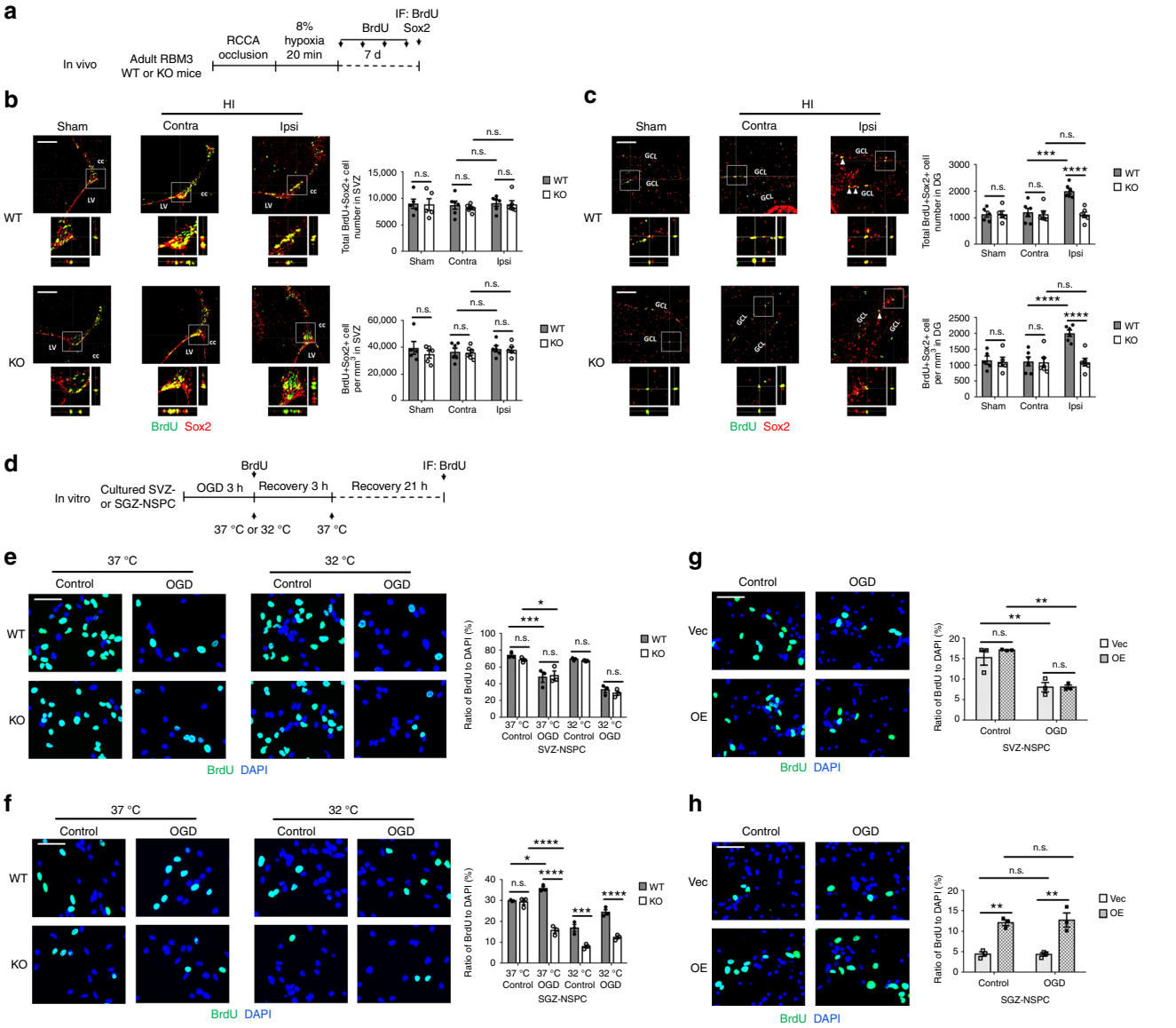

Fig. 1 RBM3 is required for HI-induced proliferation of SGZ- but not SVZ-NSPC in vivo and in vitro. **a** Illustration of in vivo HI model and analysis of NSPC proliferation. RCCA right common carotid artery, IF immunofluorescence. **b**, **c** Representative immunofluorescent staining of BrdU and Sox2 in SVZ (**b**) and DG (**c**) of RBM3 WT and KO animals treated with HI and recovered for 7 days with BrdU injection every other day. Animals in control group received sham surgery. Orthogonal view confirmed the colocalization of BrdU and Sox2. BrdU+ Sox2+ cell number and density in the SVZ or DG were estimated. Five sham animals and six HI animals were counted per group (Sham: $n = 5$, HI: $n = 6$). Sham, sham group; contra, contralateral (uninjured side) in HI group; ipsi, ipsilateral (injured side) in HI group. Scale bar: 100 µm. LV lateral ventricle, cc corpus callosum, GCL granular cell layer. Repeated measures two-way ANOVA was used for statistical analysis; n.s. not significant; ***$p < 0.001$; ****$p < 0.0001$. **d** Illustration of in vitro OGD model and analysis of NSPC proliferation. OGD oxygen-glucose deprivation, IF immunofluorescence. Only WT or KO NSPCs underwent hypothermic treatment (32 °C). Plasmid-transfected NSPCs were always cultured at 37 °C. **e**–**h** Representative immunofluorescent staining of BrdU and DAPI in NSPCs after OGD stress. SVZ-NSPCs (**e**) and SGZ-NSPCs (**f**) from RBM3 WT or KO mice were treated with OGD and reoxygenated in BrdU-containing medium at 37 or 32 °C for 3 h, followed by 37 °C for an additional 21 h. The ratio of BrdU+/DAPI+ cells were quantified (three independent experiments, $n = 3$). Three-way ANOVA was used for statistical analysis; n.s. not significant; *$p < 0.05$; ***$p < 0.001$; ****$p < 0.0001$. SVZ-NSPCs (**g**) and SGZ-NSPCs (**h**) transfected with empty vector (Vec) or RBM3 overexpression (OE) plasmid were treated with OGD and reoxygenated in BrdU-containing medium at 37 °C for 24 h. The ratio of BrdU+/DAPI+ cells was quantified (three independent experiments, $n = 3$). Scale bar: 50 µm. Two-way ANOVA was used for statistical analysis; n.s. not significant; **$p < 0.01$. All data are presented as mean ± SEM

RBM3 promotes NSPC neuronal differentiation in SVZ and SGZ. We next examined whether RBM3 regulates NSPC differentiation and contributes to neurogenesis.

In vivo, after 7 days recovery from HI treatment (Fig. 2a), newborn (BrdU+ Dcx+) neuroblasts showed significant stimulation in the HI ipsilateral SVZ and SGZ of WT mice compared to the HI contralateral and sham group (Fig. 2b, c). In RBM3-depleted mice, on the other hand, newborn neuroblast stimulation was absent in the ipsilateral SVZ and SGZ (Fig. 2b, c). In long-term studies, researchers have found that most newborn NSPCs die before maturation, with the remaining cells differentiating into mature neurons as an inadequate repair of the damaged brain tissue[18,19]. After a longer recovery period (28 days) after HI injury (Fig. 2a), only a few BrdU+ cells survived in SVZ

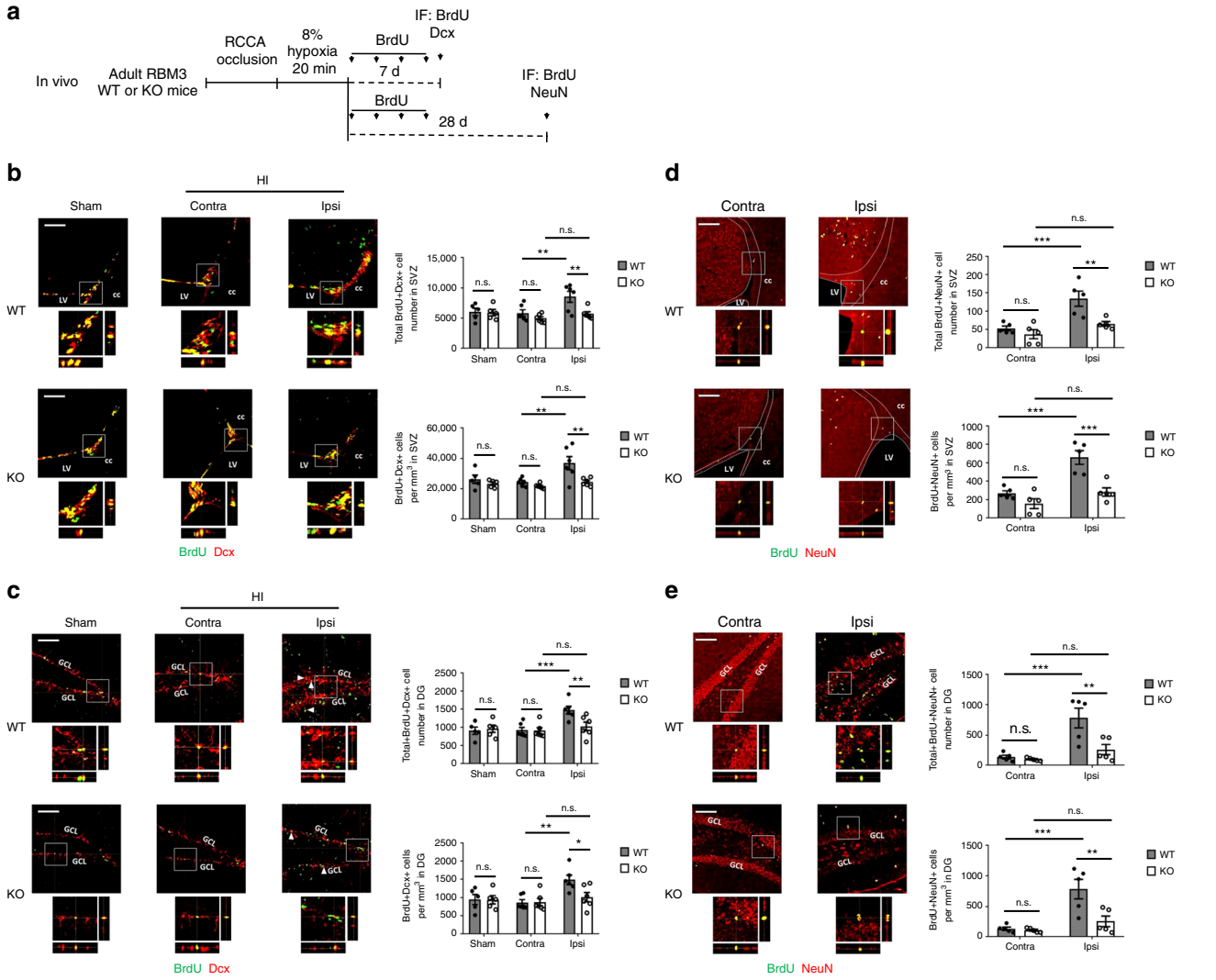

Fig. 2 RBM3 promotes neurogenesis in both SVZ and SGZ after HI injury in vivo. **a** Illustration of in vivo HI model and analysis of neurogenesis. RCCA right common carotid artery, IF immunofluorescence. **b**, **c** Representative immunofluorescent staining of BrdU and Dcx in SVZ (**b**) or DG (**c**) of RBM3 WT and KO animals treated with HI and recovered for 7 days with BrdU injection every other day. Animals in control group received sham surgery. Orthogonal view confirmed the co-localization of BrdU and Dcx. BrdU+ Dcx+ cell number and density in the SVZ or DG were estimated. Five sham animals and six HI animals were counted per group (Sham: $n = 5$, HI: $n = 6$). Sham, sham group; contra, contralateral (uninjured side) in HI group; ipsi, ipsilateral (injured side) in HI group. Scale bar: 100 μm. LV lateral ventricle, cc corpus callosum, GCL granular cell layer. Repeated measures two-way ANOVA was used for statistical analysis; n.s. not significant; $^{*}p < 0.05$; $^{**}p < 0.01$; $^{***}p < 0.001$. **d**, **e** Representative immunofluorescent staining of BrdU and NeuN in SVZ (**d**) or DG (**e**) of RBM3 WT and KO animals treated with HI and recovered for 28 days with BrdU injection every 2 days in the first week of recovery. Orthogonal view confirmed the colocalization of BrdU and NeuN. BrdU+ NeuN+ cell number and density in the SVZ or DG were estimated. Five animals were counted per group ($n = 5$). Contra, contralateral (uninjured side); ipsi, ipsilateral (injured side). Scale bar: 100 μm. LV lateral ventricle, cc corpus callosum, GCL granular cell layer. Repeated measures two-way ANOVA was used for statistical analysis; n.s. not significant; $^{**}p < 0.01$; $^{***}p < 0.001$. All data are presented as mean ± SEM

but more BrdU+ cells survived in DG (Supplementary Fig. 2e, f). A significantly higher number and density of total BrdU+ cells in the SVZ and DG was found in WT mice compared to KO mice (Supplementary Fig. 2e, f). Furthermore, we found increased numbers of mature BrdU+ NeuN+ neurons in both the ipsilateral SVZ and DG in WT mice (Fig. 2d, e) but reduced numbers in KO mice (Fig. 2d, e).

In vitro, we differentiated NSPCs into neurons by culture in growth factor-free medium for 7 days. At the same time, in order to assess the impact of OGD on differentiation, we treated NSPCs with OGD followed by reoxygenation for 7 days: in normal NSPC culture medium for the first 2 days, to allow enough time for activating downstream signaling in stem cell status, and in growth factor-free neuronal differentiation medium the remaining 5 days (Fig. 3a).

In this neuronal differentiation assay, OGD treatment induced a remarkable increase in the ratio of Dcx+ neuroblasts and microtubule-associated protein 2 (MAP2)+ neurons to all 4', 6-diamidino-2-phenylindole (DAPI)+ cells in SGZ-NSPCs (Fig. 3d, e) but not in SVZ-NSPCs (Fig. 3b, c). In the absence of RBM3, the percentages of both differentiated neuroblasts and neurons remained nearly unchanged in SVZ-NSPCs (Fig. 3b, c) while decreasing significantly in SGZ-NSPCs (Fig. 3d, e). When RBM3 was overexpressed, on the other hand, neuroblast and neuron percentages remained almost unchanged in SVZ-NSPCs (Fig. 3f, g) while increasing significantly in SGZ-NSPCs (Fig. 3h, i).

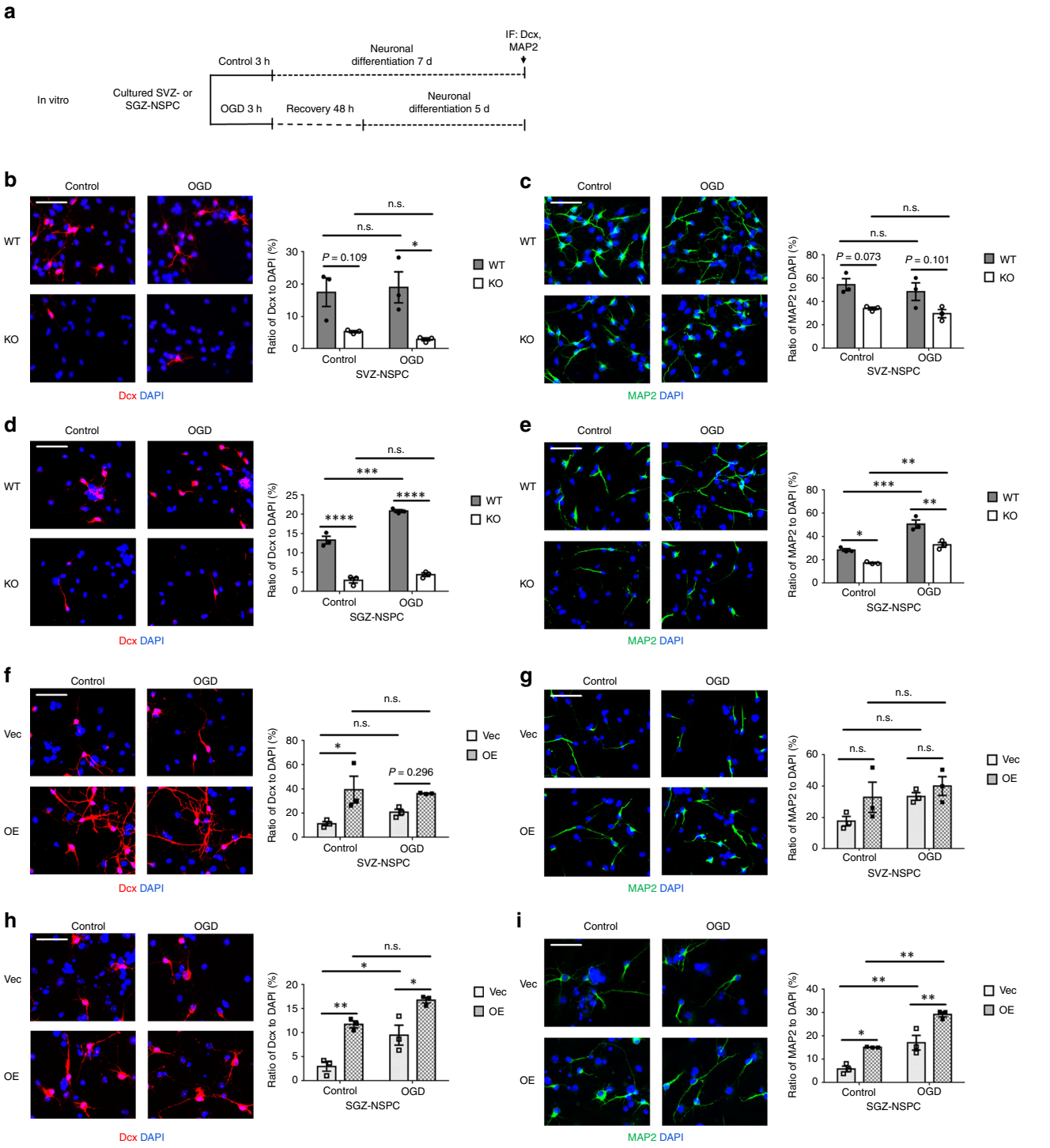

Fig. 3 RBM3 promotes neuronal differentiation of both SVZ-NSPC and SGZ-NSPC after OGD in vitro. **a** Illustration of in vitro neuronal differentiation assay. NSPCs were cultured in neuronal differentiation medium for 7 days (control), or first challenged with OGD and then reoxygenated in NSPC complete culture medium for the first 2 days, followed by switching to neuronal differentiation medium for 5 days (OGD). OGD oxygen-glucose deprivation, IF immunofluorescence. **b**–**i** RBM3 WT and KO NSPCs from SVZ (**b**, **c**) or SGZ (**d**, **e**), and WT NSPCs transfected with empty vector (Vec) or RBM3 overexpressing vector (OE) with SVZ (**f**, **g**) or SGZ (**h**, **i**) origins were used in neuronal differentiation assay. Neuroblast marker Dcx (**b**, **d**, **f**, **h**) and neuronal marker MAP2 (**c**, **e**, **g**, **i**) were stained and the ratio of immunoreactive cells to DAPI-positive cells was calculated (three independent experiments, $n = 3$). Representative images were presented and statistical data were acquired. Scale bar: 50 μm. Two-way ANOVA was used for statistical analysis; n.s. not significant; $^{*}p < 0.05$; $^{**}p < 0.01$; $^{***}p < 0.001$; $^{****}p < 0.0001$. All data are presented as mean ± SEM

Similarly, we differentiated NSPCs into astrocytes and oligodendrocytes with or without OGD treatment (Supplementary Fig. 5a). We used S100 to label glial precursors. The commonly used astrocyte marker GFAP was expressed in all the differentiated cells, and was also present in undifferentiated NSPCs (Supplementary Fig. 5b) as reported in other publications[20,21], thus not used. We found no difference when RBM3 expression was altered in an astrocyte differentiation assay (Supplementary Fig. 5c-f).

In an oligodendrocyte differentiation assay we used Olig2 to label oligodendrocyte precursor cells (OPCs), but not oligodendrocyte marker maltose binding protein (MBP) as there were only a few MBP+ cells (<1%) after 7 days of differentiation (Supplementary Fig. 5g). In contrast to astrocyte differentiation, OGD treatment induced OPC differentiation in both SVZ- and SGZ-NSPCs (Supplementary Fig. 5h-k). However, although RBM3 appeared to promote OPC differentiation in the absence of OGD, we found little difference in Olig2+ cell percentages after OGD when changing the level of RBM3 expression (Supplementary Fig. 5h-k).

In summary, we observed induction of neurogenesis after HI injury. Our results support the notion that RBM3 enhances neuronal differentiation potential in both neurogenic niches. However, as RBM3 has less influence on the neuronal differentiation of SVZ-NSPCs than of SGZ-NSPCs, we can anticipate a smaller impact on SVZ neurogenesis. RBM3 expression has no notable effect on glial cell differentiation.

RBM3 limits HI-induced apoptosis in both SVZ- and SGZ-NSPCs. To exclude the possibility that the discrepancy in proliferation rates between SVZ- and SGZ-derived NSPCs resulted from different severities of HI-induced apoptosis, we performed TUNEL staining (Fig. 4a) and found significantly more apoptotic cells at the ipsilateral side in RBM3 KO mice than in their WT littermates in both stem cell niches, in the lateral wall (Fig. 4b) and entire DG (Fig. 4c). Only few apoptotic cells were observed in the lateral tail of the SVZ (Supplementary Fig. 3d). In contrast, very few TUNEL+ cells were present at the contralateral sides in either RBM3 KO or WT HI animals (Fig. 4b, c).

To assess the anti-apoptotic effect of RBM3 in vitro, we quantified TUNEL+ cells 48 h after OGD (Fig. 4d). OGD challenge induced significant apoptosis in both SVZ- and SGZ-derived NSPCs (Fig. 4e, f). Absence of RBM3 clearly exacerbated post-OGD apoptosis (Fig. 4e, f). Hypothermia attenuated apoptosis in WT NSPCs, but only marginally in KO NSPCs, suggesting that RBM3 partially mediates hypothermic cytoprotection in NSPCs (Fig. 4e, f). On the other hand, forced RBM3 expression blocked OGD-induced apoptosis (Fig. 4g, h).

Our results suggest that RBM3 limits HI-induced apoptosis overall in vivo and in vitro thus at least partially mediating the protective effects of cooling. However, the protective effect applies to both SVZ- and SGZ-NSPCs, indicating that the discrepancy in post-OGD proliferation is not due to apoptosis.

RBM3-IMP2-IGF2 axis mediates niche-dependent proliferation. To unravel the molecular mechanism of reduced proliferation in RBM3-depleted hippocampal NSPC, we performed RNA sequencing (RNA-seq) to identify transcriptome changes in RBM3 KO mice. We used postnatal day 3 (P3) and 2–3 month adult hippocampi from RBM3 WT and KO mice without HI injury. The quality of extracted total RNA fulfilled the requirements for RNA-seq (Supplementary Data 1). As expected, rare global differences of gene expression were seen when comparing RBM3 WT and KO even when we applied a less stringent cutoff condition (Supplementary Fig. 6a-c, Supplementary Data 2 and 3), consistent with the unaltered phenotype in physiological condition (Supplementary Fig. 1a, b, e-h). Due to the limited number of differentially expressed genes (DEGs), Gene Set Enrichment Analysis (GSEA) provided limited information (Supplementary Fig. 6d). Among the few common DEGs between P3 and adult lists, we identified the transcript of *insulin-like growth factor 2* (*IGF2*) as one of the candidates, which was downregulated when RBM3 was absent (Supplementary Fig. S6a-S6c, Supplementary Data 2 and 3). At the same time, we identified candidate *IGF2* mRNA binding proteins (IMPs) from our previously published screening list of RBM3 interactors[10], known to regulate *IGF2* mRNA stability and promote its expression[22]. Based on these two independent screening approaches we focused on this IGF as in addition it had been reported to induce niche-dependent proliferation of adult NSPCs[23,24]. Consistent with previous publications[25,26], we found all three IMPs to be expressed at much lower levels in adult NSPCs than in NSPCs from postnatal day 0 (P0) mice (Supplementary Fig. 7a). *IMP1* expression was almost undetectable, while *IMP3* expression was much lower than that of *IMP2* in WT adult NSPCs (Supplementary Fig. 7a). Given additional evidence that IMP2 promotes neuronal differentiation in embryonic neocortical NSPCs[27], we tested the hypothesis that RBM3 regulates NSPC proliferation and may involve IMP2-IGF2 signaling in adult NSPCs.

First we examined RBM3-IMP2 interaction in NSPCs. In cultured NSPCs, RBM3 was expressed predominantly in nuclei but also in cytoplasm, while IMP2 expression was confined to cytoplasm (Fig. 5a). Proximity ligation assay showed that RBM3 and IMP2 were adjacent in both SVZ and SGZ-NSPCs, while OGD treatment significantly increased the number of positive signals per cell, indicating more RBM3-IMP2 interactions responding to OGD (Fig. 5b). Additionally, RBM3-IMP2 interactions were more abundant in SGZ-NSPCs than those in SVZ-NSPCs after OGD (Fig. 5b). In the SVZ and SGZ regions in vivo, RBM3 and IMP2 were co-expressed (Supplementary Fig. 7b) and showed adjacent localization in situ (Fig. 5c).

In HEK293 cells where we first identified RBM3-IMP2 interaction[10], and in NSPCs from P0 mouse brain, RBM3 and IMP2 expressions were both at high level (Supplementary Fig. 7c) and their interactions were much more abundant (Supplementary Fig. 7d), compared to adult NSPCs (Fig. 5b). Endogenous RBM3-IMP2 interactions were confirmed by co-immunoprecipitation (CoIP) directly in HEK293 cells and P0 NSPCs (Supplementary Fig. 7e). We further expressed recombinant RBM3 and IMP2 in HEK293 cells and examined, which domains were required for their interaction by using CoIP. IMP2 is known to contain two RNA-binding motifs (RRMs) and four K Homology (KH) domains, which can all bind RNA, but previous reports identified only the KH domains, and not the RRM domains as directly mediating *IGF2* mRNA binding[28]. To check which domains of IMP2 were required for RBM3-IMP2 interaction, we co-overexpressed full-length IMP2, truncated IMP2 RRMs (two RRM domains), and truncated IMP2 KHs (four K-homology domains) together with full-length RBM3 (Fig. 5d). The CoIP results indicated that the RBM3-IMP2 interaction was RNA-dependent because it was abolished by RNase treatment (Fig. 5e, f). As expected, only the KH domains and not the RRM domains, were essential for interactions with RBM3 (Fig. 5f), consistent with the finding that interaction is mediated by RNA.

Having confirmed RBM3-IMP2 interaction, we wished to determine whether RBM3 regulates IMP2 and its downstream IGF2 expression. In whole brain, we detected slightly lower protein levels of IMP2 but not IGF2 in RBM3 KO mice (Supplementary 7f). In cultured NSPCs, we observed no difference in post-OGD IMP2 expression in SVZ-NSPCs, as opposed to a slight decrease in SGZ-NSPCs, and a further decrease when RBM3 was absent (Fig. 5g). In injured hemisphere, IMP2 was generally induced in GFAP+ astrocytes in both SVZ and adjacent striatum and in the entire DG (Supplementary Fig. 7g). Therefore we intended to figure out whether the downstream effector IGF2 changes in a niche-dependent manner. We detected increased *IGF2* mRNA expression in WT SGZ-NSPCs but not in SVZ-NSPCs after OGD in vitro, and less increase in KO SGZ-NSPCs (Fig. 6a, b). In addition, using RNA-immunoprecipitation,

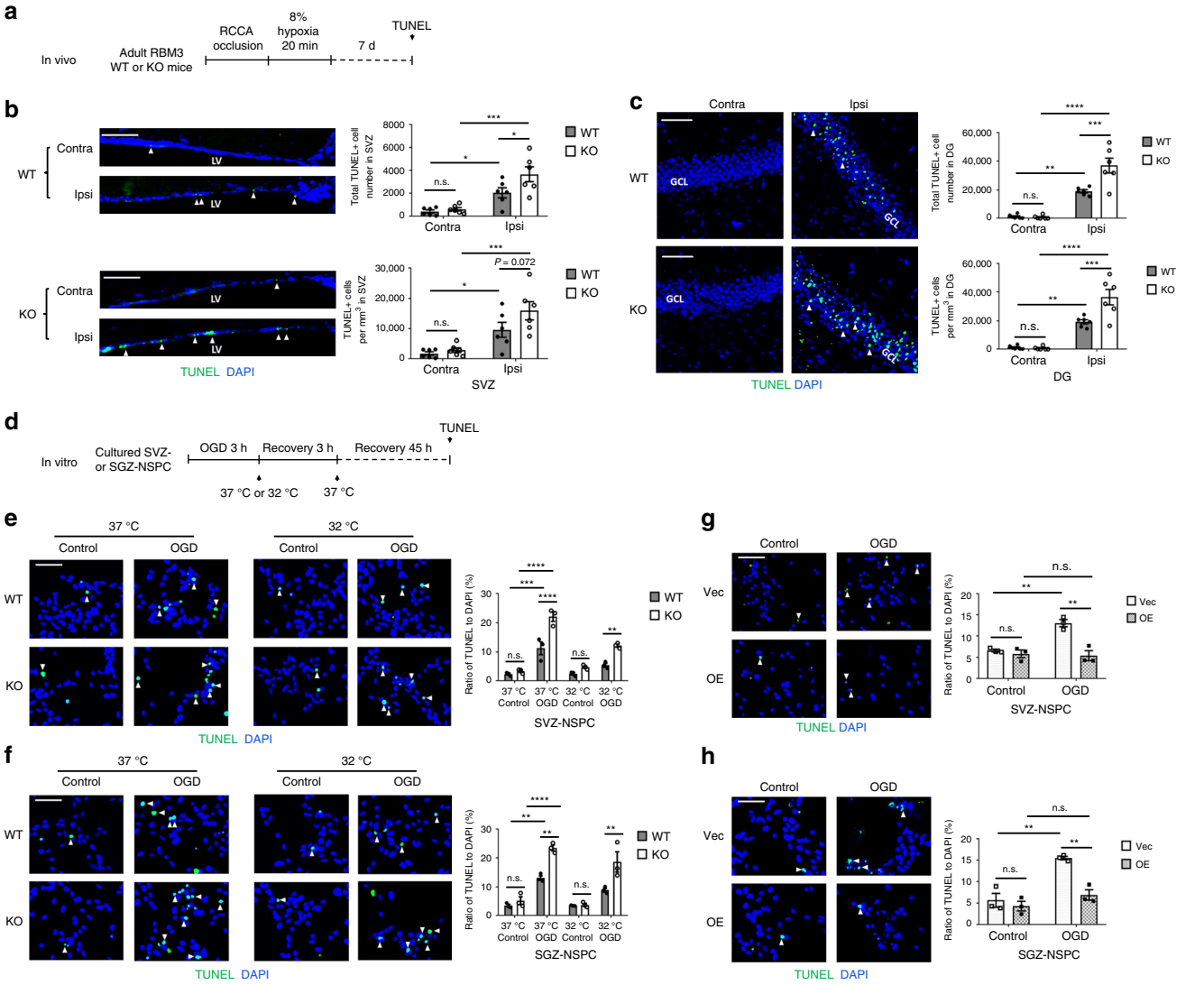

Fig. 4 RBM3 prevents HI-induced apoptosis in vivo and in vitro. **a** Illustration of in vivo HI model and analysis of apoptosis. RCCA right common carotid artery, TUNEL terminal deoxynucleotidyl transferase dUTP nick end labeling. **b**, **c** Representative immunofluorescent TUNEL staining in SVZ (**b**) or DG (**c**) of RBM3 WT and KO animals treated with HI and recovered for 7 days. Total TUNEL+ cell number and density in the SVZ or DG were estimated. Six animals were counted per group ($n = 6$). Scale bar: 50 μm. Contra contralateral (uninjured side), Ipsi ipsilateral (injured side), LV lateral ventricle, GCL granular cell layer. Repeated measures two-way ANOVA was used for statistical analysis; n.s. not significant; $^{*}p < 0.05$; $^{**}p < 0.01$; $^{***}p < 0.001$; $^{****}p < 0.0001$. **d** Illustration of in vitro OGD model and analysis of apoptosis. OGD oxygen-glucose deprivation. Only WT or KO NSPCs underwent hypothermic treatment (32 °C). Plasmid-transfected NSPCs were always cultured at 37 °C. **e**–**h** Representative immunofluorescent TUNEL in NSPCs after OGD stress. SVZ-NSPCs (**e**) and SGZ-NSPCs (**f**) from RBM3 WT or KO mice were treated with OGD and hypothermia as stated in Fig.1 legend, except for 48 h reoxygenation period instead of 24 h in total. The ratio of TUNEL+/DAPI+ cells was quantified (three independent experiments, $n = 3$). Three-way ANOVA was used for statistical analysis; n.s. not significant; $^{**}p < 0.01$; $^{***}p < 0.001$; $^{****}p < 0.0001$. SVZ-NSPCs (**g**) and SGZ-NSPCs (**h**) transfected with empty vector (Vec) or RBM3 overexpression (OE) plasmid were treated with OGD and reoxygenated at 37 °C for 48 h. The ratio of TUNEL+/DAPI+ cells was quantified (three independent experiments, $n = 3$). Scale bar: 50 μm. Two-way ANOVA was used for statistical analysis; n.s. not significant; $^{**}p < 0.01$. All data are presented as mean ± SEM

we identified more *IGF2* mRNA bound to IMP2 protein after OGD in WT SGZ-NSPCs and an upward trend in WT SVZ-NSPCs (Fig. 6c, d). In the absence of RBM3, enrichment of bound *IGF2* mRNA was clearly reduced in SGZ-NSPCs after OGD when comparing to WT, but unchanged in SVZ-NSPCs (Fig. 6c, d). Interestingly, endogenous IGF2 protein levels were reduced instead of enhanced after OGD in SGZ-NSPCs, probably due to increased secretion (Fig. 6e). When RBM3 was depleted, endogenous IGF2 protein decreased in SGZ-NSPCs after OGD (Fig. 6e). IGF2 protein levels in SVZ-NSPCs were not significantly affected by either OGD or RBM3 depletion, consistent with the unchanged *IGF2* mRNA data and the trend of IMP2 protein (Fig. 5g, 6c, e). On measuring the levels of IGF2 released into culture medium after OGD stress, we found those in SVZ-NSPC conditioned medium to be less than 50% of those in SGZ-NSPC counterpart (Fig. 6f, g). IGF2 secretion into SGZ-NSPC culture medium was significantly induced by OGD but reduced by RBM3 depletion (Fig. 6g). Conversely, RBM3 expression had no effect on IGF2 release into SVZ-NSPC culture medium (Fig. 6f). Overall, hypothermia inhibited IGF2 secretion in both SVZ- and SGZ-NSPCs after OGD, probably by reducing its expression level (Fig. 6f, g).

Additionally, we noticed that the intensity of IGF2 protein expression was enhanced in the ipsilateral SGZ but not SVZ in

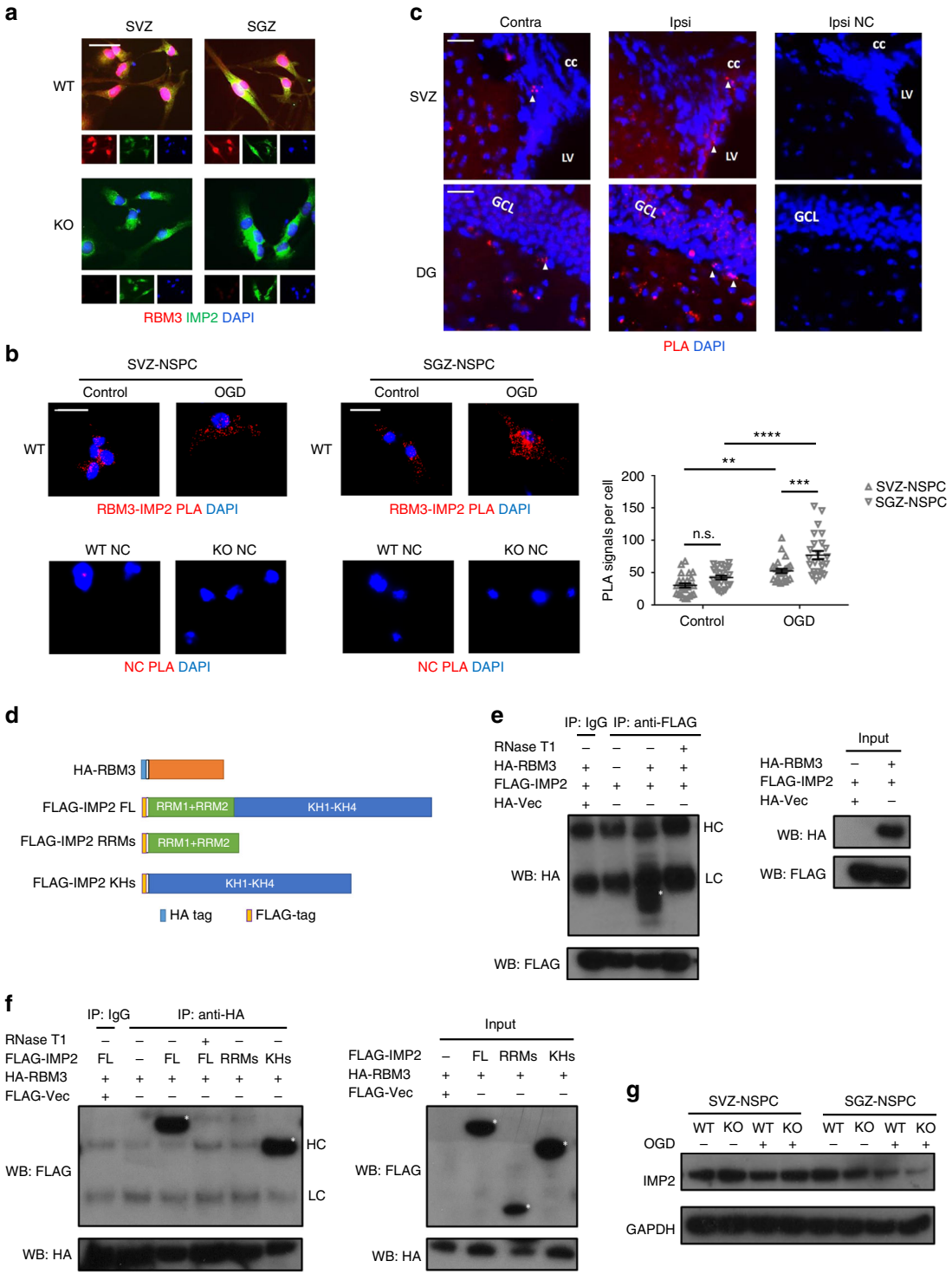

WT mice 7 days after HI injury (Fig. 7a, b). In RBM3-deficient mice, the intensity of IGF2 expression was reduced in the ipsilateral SGZ compared to WT, while remaining unchanged in the ipsilateral SVZ (Fig. 7a, b), in accordance with in vitro findings. Finally, we measured IGF2 levels in cerebrospinal fluid (CSF) by enzyme-linked immunosorbent assay (ELISA) in three groups: sham operation plus 7 days recovery, HI injury plus 7 days recovery and HI injury plus 28 days recovery. No significant change in CSF IGF2 levels was observed between WT and KO in all three groups (Fig. 7c), indicating that RBM3 does not alter IGF2 secretion from the epithelial cells of the choroid plexus, considered the main source of CSF[24]. We further found that RBM3 expression was absent in choroid plexus, while IGF2 was high as reported previously[24] (Supplementary Fig. 7h). This finding supports our notion that RBM3 does not regulate IGF2 level in CSF thus does not affect the proliferation of SVZ-NSPC.

To sum up, RBM3 interacts with IMP2 in NSPCs; however, only in SGZ-NSPC does RBM3 facilitate IMP2-mediated stabilization of *IGF2* mRNA and promote IGF2 expression and secretion after HI injury.

Fig. 5 RBM3 interacts with IMP2. **a** Representative immunofluorescent staining of RBM3 and IMP2 in SVZ-NSPCs and SGZ-NSPCs from adult WT mouse brain. RBM3 (red), IMP2 (green) and DAPI (blue) were merged. Scale bar: 25 μm. **b** Representative immunofluorescent images from proximity ligation assay. SVZ-NSPCs and SGZ-NSPCs were challenged with OGD and reoxygenated for 3 h. WT NSPCs omitting primary antibodies (WT NC) or KO NSPCs served as negative controls (KO NC). Fluorescent dots indicating single RBM3-IMP2 interactions were counted in each cell, and 25 cells per group were used for quantification ($n = 25$). RBM3-IMP2 PLA signals (red) and DAPI (blue) were merged. Scale bar: 25 μm. Two-way ANOVA was used for statistical analysis; n.s. not significant; $^{**}p < 0.01$; $^{***}p < 0.001$; $^{****}p < 0.0001$. All data are presented as mean ± SEM. **c** Representative image of proximity ligation assay of RBM3 and IMP2 in frozen brain sections from adult mice treated with HI and 7 days recovery. Scale bar: 50 μm. Contra contralateral (uninjured side), ipsi ipsilateral (injured side), LV lateral ventricle, cc corpus callosum, GCL granular cell layer, NC negative control without primary antibodies. **d** Schematic illustration of RBM3 and IMP2 constructs. Full-length (FL) RBM3 was fused with an N-terminal HA tag. Full-length (FL) IMP2 was truncated to N-terminal domain with two RNA-recognition motifs (RRMs) or C-terminal domain with four K Homology motifs (KHs); all of the constructs included an N-terminal FLAG tag. **e**, **f** Representative co-immunoprecipitation graphs of full-length or truncated RBM3 and IMP2 in HEK293 cells. Full-length FLAG-IMP2 was co-overexpressed with vector (Vec, negative control), or HA-RBM3 with or without RNase T1 pre-treatment. FLAG antibody was used to precipitate FLAG-IMP2. FLAG-IMP2 and HA-RBM3 in input or IP samples were detected by anti-FLAG or anti-HA antibodies using Western blot (**e**). A reciprocal CoIP was performed using full-length HA-RBM3 to precipitate full-length FLAG-IMP2, FLAG-RRMs or FLAG-KHs (**f**). Asterisks indicate target bands. HC heavy chain of IgG used for immunoprecipitation, LC light chain of IgG used for immunoprecipitation. **g** Representative Western blot of IMP2 expression in SVZ-NSPC and SGZ-NSPC after mock or OGD treatment in the presence or absence of RBM3

Discussion

While injured neurons lose synaptic connectivity and undergo cell death after HI, counteracting endogenous regenerative processes are activated, leading to neurogenesis and synaptogenesis[29]. Therapeutic hypothermia is widely known to protect the brain from HI injury[30,31], but there is limited and inconsistent information as to whether hypothermia promotes or inhibits injury-induced NSPC proliferation and neuronal differentiation or if anti-apoptosis is the key mechanism[16]. Here we demonstrate that under physiological conditions, RBM3 is expressed in brain, yet its deficiency has no obvious effect on brain development in vivo, probably due to other unknown compensating mechanisms. However, under pathological conditions such as HI, RBM3 is indispensable for neuroprotection and post-injury neuroregeneration. RBM3 not only protects NSPCs from HI-induced apoptosis, it also stimulates NSPC proliferation and neuronal differentiation. We demonstrate that RBM3 promotes NSPC proliferation after HI by regulating the IMP2-IGF2 pathway in SGZ-NSPCs but not SVZ-NSPCs (Fig. 7d).

Cold inducible RNA-binding protein (CIRP) is the only known homologous protein of RBM3 in mammals[6]. Like RBM3, it has been reported to promote the proliferation and suppress the apoptosis of neural stem cells in vitro[32,33]. However, CIRP has been identified as a damage-associated molecular pattern (DAMP) molecule, inducing detrimental inflammatory responses[34]. Extracellular CIRP levels increase in ischemic stroke models causing massive neuronal damage[35]. In contrast, no such deleterious effect has been reported with RBM3, which is therefore considered a safer modulator of post-injury neurogenesis than CIRP.

IMP family proteins are widely expressed and play important roles at different stages of development. In adulthood, in contrast to IMP1 and IMP3, only IMP2 remains relatively highly expressed, playing a major role in cell survival[28,36], NSPC proliferation[37], and neuronal differentiation[27]. As the main downstream factor of IMP2, IGF2 is abundant in the proliferative regions of both embryonic and adult brain[22], similarly to the temporal and spatial expression pattern of IMP2 and RBM3. In recent years, IGF2 has been identified as a positive regulator of the proliferation of embryonic and neonatal NSPCs[38,39] and adult NSPCs[23,24]. Interestingly, SVZ-NSPC responses to exogenous IGF2 follow a paracrine pattern, while SGZ-NSPCs secrete IGF2 and regulate self-renewal in an autocrine manner[23,24]. Our results support the hypothesis that RBM3 upregulates IGF2 expression and secretion in SGZ-NSPCs but not SVZ-NSPCs, explaining why only SGZ-NSPC proliferation is affected by RBM3 expression level after HI injury. Like RBM3, microprocessor complex subunit DGCR8, a key protein involved in miRNA biogenesis, can also regulate IGF2 expression and promote the proliferation of SGZ-NSPCs but not SVZ-NSPCs[40]. As IGF2 has been proved to consolidate and enhance memory, a major hippocampal function[41], a decrease in IGF2 induced by RBM3 deficiency can be expected to affect memory function after HI injury, and may also contribute to discovered memory loss by RBM3 silencing in a chronic neurodegenerative disease model[7].

It is feasible to design a small compound to stabilize the RBM3 protein and maintain its expression at high levels by targeting its typical RNA-recognition motif, in order to promote endogenous neurogenesis, particularly in the hippocampus. Such a compound could serve to treat acute brain injury and chronic disease. A preliminary successful example has already been developed with the CIRP homologue, although its activity requires further tests[42]. In addition, the safety of RBM3-based therapy will need to be carefully evaluated for potential tumorigenesis. As IMP family members and IGF2 are critical in promoting cell proliferation, they maintain stem cell stemness under physiological conditions, but are also thought to favor cancer cell progression in diverse tumor types along with their high expression[28,36]. Fortunately, clinical studies have revealed that in contrast to its CIRP homologue, high RBM3 expression is associated with favorable outcome in various cancers[6]. Although the underlying mechanisms remain largely unknown, this suggests that RBM3-targeted therapy could be safe to administer in brain disorders.

Methods

Mice. All animal experiments were approved by the veterinary office of Basel city (authorization number 2064 and 2652) and were in accordance with the guidelines on laboratory animals. RBM3 knockout (KO) C57BL/6 mice were kindly provided by Prof. Tadatsugu Taniguchi (University of Tokyo, Japan). As RBM3 is X-chromosome-linked gene, only male RBM3 WT or KO mice were used in this study. All the mice were maintained under standard conditions of 12/12 h of light/dark at 25 °C before and after surgery.

Hypoxic-ischemia (HI) model. From 2- to 3-months-old adult mice were anesthetized by 3% isoflurane. Right common carotid artery (RCCA) was exposed and permanently ligated by electrocauterization and subsequently cut. RCCA was only exposed but not ligated in sham animals. After recovery from surgery, animals were subjected to 8% hypoxia for 20 min at 37 °C. Sham animals were not treated with hypoxia. After hypoxic stress, all animals were intraperitoneally injected with 50 mg/kg BrdU. Subsequent BrdU injection was performed every other day for 7 days. Mice were sacrificed 7 days or 28 days after HI injury for further analysis.

Immunofluorescent staining. Mice were perfused transcardially with 4% paraformaldehyde (PFA). Brains were collected and post-fixed with 4% PFA for 24 h and immersed in 30% sucrose for additional 24 h both at 4 °C, then embedded in O.C.T. (TissueTek) and frozen in isopentane. Cryoprotected brains were cut into 25 μm thick coronal sections in a cryostat (Leica). For cultured NSPCs, cells were seeded onto

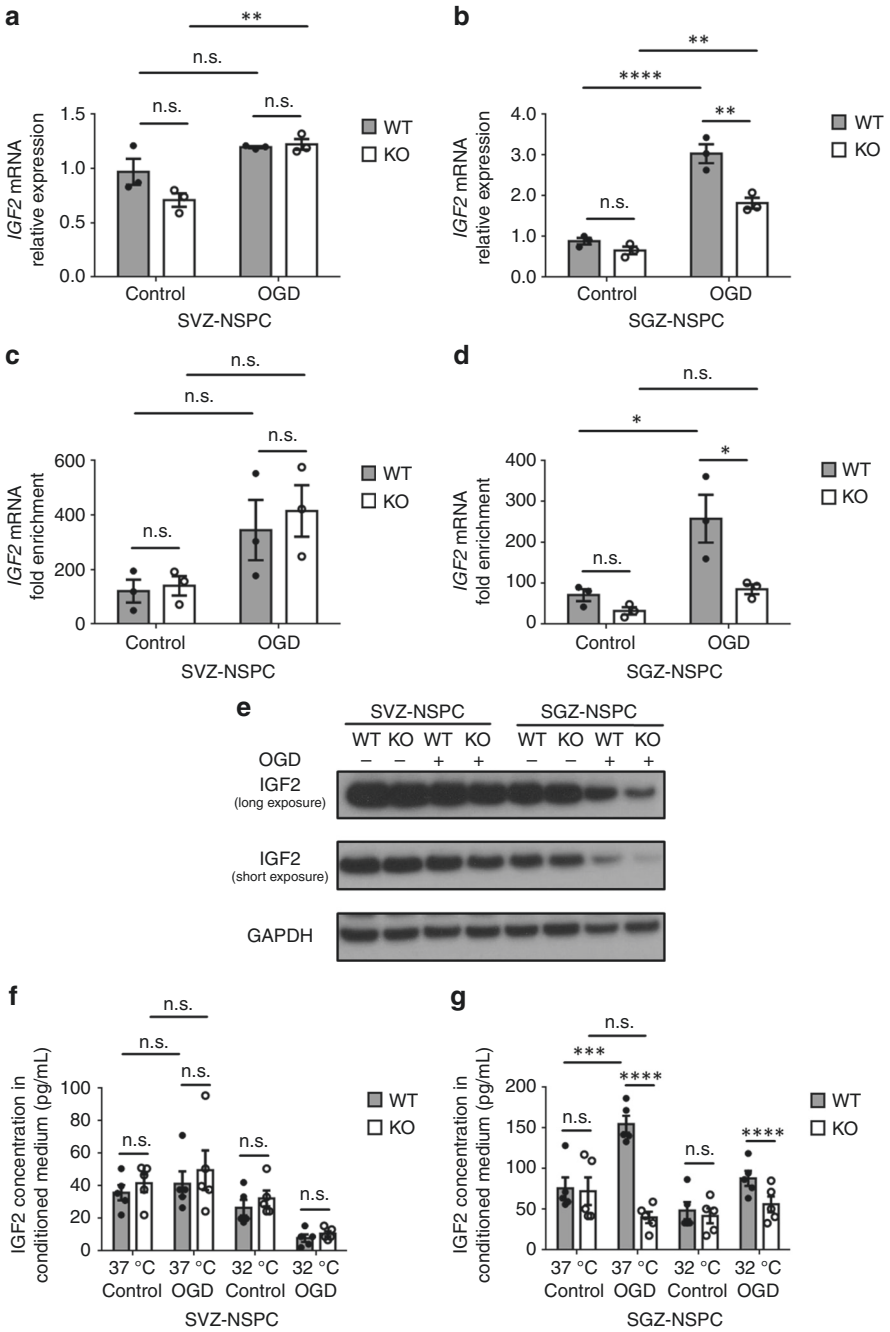

Fig. 6 RBM3 regulates IGF2 expression in SGZ- but not SVZ-NSPCs in vitro. **a**, **b** Quantitative RT-PCR of *IGF2* mRNA expression in SVZ-NSPC (**a**) and SGZ-NSPC (**b**) after 3 h OGD and 3 h reoxygenation in the presence or absence of RBM3 (three independent experiments, $n = 3$). *IGF2* mRNA level was normalized to *GAPDH* by $2^{-\Delta\Delta CT}$ method. Two-way ANOVA was used for statistical analysis; n.s. not significant; $^{**}p < 0.01$; $^{****}p < 0.0001$. **c**, **d** The abundance of bound *IGF2* mRNA to IMP2 protein in RBM3 WT or KO NSPCs after 3 h OGD and 3 h reoxygenation. Lysates from SVZ-NSPC (**c**) or SGZ-NSPC (**d**) were subjected to RNA-immunoprecipitation. Anti-IMP2 antibody was used to precipitate IMP2 protein, and the amount of bound *IGF2* mRNA was detected by quantitative RT-PCR (three independent experiments, $n = 3$). Normal mouse immunoglobulin (msIgG) was served as negative control in immunoprecipitation. *IGF2* mRNA level was normalized to input by $2^{-\Delta\Delta CT}$ method, and fold enrichment was normalized to msIgG group which was set as 1. Two-way ANOVA was used for statistical analysis; n.s. not significant; $^{*}p < 0.05$. **e** Representative Western blot of IGF2 expression in SVZ-NSPC and SGZ-NSPC after mock or OGD treatment in the presence or absence of RBM3. **f**, **g** IGF2 levels in culture medium by ELISA. SVZ-NSPCs (**f**) and SGZ-NSPCs (**g**) were stressed with OGD followed by reoxygenation at 37 or 32 °C for 3 h, then incubated at 37 °C for an additional 21 h. Culture medium was immediately collected for IGF2 measurement by ELISA (five independent experiments, $n = 5$). Three-way ANOVA was used for statistical analysis; n.s. not significant; $^{***}p < 0.001$; $^{****}p < 0.0001$. All data are presented as mean ± SEM

poly-L-lysine coated 16-well chamber slide (Nunc LabTek) and fixed with 4% PFA for 10 min at RT. To stain BrdU, brain sections or cells were treated with 2 M HCl at RT for 1 h and neutralized with 0.1 M sodium borate (pH 8.5) for 10 min before blocking. 0.5% Trition X-100 and 5% normal goat serum in phosphate buffer was used for permeabilization and blocking. Samples were incubated with primary antibodies overnight at 4 °C. Alexa Fluro dye conjugated secondary antibodies were used in 1:500 (Thermo Fisher). Nuclei were couterstained with DAPI. Information for primary antibodies was listed in Supplementary Data 4.

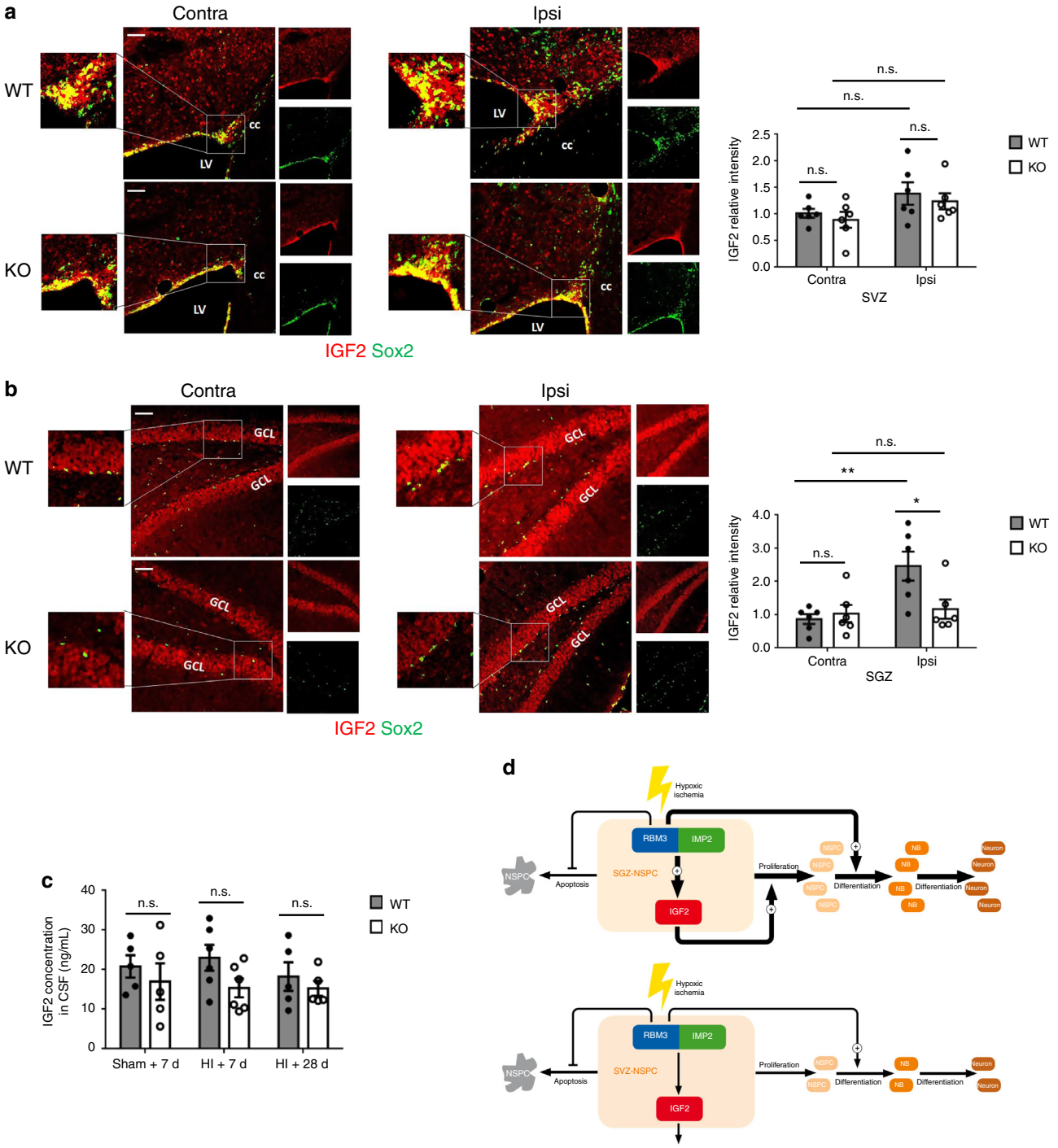

Fig. 7 RBM3 regulates IGF2 expression in SGZ but not in SVZ in vivo. **a**, **b** Representative immunofluorescent IGF2 staining in SVZ (**a**) or SGZ (**b**) of RBM3 WT and KO animals treated with HI and recovered for 7 days. All images were captured with the same parameters. Sox2+ NSPCs were co-stained to identify the SVZ or SGZ. Relative IGF2 intensity in indicated area was quantified with Image J. Six animals were counted per group ($n = 6$). Scale bar: 50 μm. LV lateral ventricle, cc corpus callosum, GCL granular cell layer, Contra contralateral (uninjured side), ipsi ipsilateral (injured side). Repeated measures two-way ANOVA was used for statistical analysis; n.s. not significant; $^{*}p < 0.05$; $^{**}p < 0.01$. **c** ELISA measurement of IGF2 levels in cerebrospinal fluid (CSF). CSF samples were collected from WT or KO mice treated with sham operation, HI plus 7 days recovery or HI plus 28 days recovery (Sham+7d: $n = 5$, HI + 7d: $n = 6$, HI + 28d: $n = 5$). Two-way ANOVA was used for statistical analysis; n.s. not significant. All data are presented as mean ± SEM. **d** Hypothesized model. In SGZ-NSPC, RBM3 interacts with IMP2 and thereby enhances IGF2 expression and release to promote SGZ-NSPC proliferation in an autocrine pattern after HI injury. On the other hand RBM3 promotes neuronal differentiation. In SVZ-NSPC, RBM3 does not promote proliferation after HI injury and affects neuronal differentiation to a lesser extent. In both cell types, RBM3 inhibits apoptosis. NB neuroblast

Cresyl violet staining. Brain cryosections were mounted on Superfrost PLUS glass slides and stained with 0.2% cresyl violet solution for 20 min at RT. Stained slides were subsequently washed in distilled water, dehydrated in 70, 80, 90, 95, and 100% ethanol, and then cleared twice in xylene. Eukitt mounting medium (Fluka) was used for mounting slides.

Stereology, imaging, and cell quantification. Stereological coordinates were identified according to adult mouse brain atlas[43]. Animals 7 days after HI injury were used for infarction volume estimation. The infarction volume estimation method was adapted from elsewhere using the Cavalieri estimator probe[44]. Fixed brains were serially cut into 25 µm thick coronal sections in a cryostat (approximately between +2.0 and −4.0 mm from the bregma), and every twelfth sections were picked (300 µm interval) for cresyl violet staining as described above, totally 20 sections. Imaging was performed in live mode with a ×5 objective using an Axio Imager Z1 microscope (Zeiss) equipped with Stereo Investigator (MBF Bioscience). The contours of direct infarction areas (mm^2), ipsilateral hemisphere areas (mm^2) and contralateral hemisphere areas (mm^2) were outlined and calculated by Cavalieri point-counting estimator from Stereo Investigator. A grid spacing of 50 µm was used. The corrected infarction areas were calculated as follows:

$$A_{\text{corrected}} = A_{\text{direct}} - \left(A_{\text{ipsi}} - A_{\text{contra}}\right) \quad (1)$$

$A_{corrected}$ is the corrected infarction area, A_{direct} is the direct infarction area, A_{ipsi} is ipsilateral hemisphere area, and A_{contra} is contralateral hemisphere area. The estimated infarction volume (mm^3) was calculated by summing up corrected infarction areas from all 20 sections and then multiplying by the 300 µm interval. The SVZ (tail and lateral wall) or DG (granular cell layer and hilus) volumes (mm^3) were estimated in a direct way without correction, using Cavalieri point-counting estimator as described above, but with 20 µm grid spacing. Four sections containing the SVZ (approximately between +1.2 and 0.0 mm from the bregma) and eight sections containing the entire DG (approximately between −1.2 and −3.6 mm from the bregma) per animal were used for volume estimation.

Cell quantification in the SVZ (approximately between +1.2 and 0.0 mm from the bregma) were estimated with every twelfth serial coronal sections (25 µm thick each, 300 µm interval), totally four sections. Cell quantification in the SGZ covering dorsal and ventral hippocampus (approximately between −1.2 and −3.6 mm from the bregma) were estimated with every twelfth serial coronal sections (25 µm thick each, 300 µm interval), totally eight sections. Double-positive cells were imaged using z-stack function with LSM710 confocal microscope (Zeiss). Stacked images were acquired every 1 µm throughout the section (25 optical sections) and presented in orthogonal view to confirm co-localization. Cell counting in the SVZ or DG was performed with Optical Fractionator from Stereo Investigator (MBF Bioscience) according to published methods[14,45–47]. The counting frame size of 30 × 30 µm was used for all the counting types. To count total BrdU+, BrdU+/Sox2+, BrdU+/Dcx+ cells in the SVZ and DG, or TUNEL + cells in the SVZ in HI + 7d groups, a 60 × 60 µm sampling grid was used. For TUNEL + cells in the DG in HI + 7d groups, a 90 × 90 µm sampling grid was used. For total BrdU + and BrdU + NeuN + cells in the SVZ and DG in HI + 28d groups, a 30 × 30 µm sampling grid was used. Cells were only counted in the optical disector with the height of 10 µm, but not counted in the top and bottom 3 µm guard zones. Total cell number (N) was estimated with the following calculation formula:

$$N = \sum Q^{-} \times (t/h) \times (1/asf) \times (1/ssf) \quad (2)$$

$\sum Q^{-}$ is total cell count in disector; t is section thickness after processing; h is optical disector height; asf is area sampling fraction (counting frame size/sampling grid size); and ssf is slice sampling fraction (1/section interval). The density of positive cells in the two neurogenic niches was determined by dividing the total positive cell number to the SVZ or DG volume, respectively. The SVZ or DG volumes (mm^3) were estimated on adjacent section series with the method as described above. For non-operating and sham animals, the mean of left and right hemisphere cell numbers was presented for each animal.

For relative intensity quantification of IGF2, all the images were captured with the same parameters. The signal in lateral ventricle was subtracted as background. The average intensity of IGF2 signal in the SVZ or SGZ from all sections prepared as above mentioned was calculated with Image J (National Institutes of Health) and was presented for each animal.

For cultured cells, images of five random fields with ×20(except ×40 for proximity ligation assay) objective lens were captured with AX70 fluorescent microscope (Olympus) for quantification per experiment. Three independent experiments were performed.

Cell culture. HEK293 cells were cultured in DMEM (Gibco) medium supplemented with 10% FBS (Gibco). SVZ-NSPCs and SGZ-NSPCs were isolated from the SVZ of lateral ventricle or DG of 2–3-months-old adult male mice respectively, according to previous protocols[48,49]. The whole brain excluding cerebellum and meninges from postnatal day 0 male mice was used for NSPC culture. In brief, cells from desired regions were dissociated by papain (Worthington) and DNase I (Sigma) digestion, and passed through 40 µm cell strainer (Sigma) to remove cell clusters. Isolated NSPCs were cultured in complete DMEM-F12 medium (Gibco) supplemented with 1 × B27 supplement (Gibco), 2 mM L-glutamine (Gibco), 20 ng/mL EGF (PeproTech) and 20 ng/mL FGF2 (PeproTech). Cells were maintained as neurospheres in uncoated dishes or as monolayer in poly-L-lysine (Sigma) coated dishes or 16-well chamber slides (LabTek). To passage neurospheres, 0.25% Typsin (Sigma) was used to digest neurospheres into single cells.

Plasmids and constructs. pCEP4-RBM3 construct used to overexpress RBM3 in primary NSPCs and control empty pCEP4 vector (Thermo Fischer) were described in previous report[9]. Commercial pCMV3-RBM3 was intended for mammalian overexpression of full-length RBM3 cDNA under CMV promoter with additional N-terminal HA tag (Sino Biological, HG16437-NY). Commercial pCMV3-IMP2 plasmid was designed for full-length IMP2 overexpression with N-terminal FLAG tag (Sino Biological, HG11116-NF). Control empty vectors with N-terminal HA or FLAG tag were purchased from Sino Biological as well (pCMV3-N-HA-NCV and pCMV3-N-FLAG-NCV).

RRM and KH domains of IMP2 including two RRMs and four KHs respectively, were cloned into pCMV3-N-FLAG-NCV with FLAG tag. IMP2-RRMs were subcloned by standard PCR using IMP2-RRMs F/R primer pairs. IMP2-KHs were amplified by overlapping PCR to conjugate DNA encoding affinity tag to DNA encoding truncated peptides. pCMV3 F/FLAG-tag R and IMP2-KHs F/R primer pairs were used for overlapping PCR. Overlapped PCR products were digested with KpnI/NotI and ligated to digested pCMV3-N-FLAG-NCV vector. Primers sequences were listed in Supplementary Data 4. All the pCMV3 constructs were transiently expressed in HEK293 cells.

Transient transfections. For co-immunoprecipitation, all pCMV3-based plasmids expressing full-length or truncated RBM3 or IMP2 were transiently transfected into HEK293 cells with FuGENE HD Transfection Reagent (Promega) for 48 h. One to two micrograms of each plasmid was used to transfect 1×10^6 HEK293 cells. For cultured NSPCs, 10 µg pCEP4 empty vector or pCEP4-RBM3 plasmid were transiently transfected into 5×10^6 NSPCs by electroporation, using Mouse Neural Stem Cell Nucleofector Kit (Lonza) and program A-33 of Nucleofector I Device (Lonza). Transfected cells were kept in 12-well plate overnight and then spun down at 100 x g at RT for 5 min to remove dead cells. The remaining viable cells were counted and seeded at the density of 1×10^4 cells/mL into poly-L-lysine coated 16-well chamber slide. Cells were incubated for another 48 h before starting further treatments.

Oxygen-glucose deprivation (OGD). NSPCs were cultured in poly-L-lysine coated 16-well chamber slide or petri dish with diameter of 10 cm for 24 h. To introduce OGD, normal NSPC culture medium was changed to glucose-free complete medium (using glucose-free DMEM-F12, Biowest) and slides or dishes were kept in hypoxic chamber (Elektrotek) with nitrogen flush for 15 min. Then the chamber was sealed and kept at 37 °C for 3 h. After OGD, glucose-free medium was switched back to normal complete culture medium and cells were incubated in normal conditions with 20% oxygen at 37 °C (normothermic group) or 32 °C (hypothermic group) for indicated period. For BrdU incorporation, 20 µM BrdU was added into the culture medium immediately after OGD or mock treatment.

Quantitative RT-PCR. Total RNA from cells or brain tissues were isolated by ReliaPrep RNA Miniprep System (Promega). One microgram total RNA was reversely transcribed into complementary DNA using GoScript Reverse Transcription System (Promega). Quantitative amplification was carried out with GoTaq qPCR Master Mix (Promega) in 15 µL reaction volume. Thermal cycles were performed on CFX Connect Real-Time PCR Detection System (Bio-Rad) at 95 °C for 5 min, followed by 40 cycles of 95 °C for 15 s and 60 °C for 1 min. $2^{-\Delta\Delta CT}$ method was used to calculate the fold change of gene expression. Three independent experiments were performed. Primers sequences were listed in Supplementary Data 4.

Western blot. Cells or brain tissues were harvested, washed with cold PBS and lysed in lysis buffer (1% Triton X-100, 50 mM Tris, 150 mM NaCl, 1 × Roche Protease Inhibitor Cocktail, pH 8.0). Brain tissues were further homogenized with Dounce tissue grinder on ice. After centrifugation at 15000 rpm for 10 min at 4 °C, supernatants were collected and normalized with RC DC Protein Assay (Bio-Rad). Lysates were loaded onto NuPAGE Novex 4–12% Bis-Tris protein gels (Invitrogen) and transferred to PVDF membranes (Amersham/GE Healthcare Life Sciences). Samples were incubated with primary antibodies overnight at 4 °C. HRP-linked anti-rabbit IgG and HRP-linked anti-mouse IgG secondary antibodies were purchased from Cell Signaling Technology and used in 1:5000. Information for primary antibodies was listed in Supplementary Data 4.

Neurosphere assay. Neurospheres assay was performed to test self-renewal capacity of cultured NSPCs. Pre-cultured NSPCs directly from dissociated tissue in the form of neurospheres were digested into single cells by trypsin and plated at the density of 100 cells per 100 µL medium in each well of 96-well plate to form primary neurospheres. Primary neurospheres were further digested into single cells and plated at the same density to form secondary neurospheres. After 48 h culture, the numbers of primary and secondary neurospheres were counted in two groups

in terms of their diameters (<20 and ≥20 μm). Triplicates were included in each group.

Differentiation assay. NSPCs were seeded in 16-well chamber slide as monolayer at the density of 1×10^5/mL and maintained for 24 h at 37 °C. Cultured cells were subjected to directed differentiation or OGD-induced differentiation. For directed differentiation, NSPCs were incubated in the following medium for 7 days before immunostaining: Neuralbasal medium supplemented with 1 × B27 supplement and 2 mM L-glutamine for neuronal differentiation; DMEM supplemented with 1 × N-2 supplement (Gibco), 2 mM L-glutamine and 1% FBS for astrocyte differentiation; Neuralbasal medium supplemented with 1 × B27 supplement, 2 mM L-glutamine and 30 ng/mL triiodothyronine (T3) solution (Calbiochem) for oligodendrocyte differentiation. For OGD-induced differentiation, cells were challenged with 3 h OGD and then reoxygenated at 37 °C for 2 days in NSPC complete culture medium, followed by 5 days in above-mentioned directed differentiation medium, respectively. The following primary antibodies were used to identify various differentiated cells: MAP2 for neurons; Dcx for neuroblasts; S100 for glia cell progenitors and Olig2 for oligodendrocyte progenitor cells (OPCs). Information for primary antibodies was listed in Supplementary Data 4. All quantifications were performed in triplicates.

TUNEL staining. TUNEL staining was used to test late apoptosis. The assay was performed with Click-iT Plus TUNEL Assay for In Situ Apoptosis Detection with Alexa Fluor 488 Dye (Invitrogen) following manufacturer's instructions. Brain cyrosections were digested with Protease K for antigen retrieval and counterstained with DAPI. Cultured NSPCs were permeabilized with Triton X-100 and counterstained with DAPI. TUNEL+ cells were counted in brain sections or cultured NSPCs, respectively. In cultured NSPCs, TUNEL+ cell percentages in all DAPI stained cells were calculated in triplicates.

Co-immunoprecipitation and RNA-immunoprecipitation. For co-immunoprecipitation (CoIP), 4 μg primary antibodies or control normal IgG were conjugated to 40 μL Dynabeads Protein G (Invitrogen) for 45 min at RT. HEK293 cells which were transfected with full-length or truncated RBM3 and IMP2 overexpressing pCMV plasmids (as described above) were harvested 48 h after transfection. HEK293 or P0 NSPC cell lysates were incubated with antibody-coupled Dynabeads Protein G overnight at 4 °C. For RNase-treated group, cell lysates were pretreated with 10 U/μl RNaseT1 (Fermentas) for 15 min at RT before subjected to beads. Proteins were eluted from beads in NuPAGE LDS Sampler Buffer (Invitrogen) containing 50 mM DTT at 70 °C for 10 min. Samples were analyzed by Western blot. RNA-immunoprecipitation (RIP) was performed in a native way similar to CoIP. After mock or OGD treatment, the starting material was adjusted to 5×10^6 cells per sample. All the reagents contained 40 U/mL RNase inhibitor RNasin (Promega) and prepared in RNase-free water (Promega) to minimize the activity of RNase from the environment. Immunoprecipiated RNA was eluted in lysis buffer from above-mentioned total RNA isolation kit at 70 °C for 10 min, and further purified by the kit. Samples were analyzed by quantitative RT-PCR.

Proximity ligation assay. Proximity ligation assay (PLA) was used to reveal protein interactions between RBM3 and IMP2 in situ using Duolink In Situ Red Starter Kit Mouse/Rabbit (Sigma). Brain sections and cultured NSPCs were counterstained with DAPI. In cultured NSPCs, PLA + dots (each dot represents one interaction) in each cell were quantified, and 25 cells per sample were analyzed for statistical analysis.

RNA sequencing. Hippocampi were isolated from postnatal day 3 (P3) or adult RBM3 WT or KO mice ($n = 3$ for each group) and homogenated in Trizol by Dounce tissue grinder on ice. Total RNA was separated by chloroform and precipitated by isopropanol, and then further cleaned up using RNA Clean & Concentrator Kit (Zymo Research). Complementary DNA libraries were constructed from messenger RNA and qualified on Agilent 2100 Bioanalyzer. RNA sequencing was carried out on Illumina Hiseq-2500 sequencing system with single reads of 50 bp read length. Differentially expressed genes (DEGs) were filtered with log2A > 3.32 (Average counts per million (CPM) > 10); |log2 FC| > 0.26 (|Fold change| > 1.2) and unadjusted P value < 0.05. Venn diagrams were generated via InteractiVenn online tool (http://www.interactivenn.net). Gene heatmap were generated via Heatmapper online tool (http://heatmapper.ca/expression). Gene set enrichment analysis (GSEA) was performed via online analysis tool (http://www.webgestalt.org). Volcano plot and M-A plot were prepared by GraphPad Prism 8.0. The raw data are available on NCBI BioProject (Project ID: PRJNA529585).

ELISA. Cerebrospinal fluid (CSF) samples were collected from cisterna magna immediately before sacrificing animals as described previously[50]. NSPC culture media were collected immediately before fixing cells. IGF2 levels in CSF or in culture medium were measured by mouse IGF2 ELISA Kit (Abnova) with the sensitivity of <5 pg/mL. Five replicates for sham and HI + 28d groups and six replicates for HI + 7d group were included. Culture medium from NSPCs were in five replicates.

Statistical analysis. All in vitro experiments were repeated at least three times. All in vivo experiments included a minimum of five mice per group. Quantification data were presented in standard error mean (SEM). For comparison of two groups, statistical significance was determined by two-tailed unpaired *t*-test with or without Welch's correction (single factor), two-way ANOVA (two factors) followed by Tukey's multiple comparison test or Sidak's multiple comparison test, and three-ANOVA (three factors) followed by Sidak's multiple comparison test. For the quantification of data involving contralateral and ipsilateral sides from the same animal, repeated measures two-way ANOVA was performed, and mixed effects model was applied for further comparison with the sham group. p value less than 0.05 was considered significant. n.s. not significant; $^*p < 0.05$; $^{**}p < 0.01$; $^{***}p < 0.001$; $^{****}p < 0.0001$. Statistical analysis was performed using GraphPad Prism 8.0 and all details are reported in Source Data file.

Reporting summary. Further information on research design is available in the Nature Research Reporting Summary linked to this article.

Data availability

The raw RNA-seq data are available on NCBI BioProject (Project ID: PRJNA529585). The source data relating to Figs. 1b, c, e–h, 2b–e, 3b–i, 4b, c, e–h, 5b, 6a–d, f, g, 7a–c and Supplementary Figs. 1a, b, e–h, 2a–f, 5c–f, h–k, 7a are provided in the Source Data file. Uncropped blots are shown in Supplementary Fig. 8. All other raw data are available from the authors upon request. A reporting summary for this article is available as a Supplementary Information file.

Received: 10 August 2018 Accepted: 1 August 2019
Published online: 04 September 2019

References

1. Hypothermia after Cardiac Arrest Study G. Mild therapeutic hypothermia to improve the neurologic outcome after cardiac arrest. *N. Engl. J. Med.* **346**, 549–556 (2002).
2. Heinz, U.E., Rollnik, J.D. Outcome and prognosis of hypoxic brain damage patients undergoing neurological early rehabilitation. *BMC Res. Notes* https://doi.org/10.1186/s13104-015-1175-z (2015).
3. Shankaran, S. et al. Whole-body hypothermia for neonates with hypoxic-ischemic encephalopathy. *N. Engl. J. Med.* **353**, 1574–1584 (2005).
4. Logan, A., Sangkachand, P. & Funk, M. Optimal management of shivering during therapeutic hypothermia after cardiac arrest. *Crit. Care Nurse* **31**, e18–30 (2011).
5. Geurts, M. et al. COOLIST (Cooling for Ischemic Stroke Trial): a multicenter, open, randomized, phase II, clinical trial. *Stroke* **48**, 219–221 (2017).
6. Zhu, X., Buhrer, C. & Wellmann, S. Cold-inducible proteins CIRP and RBM3, a unique couple with activities far beyond the cold. *Cell Mol. Life Sci.* **73**, 3839–3859 (2016).
7. Peretti, D. et al. RBM3 mediates structural plasticity and protective effects of cooling in neurodegeneration. *Nature* **518**, 236–239 (2015).
8. Bastide, A. et al. RTN3 is a novel cold-induced protein and mediates neuroprotective effects of RBM3. *Curr. Biol.* **27**, 638–650 (2017).
9. Chip, S. et al. The RNA-binding protein RBM3 is involved in hypothermia induced neuroprotection. *Neurobiol. Dis.* **43**, 388–396 (2011).
10. Zhu, X., Zelmer, A., Kapfhammer, J. P. & Wellmann, S. Cold-inducible RBM3 inhibits PERK phosphorylation through cooperation with NF90 to protect cells from endoplasmic reticulum stress. *FASEB J.* **30**, 624–634 (2016).
11. Pilotte, J., Cunningham, B. A., Edelman, G. M. & Vanderklish, P. W. Developmentally regulated expression of the cold-inducible RNA-binding motif protein 3 in euthermic rat brain. *Brain Res.* **1258**, 12–24 (2009).
12. Ming, G. L. & Song, H. Adult neurogenesis in the mammalian brain: significant answers and significant questions. *Neuron* **70**, 687–702 (2011).
13. Pincus, D. W. et al. Fibroblast growth factor-2/brain-derived neurotrophic factor-associated maturation of new neurons generated from adult human subependymal cells. *Ann. Neurol.* **43**, 576–585 (1998).
14. Boldrini, M. et al. Human hippocampal neurogenesis persists throughout aging. *Cell Stem Cell* **22**, 589–599 (2018).
15. Lindvall O, Kokaia Z. Neurogenesis following stroke affecting the adult brain. *Cold Spring Harb. Perspect. Biol.* https://doi.org/10.1101/cshperspect.a019034 (2015).
16. Yenari, M. A. & Han, H. S. Influence of therapeutic hypothermia on regeneration after cerebral ischemia. *Front. Neurol. Neurosci.* **32**, 122–128 (2013).
17. Matsuda, A. et al. Generation of mice deficient in RNA-binding motif protein 3 (RBM3) and characterization of its role in innate immune responses and cell growth. *Biochem. Biophys. Res. Commun.* **411**, 7–13 (2011).
18. Palma-Tortosa S et al. Specific features of SVZ neurogenesis after cortical ischemia: a longitudinal study. *Sci. Rep.* https://doi.org/10.1038/s41598-017-16109-7 (2017).

19. Woitke F et al. Adult hippocampal neurogenesis poststroke: more new granule cells but aberrant morphology and impaired spatial memory. *PloS ONE*. https://doi.org/10.1371/journal.pone.0183463 (2017).
20. Imura, T., Kornblum, H. I. & Sofroniew, M. V. The predominant neural stem cell isolated from postnatal and adult forebrain but not early embryonic forebrain expresses GFAP. *J. Neurosci.* **23**, 2824–2832 (2003).
21. Garcia, A. D., Doan, N. B., Imura, T., Bush, T. G. & Sofroniew, M. V. GFAP-expressing progenitors are the principal source of constitutive neurogenesis in adult mouse forebrain. *Nat. Neurosci.* **7**, 1233–1241 (2004).
22. Fernandez, A. M. & Torres-Aleman, I. The many faces of insulin-like peptide signalling in the brain. *Nat. Rev. Neurosci.* **13**, 225–239 (2012).
23. Bracko, O. et al. Gene expression profiling of neural stem cells and their neuronal progeny reveals IGF2 as a regulator of adult hippocampal neurogenesis. *J. Neurosci.* **32**, 3376–3387 (2012).
24. Ferron SR et al. Differential genomic imprinting regulates paracrine and autocrine roles of IGF2 in mouse adult neurogenesis. *Nat. Commun*. https://doi.org/10.1038/ncomms9265 (2015).
25. Nishino, J., Kim, S., Zhu, Y., Zhu, H., Morrison, S.J. A network of heterochronic genes including Imp1 regulates temporal changes in stem cell properties. *Elife* https://doi.org/10.7554/eLife.00924 (2013).
26. Mori, H. et al. Expression of mouse igf2 mRNA-binding protein 3 and its implications for the developing central nervous system. *J. Neurosci. Res.* **64**, 132–143 (2001).
27. Fujii, Y., Kishi, Y. & Gotoh, Y. IMP2 regulates differentiation potentials of mouse neocortical neural precursor cells. *Genes Cells* **18**, 79–89 (2013).
28. Bell, J. L. et al. Insulin-like growth factor 2 mRNA-binding proteins (IGF2BPs): post-transcriptional drivers of cancer progression? *Cell Mol. Life Sci.* **70**, 2657–2675 (2013).
29. Kernie, S. G. & Parent, J. M. Forebrain neurogenesis after focal Ischemic and traumatic brain injury. *Neurobiol. Dis.* **37**, 267–274 (2010).
30. Yenari, M. A. & Han, H. S. Neuroprotective mechanisms of hypothermia in brain ischaemia. *Nat. Rev. Neurosci.* **13**, 267–278 (2012).
31. Kurisu, K. & Yenari, M. A. Therapeutic hypothermia for ischemic stroke; pathophysiology and future promise. *Neuropharmacology* **134**, 302–309 (2017).
32. Zhang, Q. et al. Involvement of cold inducible RNA-binding protein in severe hypoxia-induced growth arrest of neural stem cells in vitro. *Mol. Neurobiol.* **54**, 2143–2153 (2017).
33. Saito, K. et al. Moderate low temperature preserves the stemness of neural stem cells and suppresses apoptosis of the cells via activation of the cold-inducible RNA binding protein. *Brain Res.* **1358**, 20–29 (2010).
34. Qiang, X. et al. Cold-inducible RNA-binding protein (CIRP) triggers inflammatory responses in hemorrhagic shock and sepsis. *Nat. Med* **19**, 1489–1495 (2013).
35. Zhou, M., Yang, W. L., Ji, Y., Qiang, X. & Wang, P. Cold-inducible RNA-binding protein mediates neuroinflammation in cerebral ischemia. *Biochim. Biophys. Acta* **1840**, 2253–2261 (2014).
36. Degrauwe, N., Suva, M. L., Janiszewska, M., Riggi, N. & Stamenkovic, I. IMPs: an RNA-binding protein family that provides a link between stem cell maintenance in normal development and cancer. *Genes Dev.* **30**, 2459–2474 (2016).
37. Degrauwe, N. et al. The RNA binding protein IMP2 preserves glioblastoma stem cells by preventing let-7 target gene silencing. *Cell Rep.* **15**, 1634–1647 (2016).
38. Lehtinen, M. K. et al. The cerebrospinal fluid provides a proliferative niche for neural progenitor cells. *Neuron* **69**, 893–905 (2011).
39. Ziegler, A. N. et al. IGF-II promotes stemness of neural restricted precursors. *Stem Cells* **30**, 1265–1276 (2012).
40. Ouchi, Y. et al. Reduced adult hippocampal neurogenesis and working memory deficits in the Dgcr8-deficient mouse model of 22q11.2 deletion-associated schizophrenia can be rescued by IGF2. *J. Neurosci.* **33**, 9408–9419 (2013).
41. Chen, D. Y. et al. A critical role for IGF-II in memory consolidation and enhancement. *Nature* **469**, 491–497 (2011).
42. Coderch, C. et al. In silico identification and in vivo characterization of small molecule therapeutic hypothermia mimetics. *Bioorg. Med. Chem.* **25**, 6597–6604 (2017).
43. Paxinos, G. F. & Franlin, K. B. J. *The Mouse Brain in Stereotaxic Coordinates*. 2nd edn (Academic Press, San Diego, USA, 2001).
44. Ballesteros, I. et al. Stereological and flow cytometry characterization of leukocyte subpopulations in models of transient or permanent cerebral ischemia. *J. Vis. Exp*. https://doi.org/10.3791/52031 (2014).
45. Li, L. et al. Hypoxia inducible factor-1alpha (HIF-1alpha) is required for neural stem cell maintenance and vascular stability in the adult mouse SVZ. *J. Neurosci.* **34**, 16713–16719 (2014).
46. Lindquist, R.A. et al. Identification of proliferative progenitors associated with prominent postnatal growth of the pons. *Nat. Commun*. https://doi.org/10.1038/ncomms11628 (2016).
47. Yau, S. Y. et al. Physical exercise-induced hippocampal neurogenesis and antidepressant effects are mediated by the adipocyte hormone adiponectin. *Proc. Natl Acad. Sci. USA* **111**, 15810–15815 (2014).
48. Guo, W., Patzlaff, N. E., Jobe, E. M. & Zhao, X. Isolation of multipotent neural stem or progenitor cells from both the dentate gyrus and subventricular zone of a single adult mouse. *Nat. Protoc.* **7**, 2005–2012 (2012).
49. Walker, T.L., Kempermann, G. One mouse, two cultures: isolation and culture of adult neural stem cells from the two neurogenic zones of individual mice. *J. Vis. Exp*. https://doi.org/10.3791/5614 (2014).
50. Bregere, C. et al. Neonatal hypoxia-ischemia in rat increases doublecortin concentration in the cerebrospinal fluid. *Eur. J. Neurosci.* **46**, 1758–1767 (2017).

Acknowledgements

This research is funded by Swiss National Science Foundation (SNSF, 163305 and 146632), Gottfried und Julia Bangerter-Rhyner-Stiftung, Freiwillige Akademische Gesellschaft Basel (FAG) and China Scholarship Council (CSC, 201606170071). We sincerely thank Prof. Tadatsugu Taniguchi (University of Tokyo, Japan) for providing RBM3 KO mice. We are grateful to Philippe Demougin and Dr. Robert Ivanek (University of Basel, Switzerland) for RNA sequencing and analysis. We sincerely thank Dr. Claudio Giachino and the DBM-Microscopy Core Facility (University of Basel, Switzerland) for valuable assistance with Stereo Investigator software and microscopy.

Author contributions

X.Z. and S.W. designed the project and wrote the manuscript. X.Z. and J.Y. performed most of the experiments and analyzed the data. X.Z. and C.B. performed animal experiments. A.Z. and T.G. assisted with in vitro experiments. J.P.K. and R.G. provided facilities for animal experiments. All authors discussed the results and commented on the manuscript.

Additional information

Supplementary Information accompanies this paper at https://doi.org/10.1038/s41467-019-11870-x.

Competing interests: The authors declare no competing interests.

Reprints and permission information is available online at http://npg.nature.com/reprintsandpermissions/

Peer review information: *Nature Communications* thanks the anonymous reviewers for their contribution to the peer review of this work. Peer reviewer reports are available.

Publisher's note: Springer Nature remains neutral with regard to jurisdictional claims in published maps and institutional affiliations.

2.1.2

Supplementary Information

RBM3 promotes neurogenesis in a niche-dependent manner via IMP2-IGF2 signaling pathway after hypoxic-ischemic brain injury

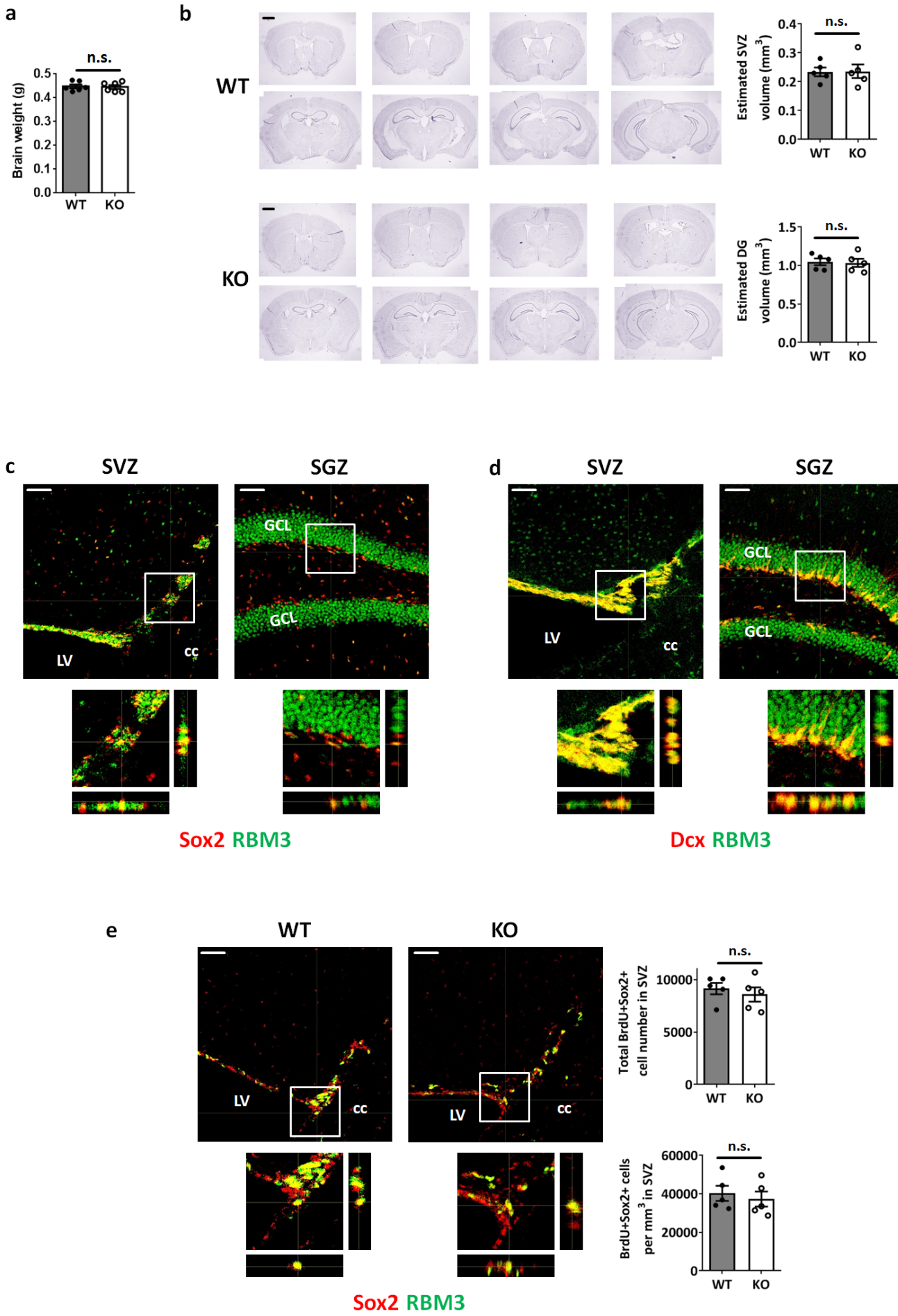

Supplementary Figure 1 (to be continued)

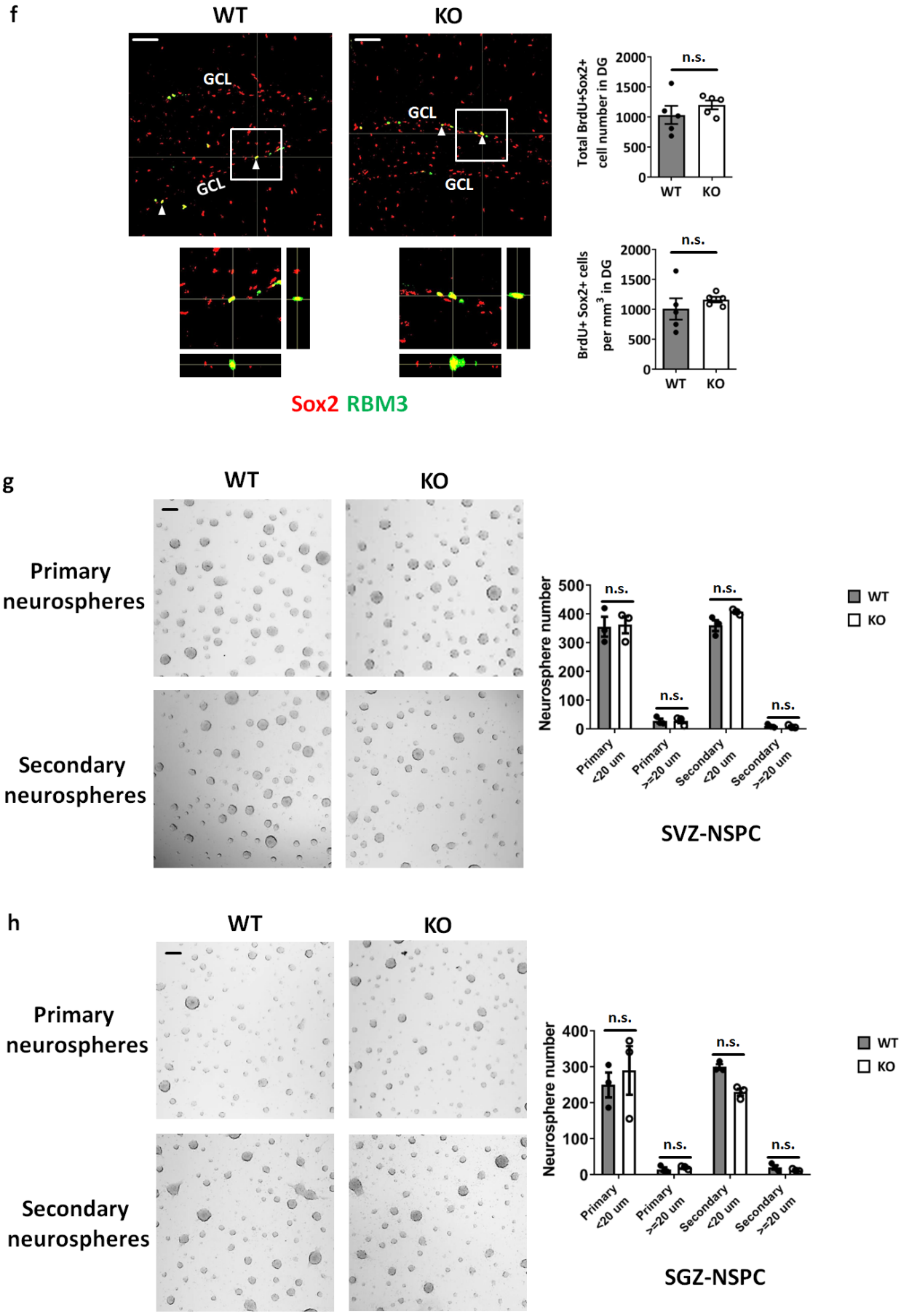

Supplementary Figure 1 (continued)

Supplementary Figure 1 RBM3 KO mouse brain does not show evident abnormality in physiological conditions.

a. Brains from adult RBM3 WT or KO mice were collected and measured (six animals per group, n=6), and analyzed by two-tailed t-test. n.s., not significant. **b.** Representative cresyl violet staining of adult RBM3 WT or KO brain without injury. Scale bar: 1 mm. The volume of SVZ and DG were estimated as described in methods, and compared between WT and KO. Five animals were counted per group (n=5). Two-tailed t-test was used for statistical analysis; n.s., not significant. **c-d.** Representative immunofluorescent staining of RBM3 and Sox2 **(c)**, or RBM3 and Dcx **(d)** in the SVZ and DG of adult WT mouse brain. Orthogonal view confirmed the co-localizations. Scale bar: 50 μm. LV: lateral ventricle; cc: corpus callosum; GCL: granular cell layer. **e-f.** RBM3 WT or KO mice were intraperitoneally injected with BrdU for 7 days to monitor NSPC proliferation. Representative immunofluorescent staining images of BrdU and Sox2 in the SVZ **(e)** or DG **(f)** were demonstrated (five animals per group, n=5). Orthogonal view confirmed the co-localization of BrdU and Sox2. Scale bar: 50 μm. LV: lateral ventricle; cc: corpus callosum; GCL: granular cell layer. Two tailed t-test was used for statistical analysis. n.s. not significant. **g-h.** SVZ-NSPCs and SGZ-NSPCs were cultured *in vitro* and seeded into 96-well plates in equal amounts for the analysis of primary neurospheres after pre-culture or passaged for analyzing secondary neurospheres in SVZ-NSPC **(g)** or SGZ-NSPC **(h)**. Neurospheres with diameters <20 μm or >=20 μm were counted and analyzed separately. Three independent experiments were performed (n=3). Scale bar: 50 μm. Three-way ANOVA was used for statistical analysis. n.s. not significant. All data are presented in SEM.

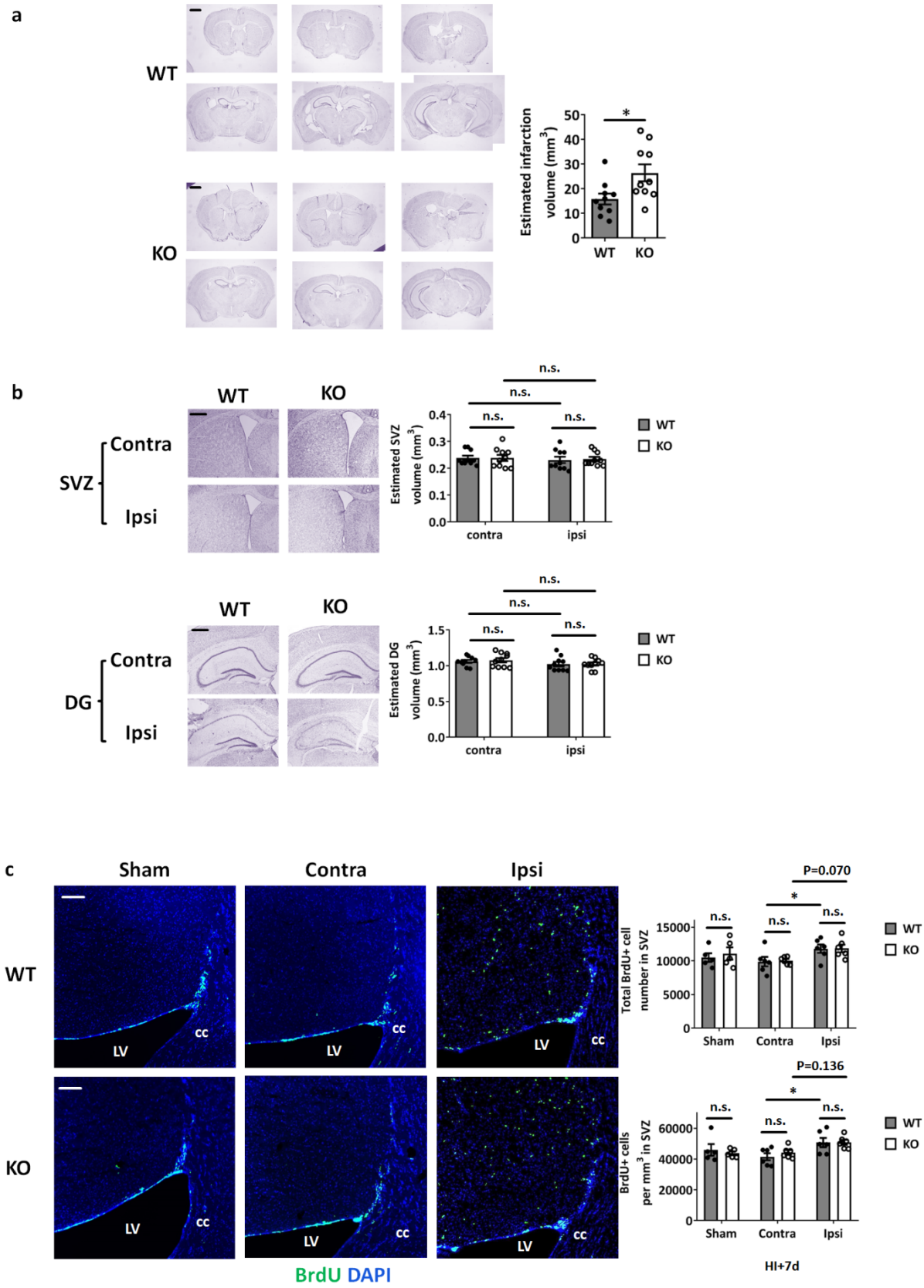

Supplementary Figure 2 (to be continued)

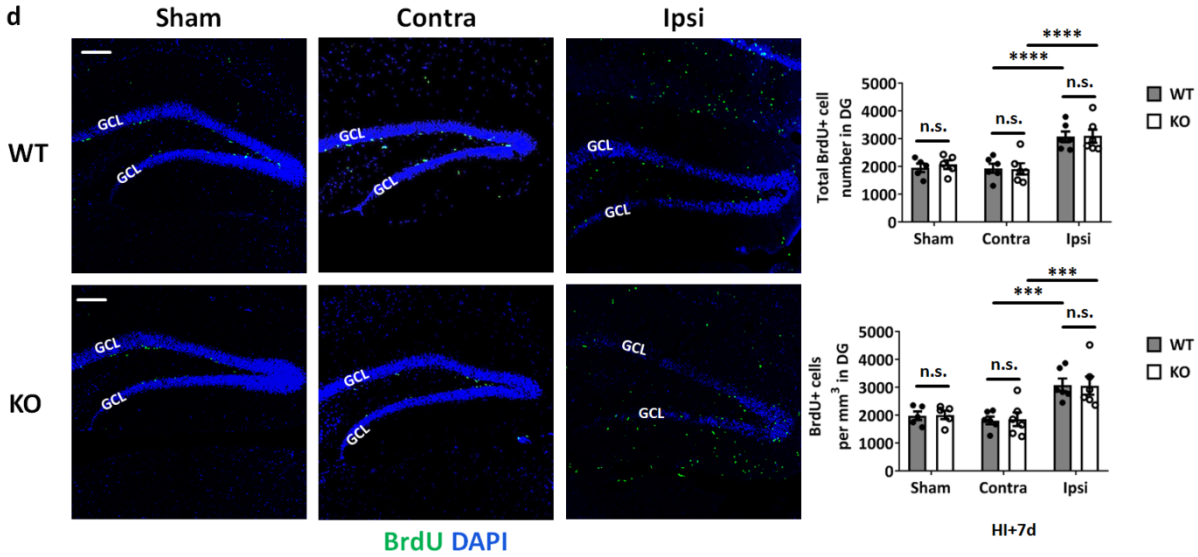

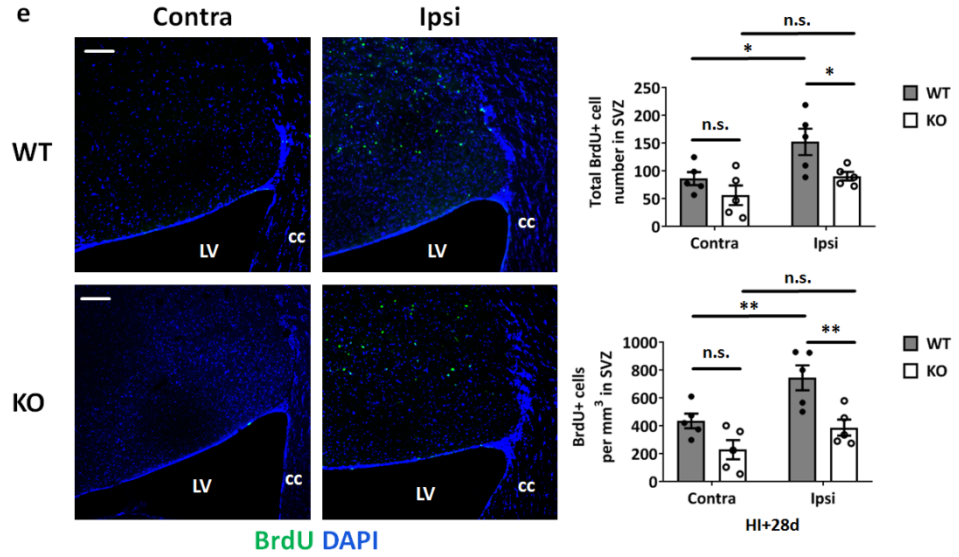

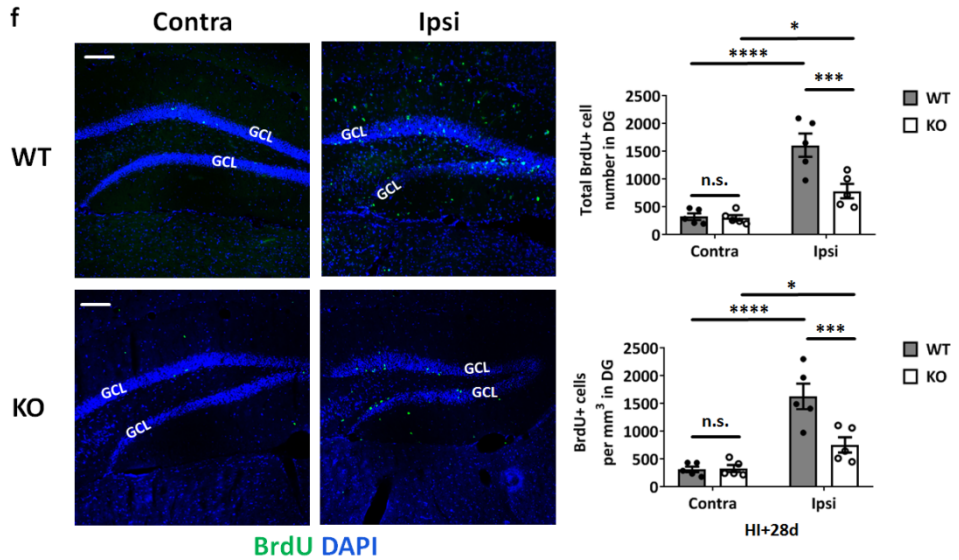

Supplementary Figure 2 (continued)

Supplementary Figure 2 HI injury caused tissue damage and activated cell proliferation in both RBM3 WT and KO mice.

a. Representative cresyl violet staining of adult RBM3 WT or KO brains after HI injury plus 7 days recovery. Scale bar: 1 mm. The infarction volumes were estimated as described in Methods. Two-tailed t-test was used for statistical analysis (ten animals per group, n=10); * $p<0.05$. **b.** High magnification of the SVZ and DG regions from **(a)**. Scale bar: 500 μm. The SVZ volumes and DG volumes were calculated as described in Methods. Repeated measures two-way ANOVA was used for statistical analysis (ten animals per group, n=10); n.s. not significant. **c-d.** Representative BrdU and DAPI staining in SVZ **(c)** and DG **(d)** of RBM3 WT and KO animals treated with HI and recovered for 7 days with BrdU injection every other day. Animals in control group received sham surgery. Total BrdU+ cell number and density in the SVZ and DG were estimated. Five sham animals and six HI animals were counted per group (Sham: n=5, HI: n=6). Sham: sham group; contra: contralateral (uninjured side) in HI group; ipsi: ipsilateral (injured side) in HI group. Scale bar: 100 μm. LV: lateral ventricle; cc: corpus callosum; GCL: granular cell layer. Repeated measures two-way ANOVA was used for statistical analysis; n.s. not significant; * $p<0.05$; *** $p<0.001$; **** $p<0.0001$. **e-f.** Representative BrdU and DAPI staining in SVZ **(e)** and DG **(f)** of RBM3 WT and KO animals treated with HI and recovered for 28 days with BrdU injection every other day in the first 7 days. Total BrdU+ cell number and density in the SVZ and DG were estimated. Five animals were counted per group (n=5). Contra: contralateral (uninjured side); ipsi: ipsilateral (injured side). Scale bar: 100 μm. LV: lateral ventricle; cc: corpus callosum; GCL: granular cell layer. Repeated measures two-way ANOVA was used for statistical analysis; n.s. not significant; * $p<0.05$; ** $p<0.01$; *** $p<0.001$; **** $p<0.0001$. All data are presented in SEM.

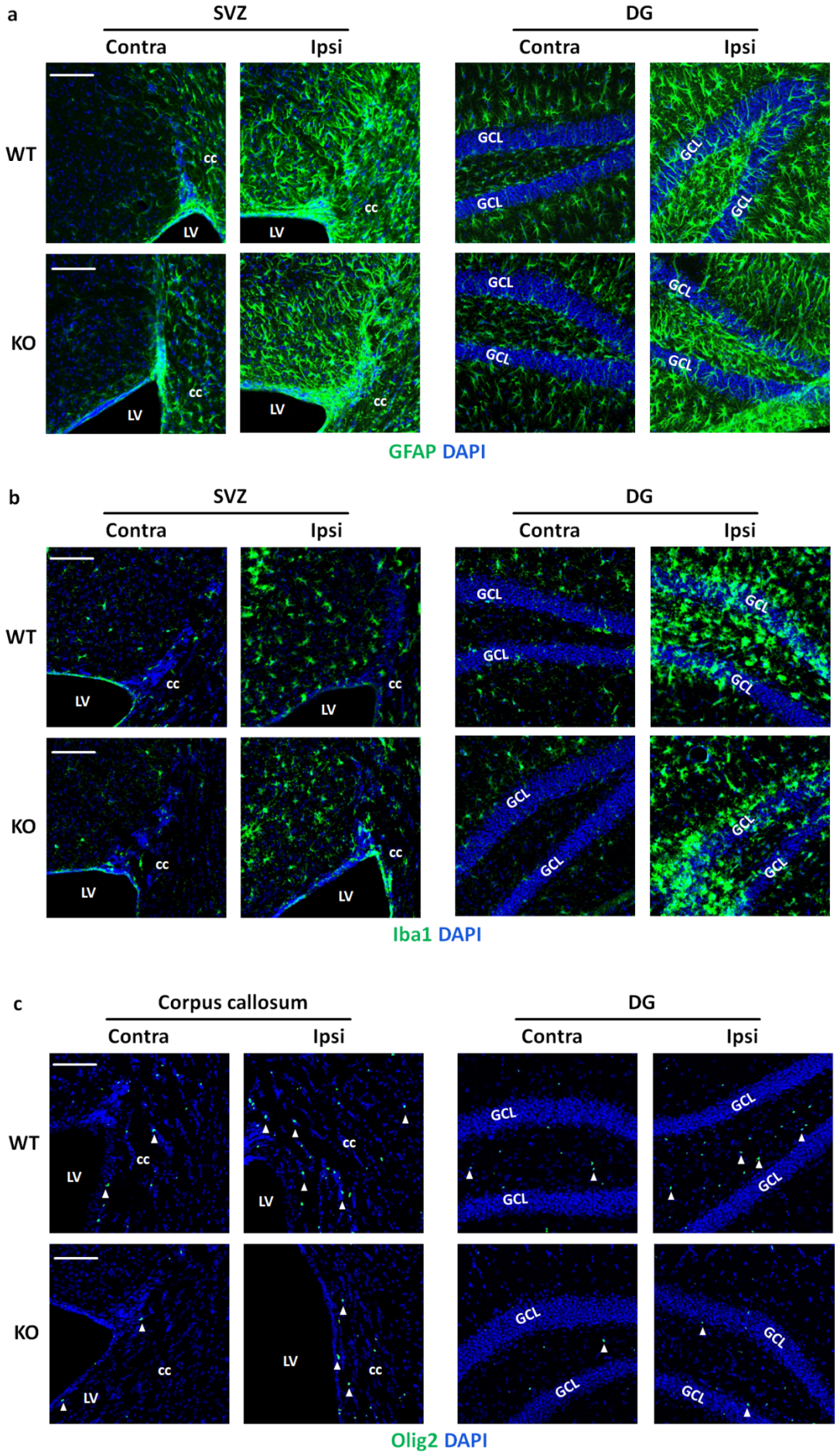

Supplementary Figure 3 (to be continued)

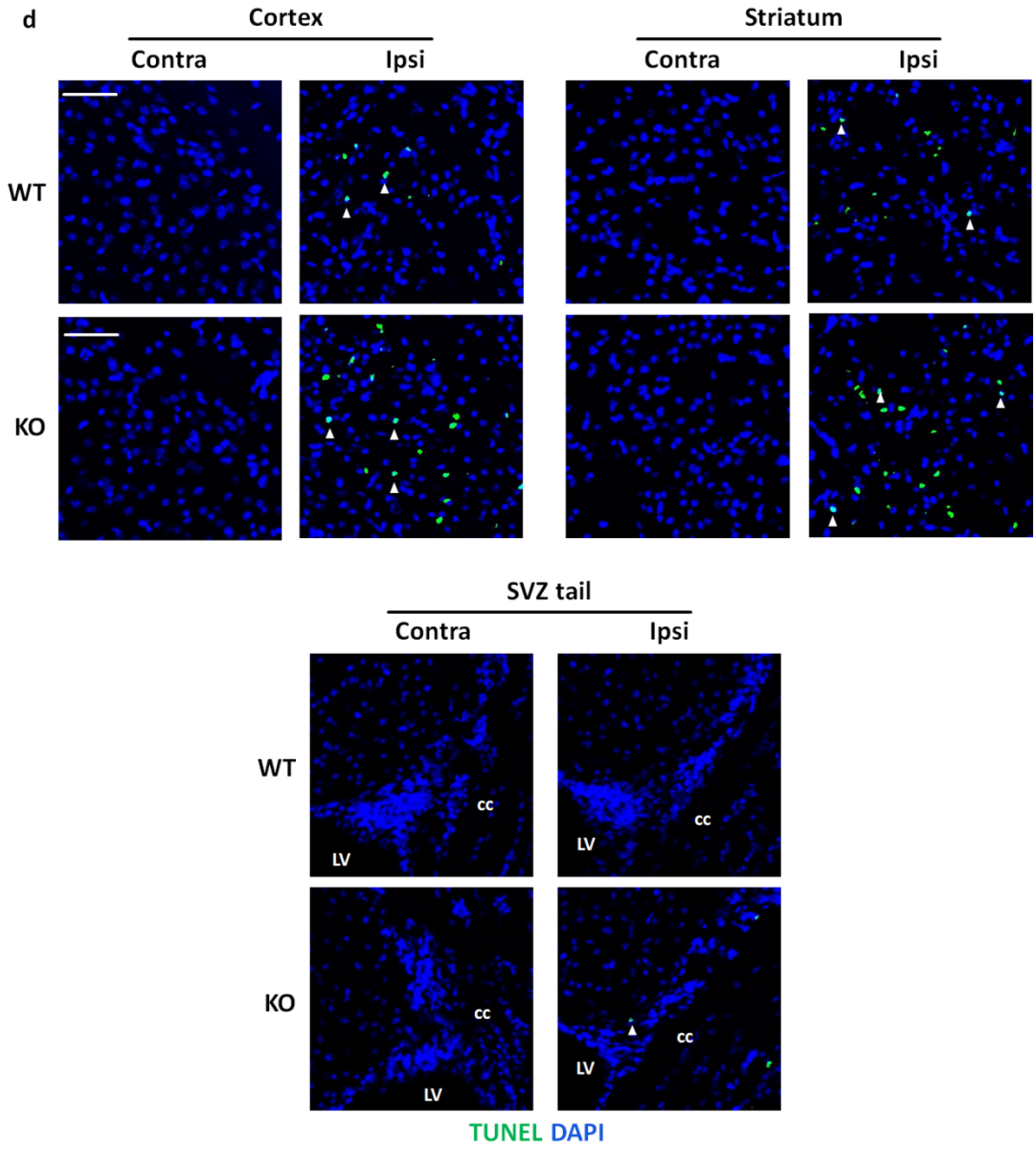

Supplementary Figure 3 (continued)

Supplementary Figure 3 HI injury caused glia cell stimulation and apoptosis in both RBM3 WT and KO mice.

a-c. Representative immunofluorescent staining of reactive astrocytes (GFAP+) **(a)**, microglia (Iba1+) **(b)** and oligodendrocyte precursors (Olig2+) **(c)** in the SVZ (corpus callosum for Olig2+) and DG as well as adjacent regions of RBM3 WT and KO animals treated with HI and recovered for 7 days. For each section, both contralateral and ipsilateral images were acquired under the same setting parameters of exposure period and gain value. Scale bar: 100 µm. LV: lateral ventricle; cc: corpus callosum; GCL: granular cell layer. **d.** Representative immunofluorescent TUNEL staining in the ischemic cores in the ipsilateral (Ipsi) side of cerebral cortex, striatum and SVZ tail of RBM3 WT and KO animals treated with HI and recovered for 7 days. The corresponding contralateral side (Contra) was represented as negative control. LV: lateral ventricle; cc: corpus callosum. Scale bar: 100 µm.

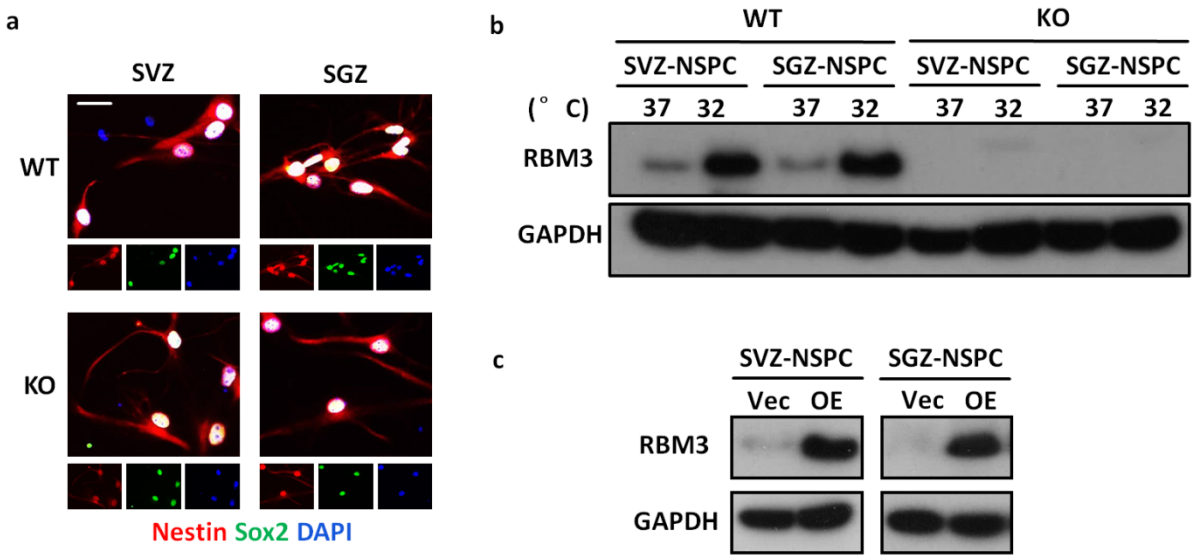

Supplementary Figure 4 RBM3 expression in cultured NSPCs.

a. Representative immunofluorescent staining of nestin and Sox2 in cultured RBM3 WT or KO NSPCs. Nestin (red), Sox2 (green) and DAPI (blue) were merged. Scale bar: 25 μm. **b.** Representative Western blot of RBM3 expression after hypothermic treatment in cultured WT NSPCs. **c.** Representative Western blot of RBM3 expression in WT NSPCs which were transfected with pCEP4 or pCEP4-RBM3 plasmids by electroporation. Vec: empty vector; OE: RBM3 overexpression.

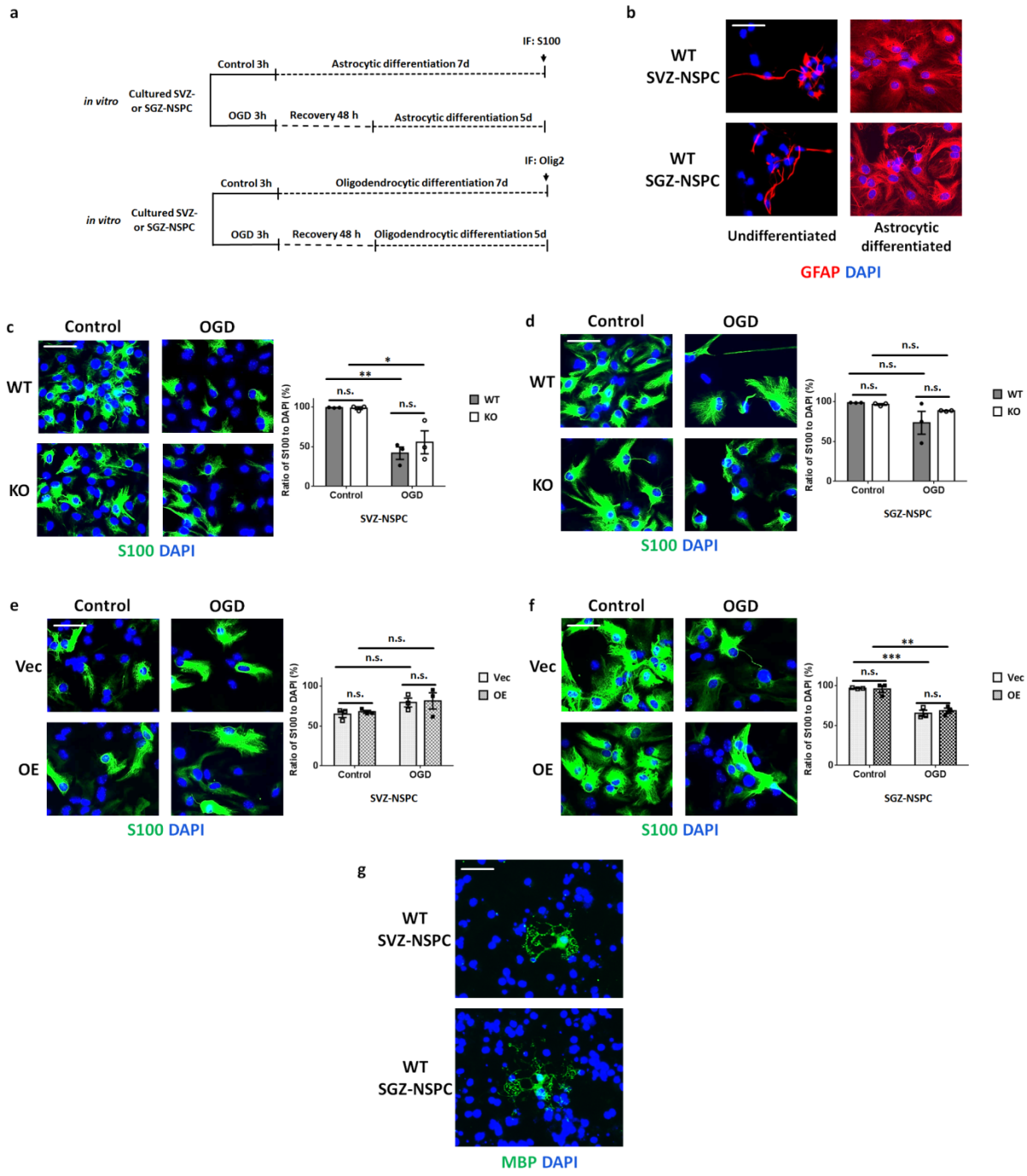

Supplementary Figure 5 (to be continued)

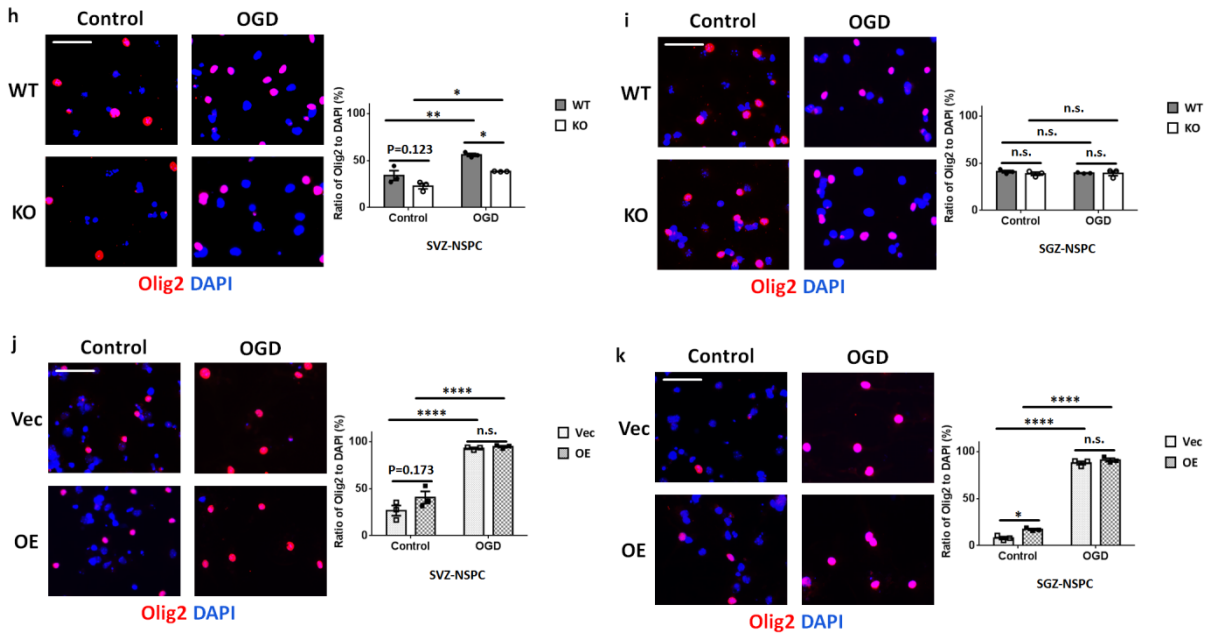

Supplementary Figure 5 (continued)

Supplementary Figure 5 RBM3 did not significantly affect glial differentiation of SVZ-NSPC and SGZ-NSPC *in vitro*.

a. Illustration of *in vitro* glial differentiation assay. NSPCs were cultured in astrocytic or oligodendrocytic differentiation medium for 7 days (control), or first challenged with OGD and then reoxygenated in NSPC complete culture medium for the first 2 days, followed by switching to astrocytic or oligodendrocytic differentiation medium for 5 days (OGD). OGD: oxygen-glucose deprivation; IF: immunofluorescence. **b.** Representative immunostaining of GFAP in undifferentiated or 7-day astrocytic differentiated WT NSPCs derived from SVZ or SGZ. Scale bar: 50 µm. **c-f.** RBM3 WT and KO NSPCs from SVZ **(c)** or SGZ **(d)**, and WT NSPCs transfected with empty vector (Vec) or RBM3 overexpressing vector (OE) with SVZ **(e)** or SGZ **(f)** origins were used in astrocytic differentiation assay. NSPSc were stained with glia cell marker S100 and the ratio of immunoreactive cells to DAPI positive cells were calculated (three independent experiments, n=3). Representative images were presented. Scale bar: 50 µm. Two-way ANOVA was used for statistical analysis. n.s. not significant; * p<0.05; ** p<0.01; *** p<0.001. **g.** Representative immunostaining of oligodendrocyte marker MBP in 7-day oligodendrocytic differentiated WT NSPCs derived from SVZ or SGZ. Scale bar: 50 µm. **h-k** RBM3 WT and KO NSPCs from SVZ **(h)** or SGZ **(i)**, and WT NSPCs transfected with empty vector (Vec) or RBM3 overexpressing vector (OE) with SVZ **(j)** or SGZ **(k)** origins were used in oligodendrocytic differentiation assay. NSPSc were stained with oligodendrocyte precursor cell marker Olig2 and the ratio of immunoreactive cells to DAPI positive cells were calculated (three independent experiments, n=3). Representative images were presented. Scale bar: 50 µm. Two-way ANOVA was used for statistical analysis. n.s. not significant; * p<0.05; ** p<0.01; **** p<0.0001. All data are presented in SEM.

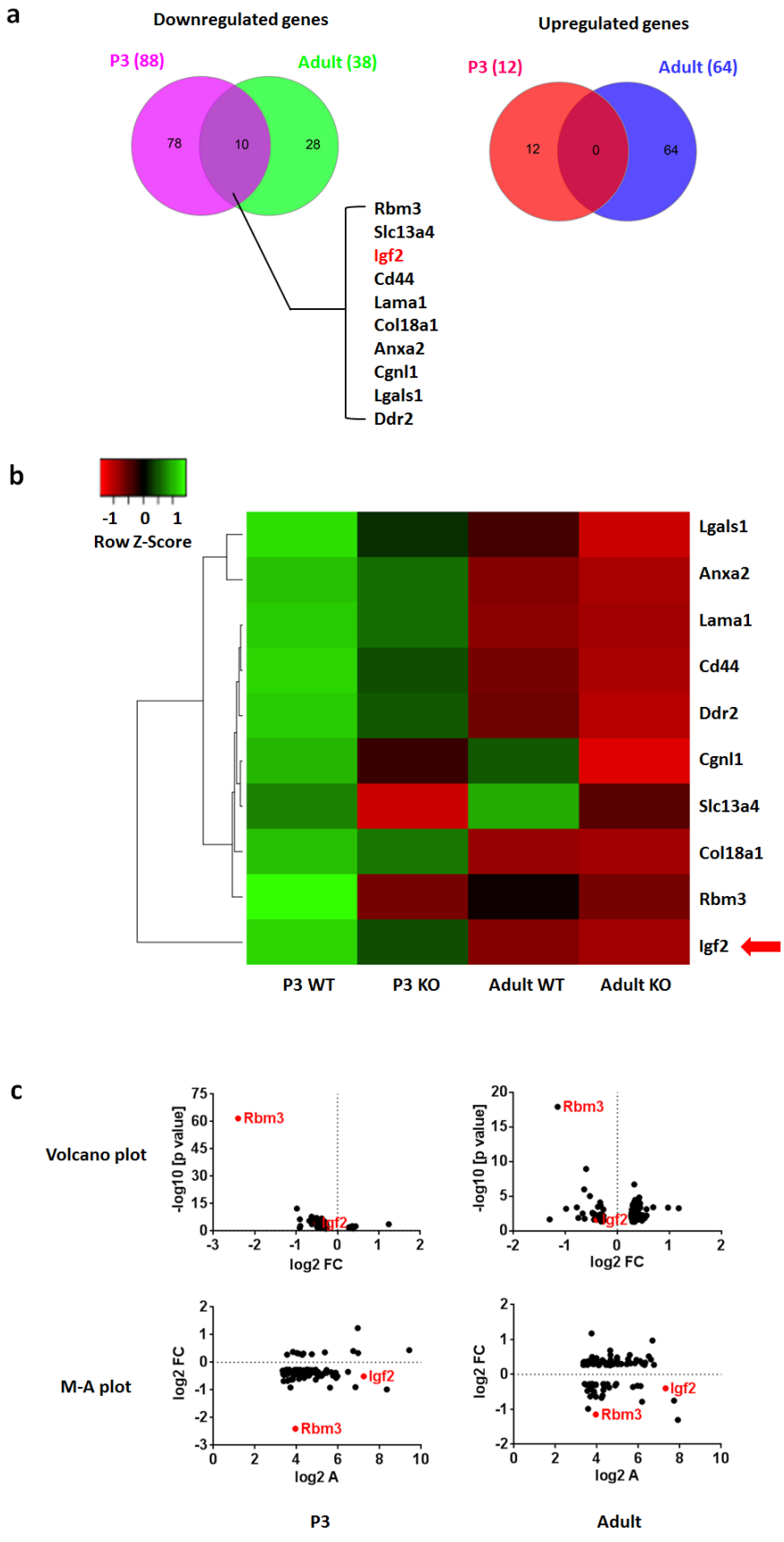

Supplementary Figure 6 (to be continued)

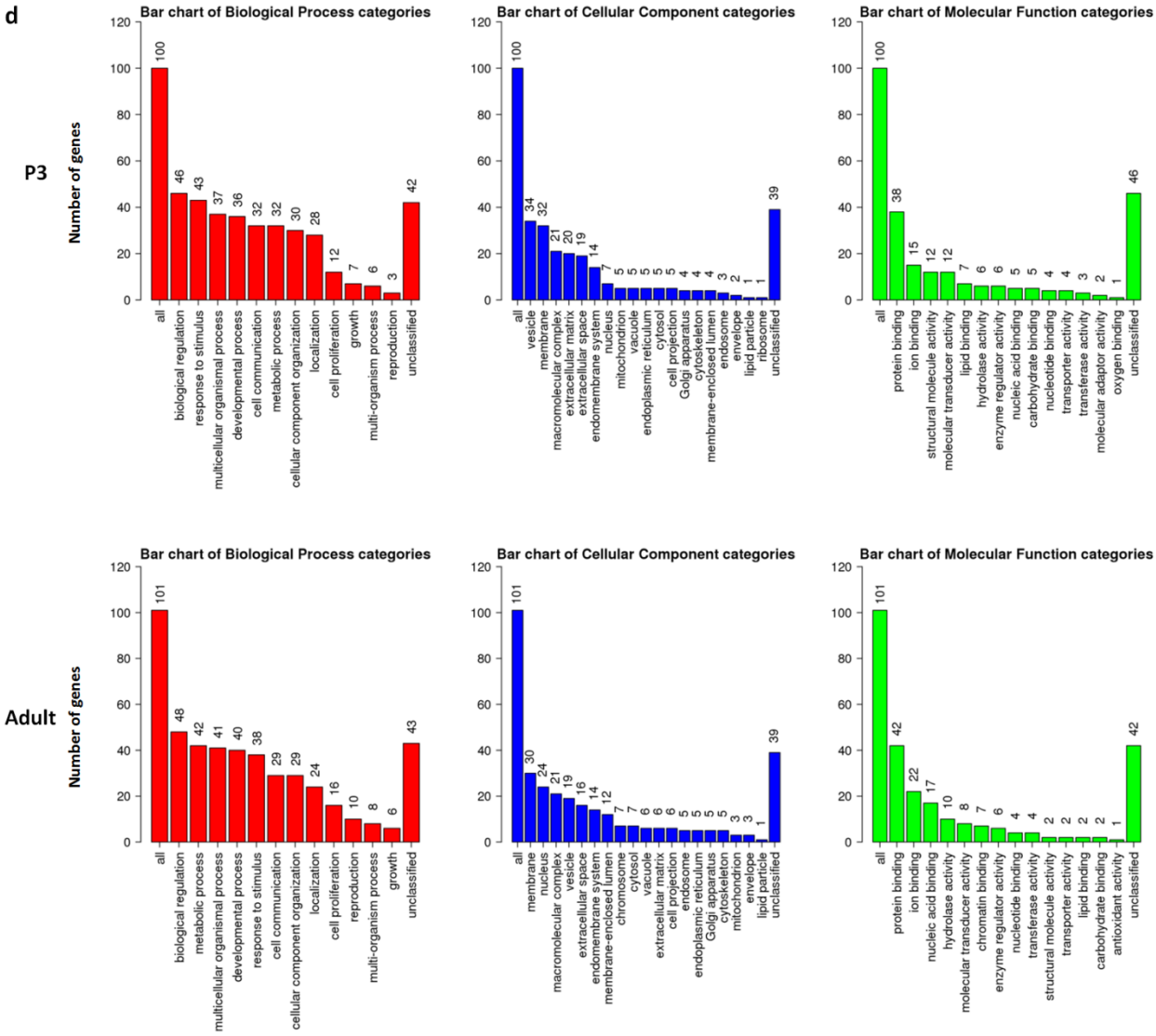

Supplementary Figure 6 (continued)

Supplementary Figure 6 RNA-seq analysis of RBM3 WT or KO hippocampi from postnatal day 3 (P3) or adult mice.

Differentially expressed genes (DEGs) were filtered with the following cutoffs: log2A > 3.32 (Average counts per million > 10); |log2 FC| > 0.26 (|Fold change| > 1.2) and unadjusted P value < 0.05.

a. Venn Diagrams of commonly downregulated or upregulated DEGs from P3 (KO vs WT) and adult (KO vs WT) lists. Ten commonly downregulated genes are listed, and *Igf2* is highlighted. **b.** Heatmap of the ten common DEGs generated by their Reads Per Kilobase Million (RPKM). Clustering distance was measured by Euclidean method. **c.** Volcano plot and M-A plot of all DEGs in P3 and adult samples, respectively. *Rbm3* and *Igf2* were highlighted. FC: fold change; A: average counts per million (average CPM). **d.** Gene set enrichment analysis (GSEA) in the three categories of biological process, cellular components and molecular functions of all DEGs in P3 and adult samples, respectively.

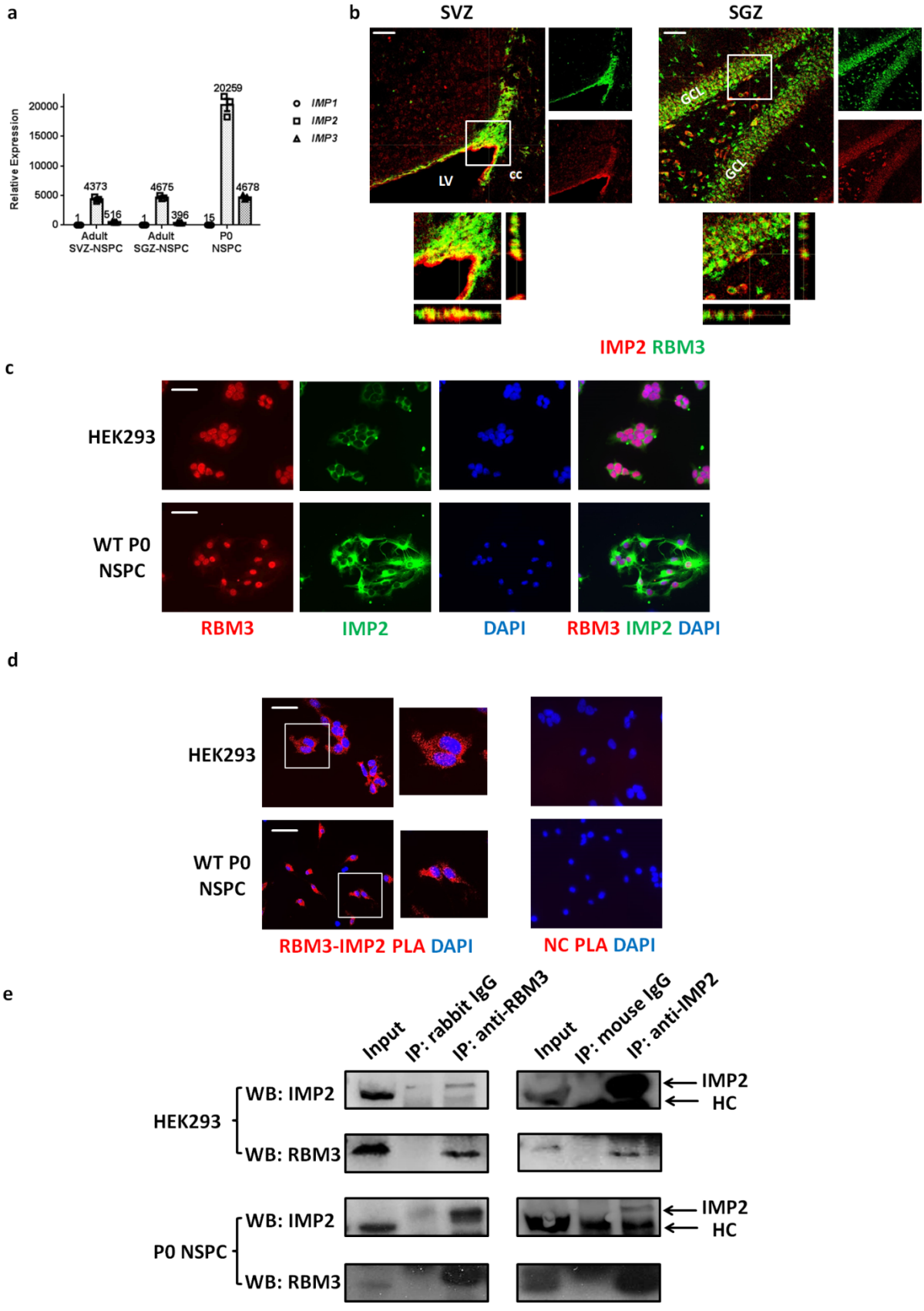

Supplementary Figure 7 (to be continued)

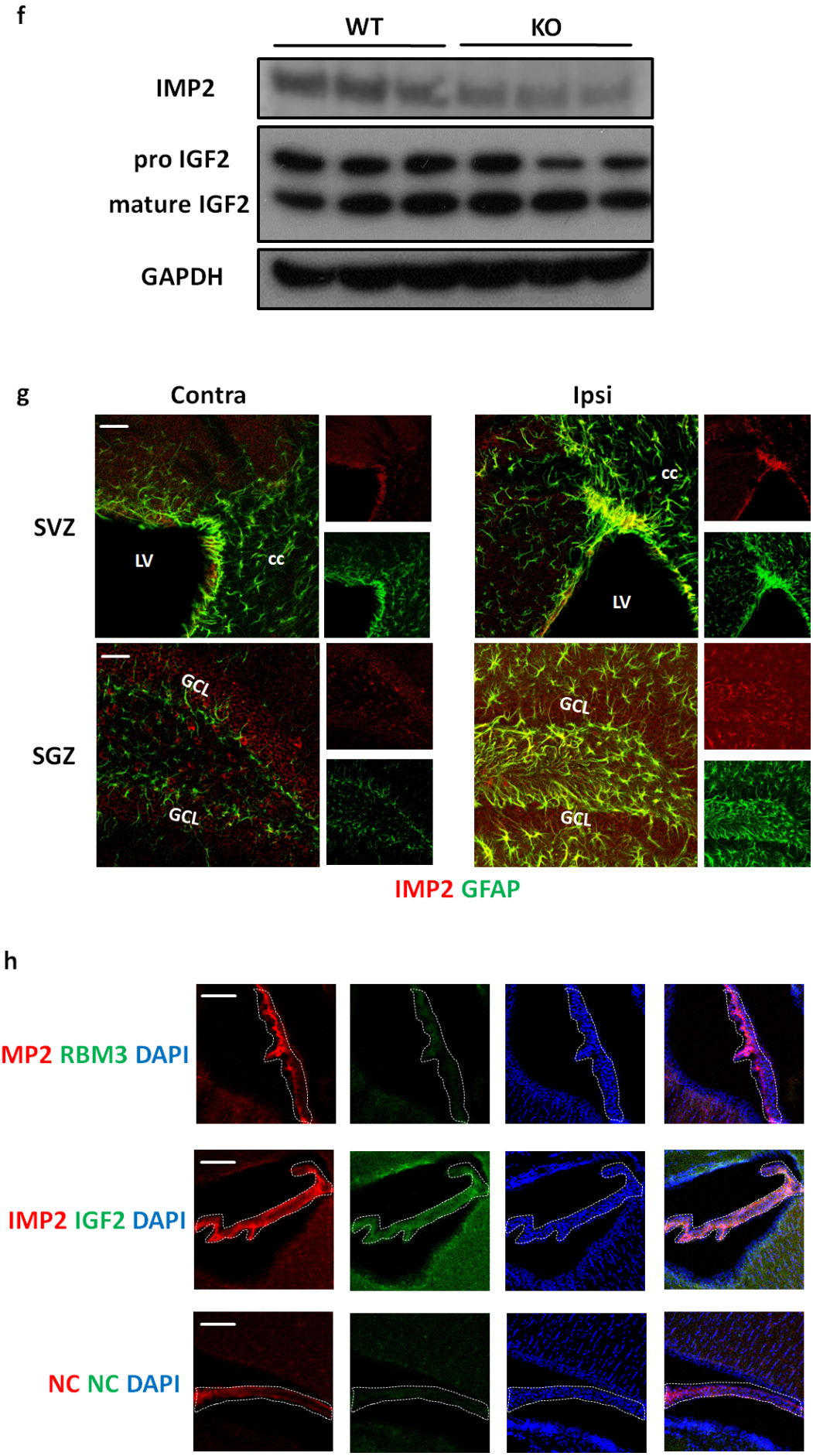

Supplementary Figure 7 (continued)

Supplementary Figure 7 Additional evidences of the involvement of IMP2-IGF2 pathway in RBM3 function on NSPC proliferation.

a. Quantitative RT-PCR of *IMP1*, *IMP2* and *IMP3* mRNA expressions in cultured adult SVZ-NSPC and SGZ-NSPCs. NSPCs from the whole brain of postnatal day 0 (P0) mouse was used as a positive control (three independent experiments, n=3). *IMP1*, *IMP2* and *IMP3* mRNA level was normalized to *GAPDH* by $2^{-\Delta\Delta CT}$ method. Relative amount of mRNA was listed on top of each column. All data are presented in SEM. **b.** Representative immunofluorescent staining of RBM3 and IMP2 in the SVZ and DG of adult WT mouse brain. Orthogonal view confirmed the co-localization of RBM3 and IMP2. Scale bar: 50 μm. LV: lateral ventricle; cc: corpus callosum; GCL: granular cell layer. **c.** Immunofluorescent co-staining of RBM3 and IMP2 in HEK 293 and WT P0 NSPC. Scale bar: 25 μm. **d.** Proximity ligation assay of endogenous RBM3 and IMP2 in HEK 293 and WT P0 NSPC. NC: negative control omitting both primary antibodies. Scale bar: 25 μm. **e.** CoIP of endogenous RBM3 and IMP2 in HEK293 and P0 NSPC. Rabbit polyclonal RBM3 antibody and mouse monoclonal IMP2 antibody were used for immunoprecipitation, respectively. Rabbit IgG was used as negative control for RBM3 antibody, mouse IgG was used as negative control for IMP2 antibody. HC: heavy chain of IgG used for immunoprecipitation. **f.** Western blot of IMP2 and IGF2 expression in whole brain lysate from adult WT or KO mice without treatment (three animals per group, n=3). Dual bands were observed for IGF2 at around 20kDa and 10kDa, indicating pro IGF2 and mature IGF2, respectively. **g.** Representative immunofluorescent staining of IMP2 and GFAP in the SVZ and DG of adult WT mice after HI injury plus 7 days recovery. LV: lateral ventricle; cc: corpus callosum; GCL: granular cell layer. Contra: contralateral (uninjured side); ipsi: ipsilateral (injured side). Scale bar: 50 μm. **h.** RBM3, IMP2 and IGF2 expressions in the choroid plexus of adult WT mice. NC: Negative control with secondary antibodies only but without primary antibody. Scale bar: 100 μm.

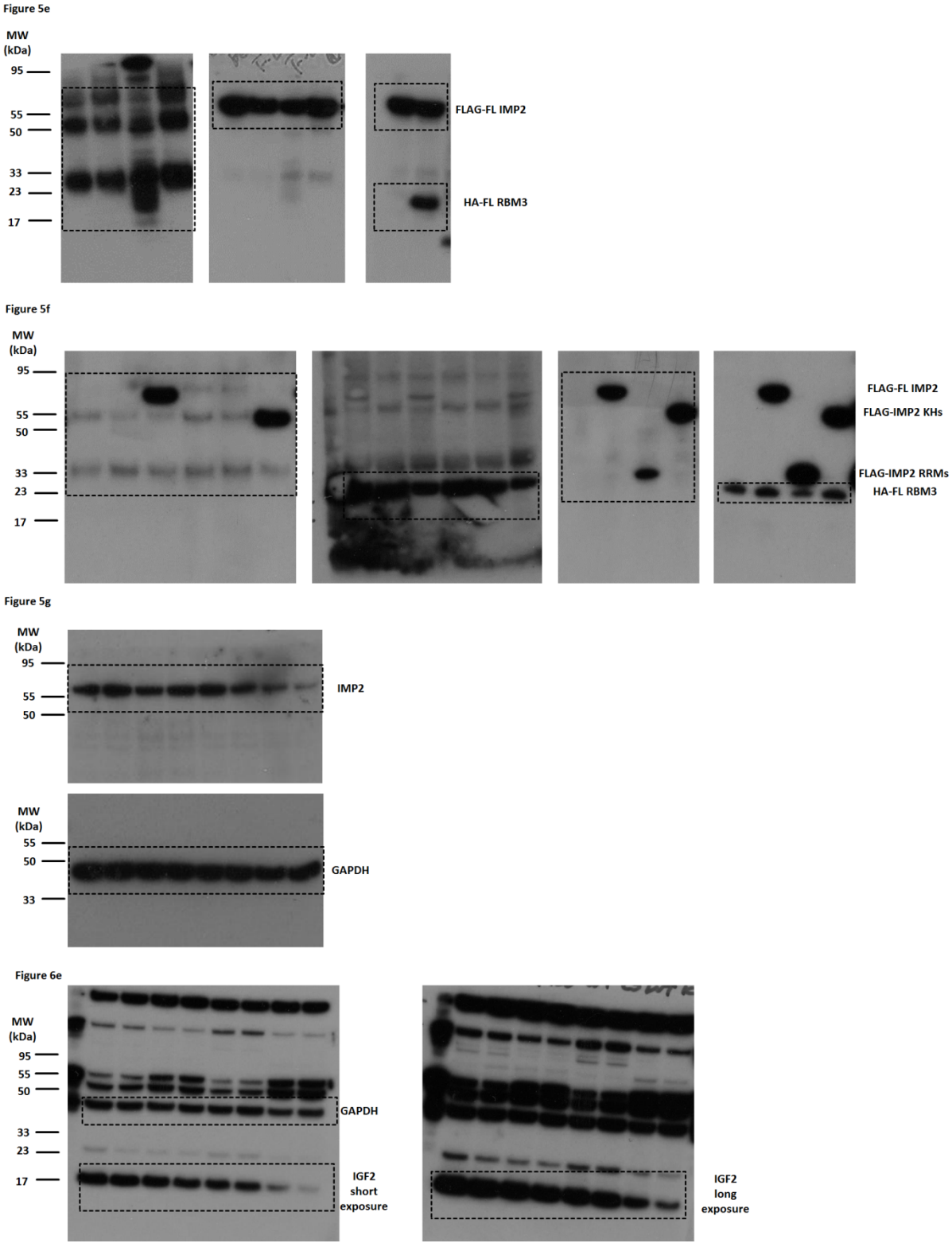

Supplementary Figure 8 (to be continued)

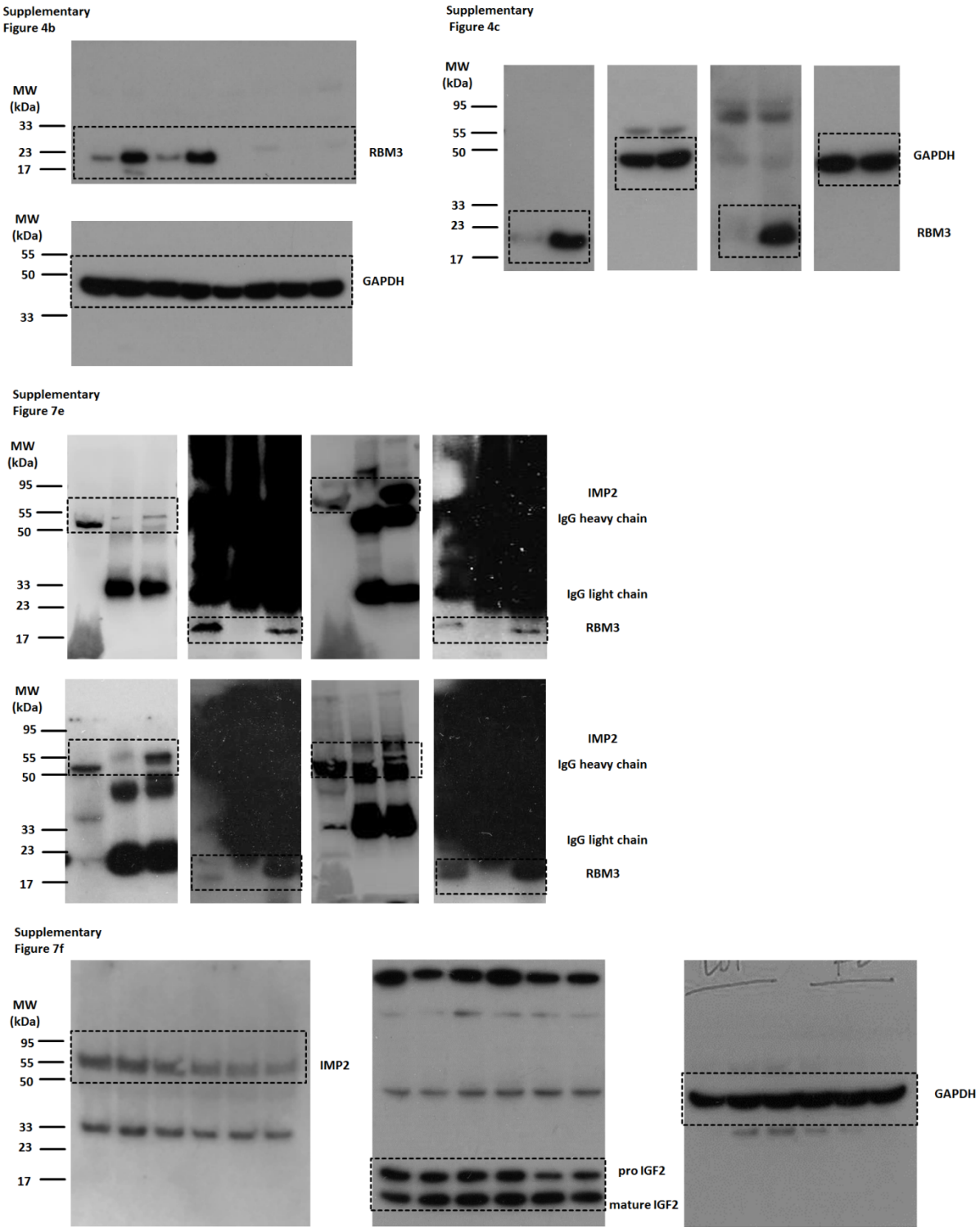

Supplementary Figure 8 (continued)

Supplementary Figure 8 Uncropped Western blot images.

Description of Additional Supplementary Files

File Name: Supplementary Data 1
Description: Summary of RNA quality and total reads number

File Name: Supplementary Data 2
Description: Differentially expressed genes (DEGs) in RBM3 KO hippocampi from postnatal day 3 (P3) mice compared to WT, ranked by fold change. The cutoff settings were described in the table, and a full list without cutoffs was also provided.

File Name: Supplementary Data 3
Description: Differentially expressed genes (DEGs) in RBM3 KO hippocampi from adult mice compared to WT, ranked by fold change. The cutoff settings were described in the table, and a full list without cutoffs was also provided.

File Name: Supplementary Data 4
Description: Information for primary antibodies and primers

(available at: https://www.nature.com/articles/s41467-019-11870-x#data-availability)

2.2 Research Article II

The RNA-Binding Protein RBM3 Promotes Neural Stem Cell Proliferation Under Hypoxia

Jingyi Yan [1#], Tessa Goerne[1#], Andrea Zelmer[1], Raphael Guzman[2], Josef P. Kapfhammer[2], Sven Wellmann[1,3,] *, Xinzhou Zhu[1,] *

1. University Children's Hospital Basel (UKBB), University of Basel, Basel, 4056 Switzerland
2. Department of Biomedicine, University of Basel, Basel, 4056 Switzerland
3. University Children's Hospital Regensburg (KUNO), University of Regensburg, Regensburg, 93053 Germany

* Corresponding author.

# Contributed equally.

Front. Cell Dev. Biol., 21 November 2019

https://doi.org/10.3389/fcell.2019.00288

Contribution statement: I performed most of the experiments and analyzed the data.

frontiers in Cell and Developmental Biology

ORIGINAL RESEARCH
published: 21 November 2019
doi: 10.3389/fcell.2019.00288

The RNA-Binding Protein RBM3 Promotes Neural Stem Cell (NSC) Proliferation Under Hypoxia

Jingyi Yan[1†], Tessa Goerne[1†], Andrea Zelmer[1], Raphael Guzman[2], Josef P. Kapfhammer[2], Sven Wellmann[1,3] and Xinzhou Zhu[1*]*

[1] Department of Neonatology, University Children's Hospital Basel (UKBB), Basel, Switzerland, [2] Department of Biomedicine, University of Basel, Basel, Switzerland, [3] Department of Neonatology, University Children's Hospital Regensburg (KUNO), Regensburg, Germany

OPEN ACCESS

Edited by:
Daniele Bottai,
University of Milan, Italy

Reviewed by:
Xinyu Zhao,
University of Wisconsin–Madison, United States
Juan Andres Rubiolo,
University of Santiago de Compostela, Spain
Ola Hermanson,
Karolinska Institutet (KI), Sweden

***Correspondence:**
Sven Wellmann
sven.wellmann@ukbb.ch
Xinzhou Zhu
xinzhou.zhu@unibas.ch

[†]These authors share first authorship

Specialty section:
This article was submitted to Stem Cell Research, a section of the journal Frontiers in Cell and Developmental Biology

Received: 21 June 2019
Accepted: 04 November 2019
Published: 21 November 2019

Citation:
Yan J, Goerne T, Zelmer A, Guzman R, Kapfhammer JP, Wellmann S and Zhu X (2019) The RNA-Binding Protein RBM3 Promotes Neural Stem Cell (NSC) Proliferation Under Hypoxia. Front. Cell Dev. Biol. 7:288. doi: 10.3389/fcell.2019.00288

Neural stem cells (NSCs) reside physiologically in a hypoxic niche to maintain self-renewal and multipotency. Whereas mild hypoxia is known to promote NSC proliferation, severe hypoxia in pathological conditions exerts the reverse effect. The multi-functional RNA-binding protein RBM3 is abundant in NSCs and can be regulated by hypoxic exposure. Although RBM3 has been shown to accelerate cell growth in many cell types, whether and how it affects NSC proliferation in hypoxic environment remains largely unknown. In this study, we tested how RBM3 regulates cell proliferation under hypoxia in C17.2 mouse NSC cell line and in primary mouse NSCs from both the forebrain of postnatal day 0 (P0) mice and the subgranular zone (SGZ) of adult mice. Our results demonstrated that RBM3 expression was highly sensitive to hypoxia, and NSCs were arrested in G0/G1 phase by 5, 2.5, and 1% O_2 treatment. When we overexpressed RBM3, hypoxia-induced cell cycle arrest in G0/G1 phase was relieved and more cell transit into S phase was observed. Furthermore, cell viability under hypoxia was also increased by RBM3. In contrast, in RBM3-depleted primary NSCs, less BrdU-incorporated cells were detected, indicating exacerbated cell cycle arrest in G1 to S phase transition. Instead, overexpressed RBM3 significantly increased proliferation ratio in primary NSCs. Our findings indicate RBM3 as a potential target to maintain the proliferation capacity of NSCs under hypoxia, which can be important in NSC-based therapies of acute brain injury and chronic neurodegenerative diseases.

Keywords: RBM3, CIRP, oxygen, neural stem cell, cell cycle

INTRODUCTION

Physiological oxygen levels in organisms are considerably lower than ambient oxygen tension (21%) and vary widely in different tissues to adapt oxygen consumption requirements of diverse cell types (Panchision, 2009; De Filippis and Delia, 2011). Neural stem cells (NSCs) are the main sources to generate neuronal and glial cells of the central nervous system during embryonic and postnatal development and are maintained in specific regions during adulthood for consistent neurogenesis (Gage and Temple, 2013; Bond et al., 2015). They also contribute to neuro-regeneration after acute injuries in the brain or spinal cord (Gage and Temple, 2013; Ludwig et al., 2018). Neurogenic niches, which are the microenvironment for NSC self-renewal and differentiation, contain a relatively wide range of oxygen tension from <1 to 8% (Mohyeldin et al., 2010). The heterogeneity of oxygen

tension exerts opposite functions on NSC proliferation. While mild hypoxia substantially promotes NSC proliferation, severe hypoxia suppresses their growth and maintains them in quiescent status (Santilli et al., 2010; Felfly et al., 2011). Furthermore, different severity of hypoxia can also have opposite effects on NSC differentiation and neurogenesis (Francis and Wei, 2010; De Filippis and Delia, 2011; Vieira et al., 2011). Therefore, the precise control of hypoxic environment is critical for the maintenance of NSC quiescence/activation status and NSC amount in the pool, as well as for the regulation of their differentiation upon diverse demands.

The appropriate oxygen concentration can be different for *in vivo* animal studies and for *in vitro* cell models when investigating NSCs. Traditionally, 21% O_2 is used as the standard laboratory oxygen supply concentration for cell culture (including NSC culture) *in vitro*, but some researchers questioned whether 21% O_2 results in a relatively hyperoxic environment and may change the physiological characters of NSCs (Clarke and Van Der Kooy, 2009; Yuan et al., 2015; Mas-Bargues et al., 2019). Atmospheric oxygen tension *in vitro* may lead to a shift of NSC proliferation pattern. Therefore, lower oxygen level can be superior for NSC culture *in vitro*, when intending to mimic *in vivo* NSC characters. Instead, 8% O_2 is considered as physiological oxygen tension in neurogenic niche, 2.5% O_2 is considered as moderate hypoxia, and 1% O_2 is considered as severe hypoxia (Panchision, 2009; De Filippis and Delia, 2011).

The multi-functional RNA-binding protein RBM3 is typically inducible by cold exposure (Danno et al., 2000; Zhu et al., 2016). Besides cold stress, RBM3 responds to hypoxia as well (Wellmann et al., 2004). During development, RBM3 expression is abundant in neurogenic niches and co-localizes with NSC marker nestin (Pilotte et al., 2009). RBM3 has been recently reported to promote neurogenesis via Yap during embryonic stage (Xia et al., 2018). Other studies also suggest that RBM3 plays an important role in the proliferation of cancer cells, fibroblasts, and HEK293 cells (Sureban et al., 2008; Wellmann et al., 2010; Matsuda et al., 2011; Chen et al., 2019). Besides, in recent years, a series of studies have demonstrated that RBM3 can promote the survival of neuroblastoma cells, which are widely used to replace NSCs in neuronal differentiation assays *in vitro*, upon diverse stressful treatments (Yang et al., 2017; Zhuang et al., 2017; Ushio and Eto, 2018). However, it remains unclear how RBM3 regulates NSC proliferation under hypoxic conditions.

In this study, we investigated whether RBM3 expression is affected under hypoxic conditions and elucidated the role of RBM3 in the regulation of cell cycle in mouse NSC cell line and primary murine NSCs exposed to hypoxia.

MATERIALS AND METHODS

Animals

The research protocol, approved by the Cantonal Veterinary Office of Basel, was conducted according to the Ethical Principles and Guidelines for Experiments on Animals of the Swiss Academy of Medical Sciences and the Swiss Academy of Sciences. RBM3 wild type (WT) and knockout (KO) mice with C57BL/6 background were generated by Prof. Tadatsugu Taniguchi (University of Tokyo, Japan) (Matsuda et al., 2011) and were kindly provided by his group. Since *RBM3* is X-chromosome gene, only male mice were used in this study.

Cell Isolation and Culture

Primary NSCs were isolated from the whole brain excluding cerebellum of postnatal day 0 (P0) mice or from the subgranular zone (SGZ) of 2-month-old adult mice as described previously (Zhu et al., 2019). Briefly, the forebrains from P0 mice or the dentate gyrus from adult mice were dissociated with papain (Worthington) and DNase I (Sigma) and then undissociated cell clusters were removed by a cell strainer (Sigma). Dissociated cells were cultured in serum-free DMEM-F12 (Gibco) supplemented with B27 supplement (Gibco), 2 mM L-glutamine (Gibco), 20 ng/ml EGF (PeproTech), and 20 ng/ml FGF2 (PeproTech). After glial cells and neurons died, primary NSCs were maintained as neurospheres in uncoated dishes.

C17.2 mouse NSC line was purchased from Sigma and cultured in DMEM (Gibco) supplemented with 10% FBS (Gibco) and 2 mM L-glutamine (Gibco).

Plasmid Transient Transfection

pCEP4 mammalian expression vector was purchased from ThermoFisher Scientific. *rbm3* gene was cloned into pCEP4 vector in our previous work for exogenous overexpression (Chip et al., 2011). The empty vector or RBM3-overexpressing vector was transiently transfected into C17.2 cells by electroporation with Cell Line Nucleofector Kit V (Lonza) using the Nucleofector I device (Lonza). For transfections in primary NSCs, cells were first dissociated from neurospheres to single cells by Trypsin (Sigma) and then transfected with DNA vectors using the Mouse Neural Stem Cell Nucleofector Kit (Lonza) and the Nucleofector I device (Lonza).

Hypoxia Exposure

Before hypoxic treatment, primary NSCs in the form of neurospheres were dissociated into single cells by Trypsin (Sigma) and seeded into poly-L-lysine pre-coated 16-well chamber slides (Labtek) at a density of 1×10^4/well as monolayer culture in ambient normoxic condition (21% O_2). For transfected primary NSCs, additional overnight recovery in uncoated 12-well plate was required before seeding to chamber slides. After 24 h (for non-transfected NSCs) or 48 h (for transfected NSCs) growth, 20 μM BrdU was added into the medium and the slides were transferred to a hypoxic incubator (MiniGalaxy A, RS Biotech) with indicated oxygen levels. Slides in an ambient normoxic incubator served as a control group.

Non-transfected and transfected C17.2 cells were seeded either in six-well plates or in 15-cm-diameter dishes, and transferred to a hypoxic incubator with indicated oxygen levels. Plates or dishes in ambient normoxic incubator served as a control group.

RNA Isolation and Real-Time PCR

Total RNA were purified from 2×10^5 cultured cells by the ReliaPrep RNA Cell Miniprep System (Promega). cDNA was

synthesized from 1 μg total RNA using the GoScript Reverse Transcription System (Promega). Real-time PCR was performed in 15 μl volume with the GoTaq qPCR System (Promega) on the CFX Connect Real-Time PCR Detection System (Bio-Rad). The PCR cycle was run as follows: pre-denaturation by 95°C for 5 min, and then 95°C for 15 s and 60°C for 1 min for 40 cycles. To calculate relative gene expression, the $2^{-\Delta\Delta CT}$ method was used. Primer sequences for real-time PCR are listed below. To correct for differences in both RNA quality and quantity between samples as well as changes in oxygen exposure, six housekeeping genes were used, namely, beta-actin (*actb*), glyceraldehyde 3-phosphate dehydrogenase (*gapdh*), ribosomal protein L13a (*rpl13a*), 45S pre-ribosomal RNA (*rn45s*), 28S ribosomal RNA (*rn28s1*), and alpha-tubulin-1 (*tuba1*):

Mouse-*rbm3*-forward: 5′ CTT CAG CAG CTT TGG GCC TA 3′
Mouse-*rbm3*-reverse: 5′ CCC ATC CAG GGA CTC TCC AT 3′
Mouse-*cirp*-forward: 5′ CCA AGT ATG GGC AGA TCT CCG A 3′
Mouse-*cirp*-reverse: 5′ CTG CCG CCC GTC CAC AGA CT 3′
Mouse-*kdm3a*-forward: 5′ GAG CTG TTT CCC ACA CCG A 3′
Mouse- *kdm3a* -reverse: 5′ TGC TTT TCT CTG AAG GCT 3′
Mouse-*actb*-forward: 5′ GGC CAA CCG TGA AAA GAT GA 3′
Mouse-*actb*-reverse: 5′ CAC AGC CTG GAT GGC TAC GT 3′
Mouse-*gapdh*-forward: 5′ AAC GAC CCC TTC ATT GAC 3′
Mouse-*gapdh*-reverse: 5′ TCC ACG ACA TAC TCA GCA C 3′
Mouse-*rpl13a*-forward: 5′ GCG GAT GAA TAC CAA CCC 3′
Mouse-*rpl13a*-reverse: 5′ GTA GGC TTC AGC CGA ACA AC 3′
Mouse-*rn45s*-forward: 5′ GTA ACC CGT TGA ACC CCA TT 3′
Mouse-*rn45s*-reverse: 5′ CCA TCC AAT CGG TAG TAG CG 3′
Mouse-rn*28s1*-forward: 5′ TTG AAA ATC CGG GGG AGA G 3′
Mouse-*rn28s1*-reverse: 5′ ACA TTG TTC CAA CAT GCC AG 3′
Mouse-*tuba1*-forward: 5′ ACA GGA TTC GCA AGC TGG C 3′
Mouse-*tuba1*-reverse: 5′ CCA AGA AGC CCT GGA GAC C 3′

Protein Isolation and Western Blot

Total proteins were extracted from cultured cells or homogenized mouse brain with lysis buffer (1% Triton X-100, 50 mM Tris, 150 mM NaCl, 1 × Roche Protease Inhibitor Cocktail, pH 8.0). Total protein concentrations in cleared cell lysates were determined with RC DC Protein Assay (Bio-Rad). Lysates were loaded onto Mini-Protean TGX pre-cast gels (Bio-Rad) and transferred to PVDF membranes (Amersham/GE Healthcare Life Sciences). Membranes were incubated with primary antibodies overnight at 4°C and then with HRP-linked secondary antibodies for 1 h at room temperature (RT).

Primary and secondary antibodies:

Anti-mouse RBM3 (Proteintech, 14363-1-AP): rabbit polyclonal, 1:1000 diluted
Anti-mouse CIRP (Proteintech, 10209-1-AP): rabbit polyclonal, 1:1000 diluted
Anti-mouse GAPDH (Abeam, ab8245): mouse monoclonal, 1:2000 diluted
HRP-linked anti-rabbit secondary antibody (Cell Signaling Technology, 7074S): 1:5000 diluted
HRP-linked anti-mouse secondary antibody (Cell Signaling Technology, 7076S): 1:5000 diluted.

Band relative quantification was performed by Image J (NIH). Each band was outlined and the mean grayscale value was measured. Background intensity was subtracted from the measured values. The ratios of target proteins (RBM3 and CIRP) and loading control (GAPDH) were calculated.

Flow Cytometry

Flow cytometry analysis was performed with C17.2 cells on FACSCANTO II device (BD Biosciences). After hypoxic treatment, cells were fixed with ethanol for viability and cell cycle analysis. Cell viability was measured with 1×10^6 cells using LIVE/DEAD Viability/Cytotoxicity Kit (ThermoFisher Scientific). For cell cycle analysis, 1×10^6 cells were analyzed with propidium iodide (Sigma).

Immunofluorescent Staining

After hypoxic treatment, cells in chamber slides were fixed 4% paraformaldehyde for 10 min at RT. For BrdU staining, fixed cells were treated 2 M HCl for 30 min and neutralized with 0.1 M sodium borate (pH 8.5) for 10 min before blocking. For permeabilization and blocking, cells were treated with 0.5% Triton X-100 and 5% normal goat serum in phosphate buffer for 1 h at RT. Cells were incubated with primary antibodies overnight at 4°C and then with Alexa Fluor dye-conjugated secondary antibodies for 2 h at RT. Nuclei were counterstained with DAPI for 15 min at RT. Images were acquired with an Olympus AX-70 fluorescent microscope equipped with a Spot Insight digital camera. For cell quantification, images of five random fields in each experiment were captured under 20 × magnifications, and the total numbers of BrdU + and DAPI + cells in each image were counted. The average percentage of BrdU + /DAPI + cells from five images was used to represent the value of one experiment. Three independent experiments were performed.

Primary antibodies:

Anti-Nestin (Novus, NBP1-02419), rabbit polyclonal, 1:200 diluted
Anti-Sox2 (R&D, MAB2018), mouse monoclonal, 1:250 diluted

Anti-Dcx (Millipore, AB2253), guinea pig polyclonal, 1:1000 diluted
Anti-Tuj1 (Tubulin III) (Millipore, AB1637), mouse monoclonal, 1:250 diluted
Anti-BrdU (Abcam, ab6326), rat monoclonal, 1:250 diluted.

Statistical Analysis

All experiments were repeated three times independently. Quantification data are presented in standard error of the mean (SEM). Statistical analysis was performed by GraphPad Prism 8.0. To compare two groups with a single factor, unpaired *t* test was used. To compare more than two groups with a single factor, statistical significance was determined by one-way ANOVA followed by Dunnett's multiple comparison. To compare two groups and two factors, statistical significance was determined by two-way ANOVA followed by Tukey's multiple comparison. *p* value less than 0.05 was reported as significant difference. N.S., not significant; $^{*}p < 0.05$; $^{**}p < 0.01$.

RESULTS

RBM3 Expression Is Sensitively Inhibited by Hypoxia in NSC

C17.2 mouse NSC line was used for this study, as it harbors NSC properties and is widely investigated with hypoxic treatments (Felfly et al., 2011; Wang et al., 2014; Zhang et al., 2017). We first confirmed the NSC property of C17.2 cells by immunostaining with specific markers. C17.2 cells express NSC marker nestin and sex determining region Y-box 2 (Sox2), but not neuroblast marker doublecortin (Dcx) and neuronal marker neuron-specific Class III β-tubulin (Tuj1) (**Figure 1A**), indicating their properties as undifferentiated NSCs.

To test how different oxygen levels influenced RBM3 expression, we exposed C17.2 cells to ambient normoxia (21% O_2), very mild hypoxia (18 and 16% O_2), mild hypoxia (12 and 8% O_2), moderate hypoxia (5 and 2.5% O_2), and severe hypoxia (1% O_2). Beta-actin gene (*actb*) was selected as reference gene for real-time PCR, as it showed the highest stability under hypoxic conditions among six commonly used housekeeping genes (**Supplementary Table S1**). The mRNA level of *rbm3* was remarkably suppressed even under very mild hypoxic condition, and remained suppressed with mild, moderate, and severe hypoxia (**Figure 1B**). Notably, at 2.5% O_2, *rbm3* expression was recovered to some extent, but remained lower than ambient normoxic condition (**Figure 1B**). *kdm3a*, a well-characterized hypoxia-inducible gene, was used as positive control (Wellmann et al., 2008), and its expression was upregulated by moderate to severe hypoxia (**Figure 1D**). At 2.5% O_2 level, *kdm3a* expression reached the peak (**Figure 1D**). Interestingly, the only known vertebrate homolog of RBM3, cold inducible RNA-binding protein (CIRP) (Zhu et al., 2016), showed a similar reduction of mRNA as *rbm3* under hypoxic conditions, but not as sensitive as *rbm3* at 18% O_2 level (**Figure 1C**). Consistently, RBM3 and CIRP protein expressions were also downregulated by 2.5% hypoxia (**Figures 1E,F**). In general, our results show that RBM3 expression is extremely sensitive to hypoxic exposure in C17.2 mouse NSC line.

Moderate to Severe Hypoxia Inhibits C17.2 Cell Proliferation

In general, NSCs are exposed to moderate hypoxia physiologically and to severe hypoxia pathologically *in vivo* (De Filippis and Delia, 2011). Here, we evaluated how different degrees of moderate to severe hypoxia influenced the cell cycle of C17.2 cells. Cells were treated with 21, 5, 2.5, and 1% O_2 for 24 h, and then stained with propidium iodide and analyzed for cell cycle change by flow cytometry. We observed that moderate (5 and 2.5% O_2) and severe hypoxia (1% O_2) lead to a remarkable cell cycle arrest, with increased cell number in G0/G1 phase and decreased cell number in S phase (**Figure 2**). Cell numbers in S phase and G2/M phase were reduced in all hypoxic groups (**Figure 2**). In accordance to a previous report, our data supported the idea that severe hypoxia (1% O_2) inhibited cell cycle in C17.2 cells (Zhang et al., 2017). However, with moderate hypoxia (5 and 2.5% O_2), we observed an inhibitory effect as well (**Figure 2**) rather than a stimulating effect on NSC proliferation (Zhang et al., 2017). As moderate hypoxia (2.5% O_2) demonstrated more cell arrest in S phase than 5 and 1% hypoxia (**Figure 2**), and a recovery of expression was observed (**Figure 1B**), in the following RBM3-overexpressing experiments, we selected this oxygen concentration to examine the function of RBM3 on NSC proliferation and survival.

Overexpression of RBM3 Rescues C17.2 Cell From Hypoxia-Induced Cell Cycle Arrest

To explore the role of RBM3 in hypoxia-induced cell cycle arrest, we overexpressed RBM3 in C17.2 cells by transient transfection (**Figure 3A**) before exposing them to moderate hypoxia (2.5% O_2). As RBM3 was found to be cytoprotective (Yang et al., 2017; Zhuang et al., 2017; Ushio and Eto, 2018), we examined the viability of NSCs after moderate hypoxic treatment. Forced RBM3 expression significantly enhanced live cell proportion and reduced dead cell proportion (**Figure 3B**). While cells were arrested in G0/G1 phase after hypoxic treatment, RBM3 overexpression caused the cells to overcome the arrest (**Figure 3C**). These data provide evidence that RBM3 positively regulates NSC growth under moderate hypoxic condition by promoting G1 to S phase transition.

RBM3 Positively Regulates Primary NSC Proliferation Under Hypoxia

To further confirm the role of RBM3, we took advantage of primary NSCs isolated from the forebrain of postnatal day 0 (P0) RBM3 WT and KO mice. Similar to C17.2 cells, both WT and KO NSCs express NSC marker nestin and Sox2, but neither the neuroblast marker Dcx nor the neuronal marker Tuj1 (**Figure 4A**). RBM3 depletion in KO NSCs was confirmed by Western blot (**Figure 4B**). We further treated primary NSCs with ambient normoxia (21% O_2), moderate hypoxia (5 and 2.5% O_2), or severe hypoxia (1% O_2), and labeled cells by BrdU, a

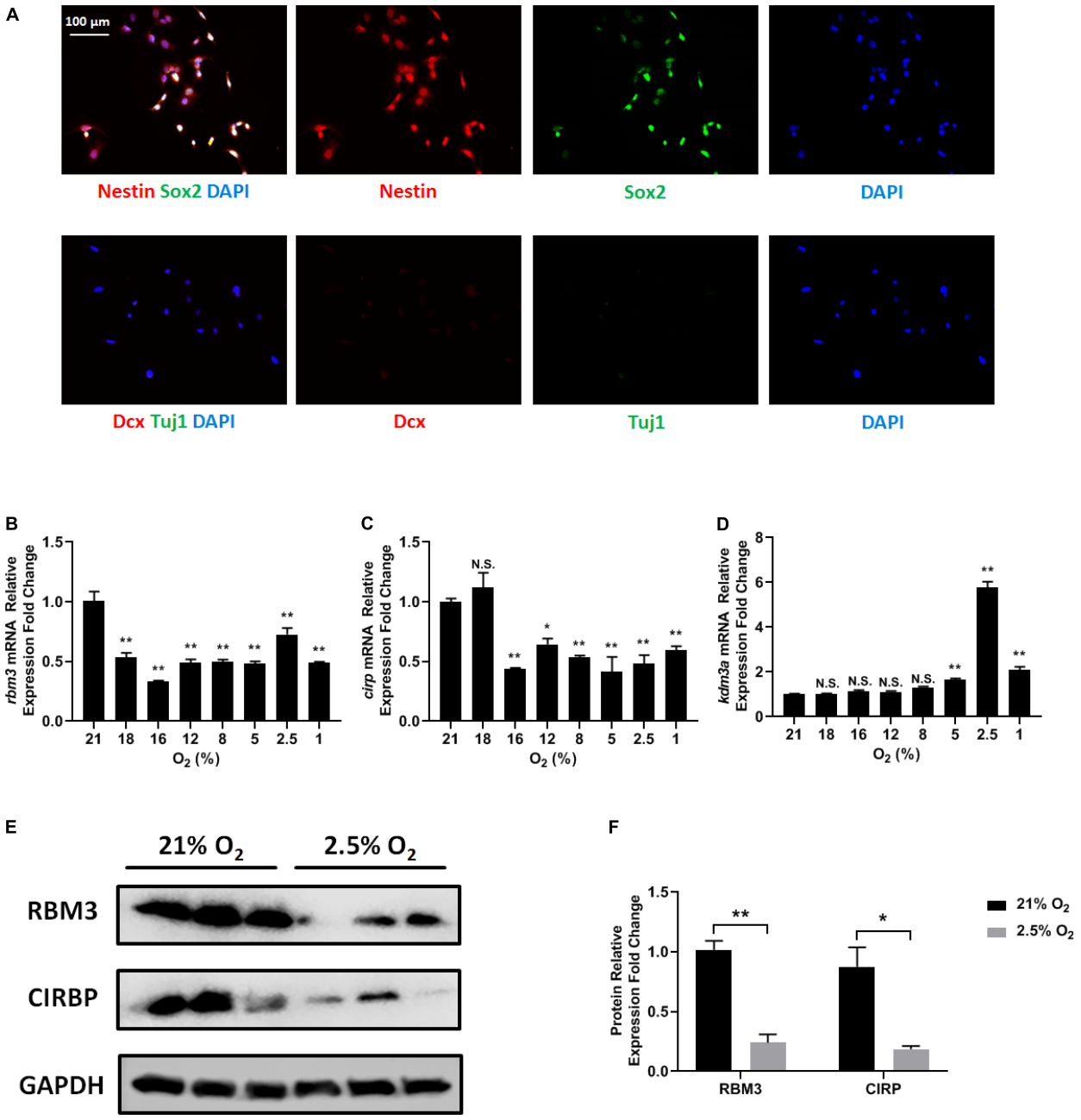

FIGURE 1 | Oxygen-sensitive gene expression in NSCs upon hypoxic exposure. **(A)** Representative Nestin/Sox2 and Dcx/Tuj1 double stainings of C17.2 cells cultured in standard condition with 21% O_2; nuclei were counterstained with DAPI. **(B–D)** mRNA expression of *rbm3* **(B)**, *cirp* **(C)**, and *kdm3a* **(D)** was measured 16 h after ambient normoxic (21% O_2) or indicated hypoxic treatment. *Actb* was used as an internal control. One-way ANOVA followed by Dunnett's test was used to compare each hypoxic condition to the normoxic group. N.S. not significant; $*p < 0.05$; $**p < 0.01$. **(E)** Representative Western blot, RBM3, and CIRP were measured 24 h after ambient normoxic (21% O_2) or moderate hypoxic (2.5% O_2) treatment; GAPDH was used as a loading control. **(F)** Band relative intensity in panel **(E)** was normalized, and unpaired *t* test was used for statistical analysis. N.S., not significant; $*p < 0.05$; $**p < 0.01$.

commonly used proliferation marker for S phase (Lengronne et al., 2001). After 24 h incorporation with BrdU, a significant decrease of proliferation ratio (% of BrdU + /DAPI + cells) from ambient normoxia (21% O_2) to severe hypoxia (1% O_2) was detected, but not from ambient normoxia (21% O_2) to moderate hypoxia (5 and 2.5% O_2) (**Figures 4C,D**), probably due to the robustness of P0 NSCs with high proliferation rate and resistance to hypoxic stress. The proliferation ratio was remarkably downregulated in KO NSCs when comparing to WT NSCs under ambient normoxic condition (21% O_2) or moderate hypoxic conditions (5 and 2.5% O_2), but not significant under severe hypoxic conditions (1% O_2) (**Figures 4C,D**). In addition,

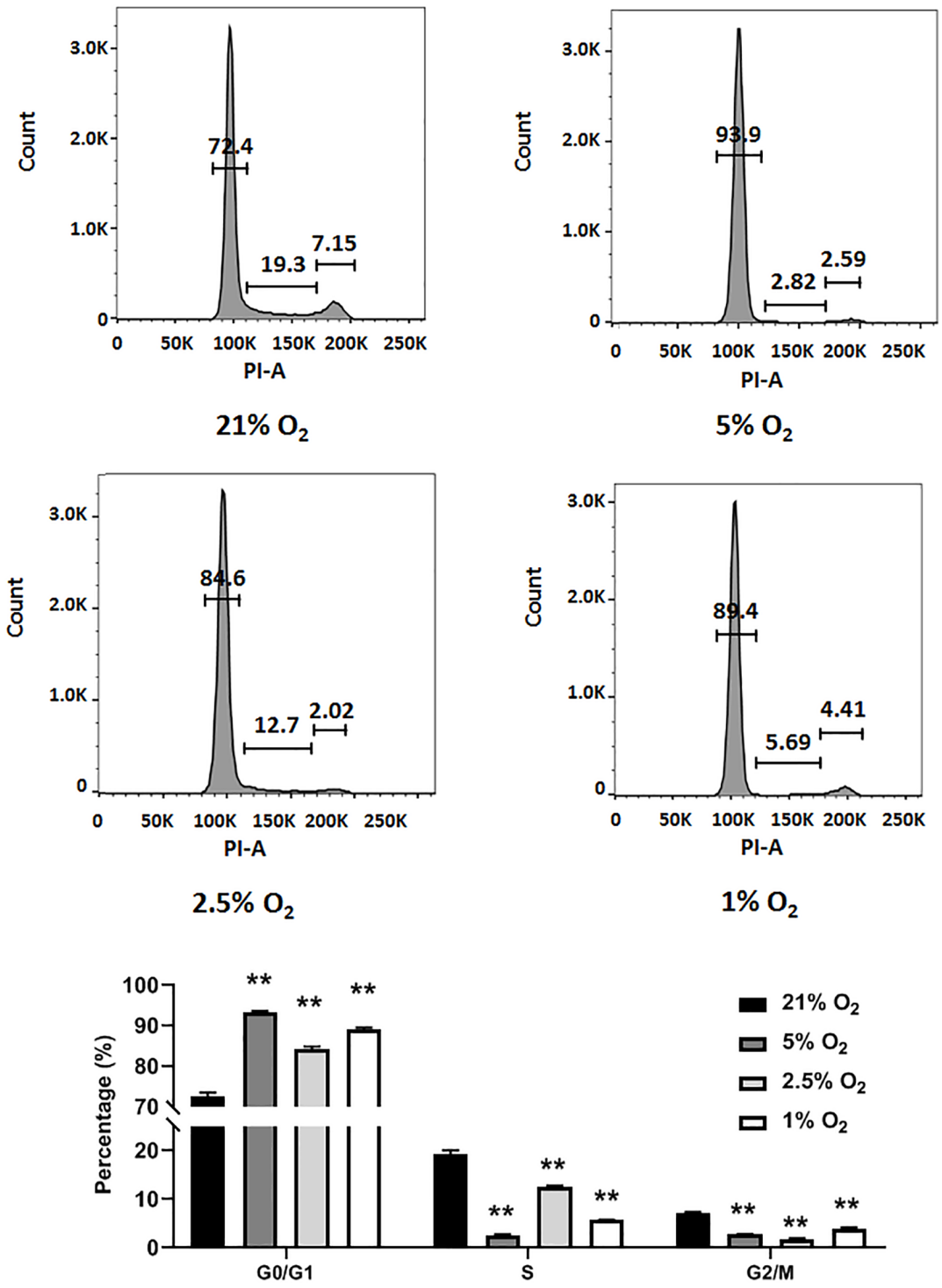

FIGURE 2 | Hypoxia induces cell cycle arrest in NSCs. Cell cycle analysis of C17.2 cells after 24 h 5% O_2, 2.5% O_2, and 1% O_2 hypoxic treatment. Ambient normoxic (21% O_2) was used as control. Representative flow cytometry DNA histogram with propidium iodide (PI) staining. One-way ANOVA followed by Dunnett's test was used for statistical analysis in G0/G1 phase, S phase, and G2/M phase ($n = 3$). N.S., not significant; $^{**}p < 0.01$.

we overexpressed exogenous RBM3 in primary P0 NSCs by electroporation (**Figure 4B**). Electroporation-based transfection significantly reduced proliferation ratio to around 70% under normoxic conditions (21% O_2), while both moderate hypoxia (5 and 2.5% O_2) and severe hypoxia (1% O_2) further inhibited proliferation ratio remarkably (**Figures 4E,F**). In contrast to

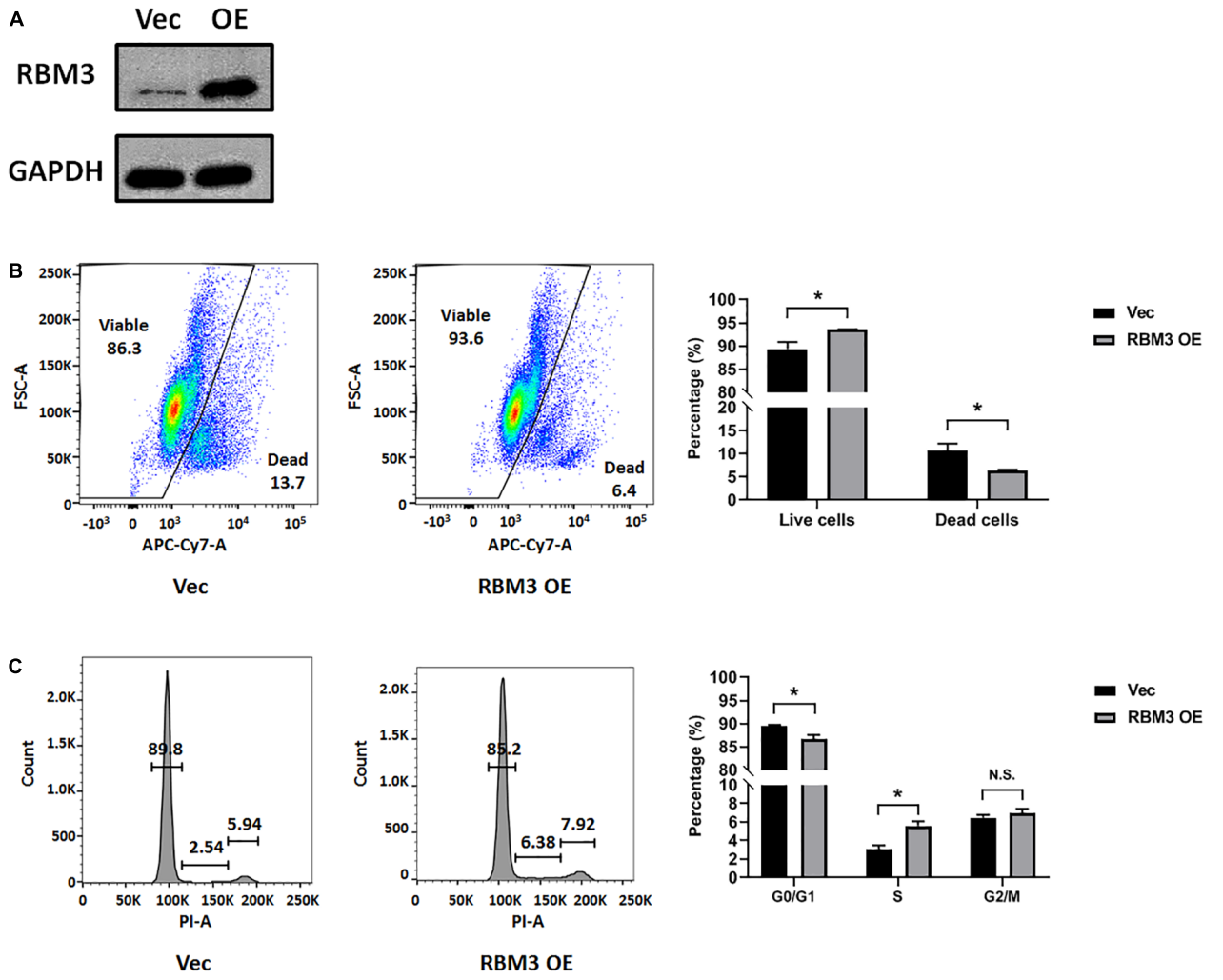

FIGURE 3 | RBM3 overexpression increases NSC viability and proliferation under moderate hypoxia. **(A)** RBM3 protein expression after transient transfection with overexpressing vector. Vec: empty vector; RBM3 OE: RBM3-overexpressing vector. **(B)** Representative flow cytometry dot plots of transfected C17.2 cells with LIVE/DEAD viability staining after 24 h moderate hypoxia (2.5% O_2). Unpaired *t* test was used for statistical analysis ($n = 3$). *$p < 0.05$. **(C)** Representative flow cytometry DNA histogram of transfected C17.2 cells with propidium iodide (PI) staining after 24 h moderate hypoxic (2.5% O_2) treatment. Vec: empty vector; RBM3 OE: RBM3-overexpressing vector. Unpaired *t* test was used for statistical analysis in G0/G1 phase, S phase and G2/M phase ($n = 3$). N.S., not significant; *$p < 0.05$.

depletion, forced RBM3 expression rescued hypoxia-induced proliferation inhibition partially, but did not alter proliferation under normoxia (21% O_2) (**Figures 4E,F**).

To confirm that the effect of RBM3 in NSC proliferation is general, we isolated NSCs from the SGZ of adult mice, one of the two well-characterized neurogenic niches in adults (Fuentealba et al., 2012). We did not use subventricular zone (SVZ)-derived NSCs because our previous study showed that RBM3 plays a less important role in the proliferation of SVZ-NSCs than SGZ-NSCs after hypoxic–ischemic (HI) injury (Zhu et al., 2019). The characters of SGZ-derived NSCs were confirmed by positive staining of nestin/Sox2 and negative staining of Dcx/Tuj1 (**Figure 5A**). We also confirmed RBM3 depletion in KO SGZ-NSCs and RBM3 overexpression in electroporation-transfected WT SGZ-NSCs (**Figure 5B**). We also observed a reduction of proliferation of SGZ-NSC in the absence of RBM3 under hypoxia (**Figures 5C,D**). On the other hand, overexpressed RBM3 elevated SGZ-NSC proliferation ratio under hypoxic conditions (**Figures 5E,F**).

DISCUSSION

In this study, we exposed murine NSCs to various degrees of hypoxia and noticed a remarkable downregulation of RBM3 even at very mild hypoxia (18% O_2) with little further change at lower oxygen levels (**Figure 1B**). The sensitivity of RBM3 expression to hypoxic response is higher than its homolog CIRP (**Figures 1B,C**). Such a high sensitivity of RBM3 has also been reported in response to environmental temperature change, more than CIRP. Even a 1°C change from 37 to 36°C is sufficient to stimulate RBM3 expression in primary

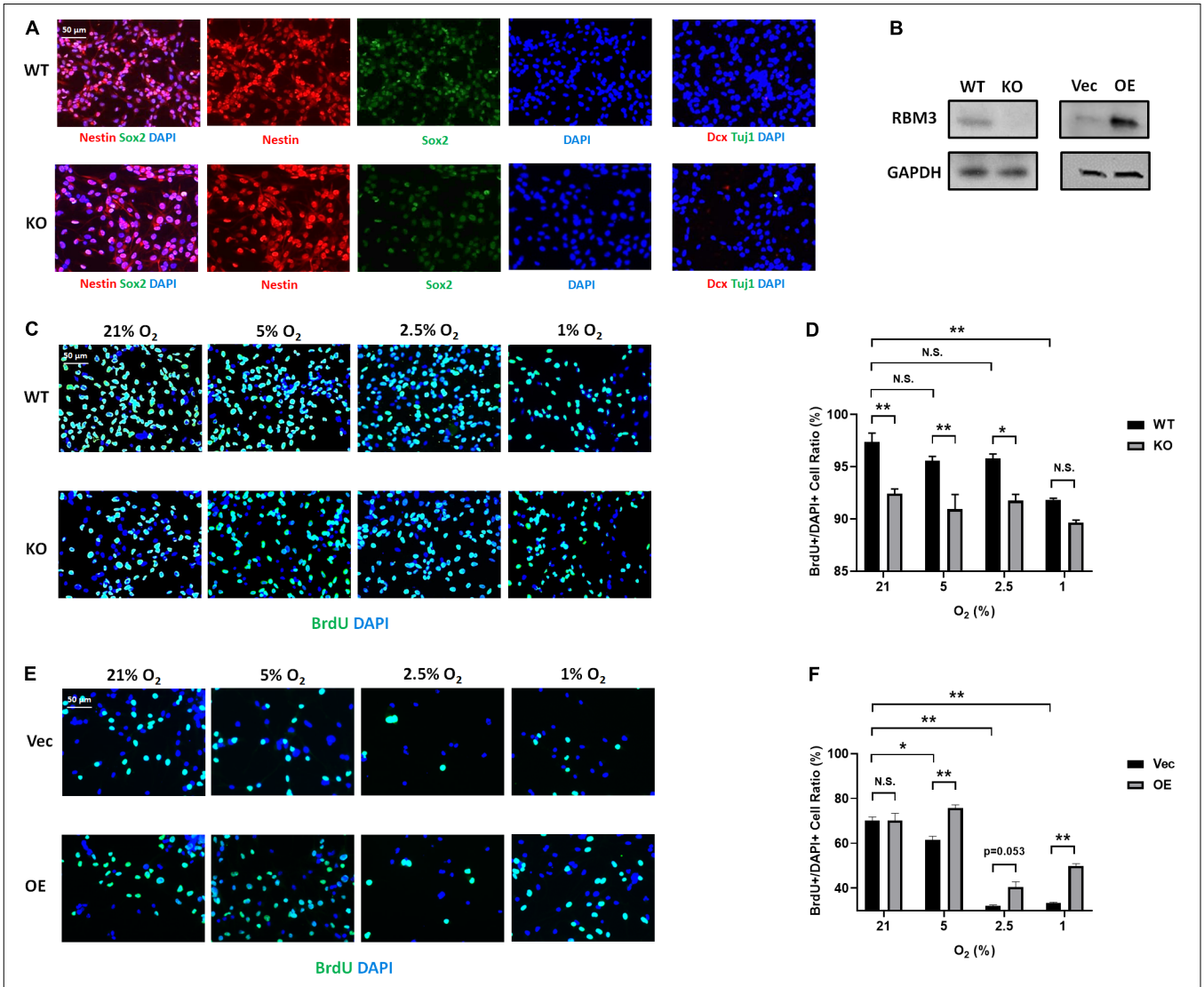

FIGURE 4 | RBM3 positively regulates proliferation in primary NSC from P0 mice under hypoxia. **(A)** Representative Nestin/Sox2 and Dcx/Tuj1 double staining of primary RBM3 WT and KO NSCs from the forebrains of P0 mice. Nuclei were counterstained with DAPI. **(B)** RBM3 protein expression in RBM3 WT and KO primary NSCs, and vector transfected WT NSCs from the forebrains of P0 mice. Vec: empty vector; OE: RBM3-overexpressing vector. **(C)** Representative BrdU and DAPI staining of P0 WT or KO NSCs after 24 h 21, 5, 2.5, or 1% O_2 treatment. **(D)** Two-way ANOVA followed by Tukey's test was used for the comparisons in panel **(C)**. N.S., not significant; $^*p < 0.05$; $^{**}p < 0.01$. **(E)** Representative BrdU and DAPI staining of P0 WT NSCs transfected with empty or RBM3-overexpressing vector after 24 h 21, 5, 2.5, or 1% O_2 treatment. **(F)** Two-way ANOVA followed by Tukey's test was used for the comparisons in panel **(E)**. N.S., not significant; $^*p < 0.05$; $^{**}p < 0.01$.

cortical neurons and astrocytes (Jackson et al., 2015). Regarding hypoxia, CIRP expression was also reported to decrease in moderate (3%) and severe (1%) hypoxic conditions (Zhang et al., 2017). However, RBM3 was previously found to be induced by moderate (5%) and severe (1%) hypoxia in HeLa and Hep3B cancer cells (Wellmann et al., 2004). The discrepancy in different cell types indicates that the subtle regulation patterns of the two cold-inducible RNA-binding proteins RBM3 and CIRP by hypoxia can be cell type specific and may involve different regulatory mechanisms. Indeed, cancer stem cells reside in a more hypoxic niche than NSCs and utilize oxygen in different signaling pathways compared to NSCs, in the maintenance of their stemness (Panchision, 2009; Mohyeldin et al., 2010). Notably, in C17.2 cell line, both RBM3 and CIRP are downregulated under moderate to severe hypoxic conditions (**Figures 1B,C**; Zhang et al., 2017), and both proteins promote G1/S transition in the cell cycle of NSCs upon hypoxic exposure (**Figure 3C**; Zhang et al., 2017), in accordance with their homogeneous structure and functions as reviewed before (Zhu et al., 2016). We additionally demonstrated consistent effects of RBM3 on NSC proliferation in neonatal and adult primary NSCs (**Figures 4**, **5**). Based on these functions, both RBM3 and CIRP are suggested for potential prevention of hypoxia-induced brain injury. However, considering that CIRP is also

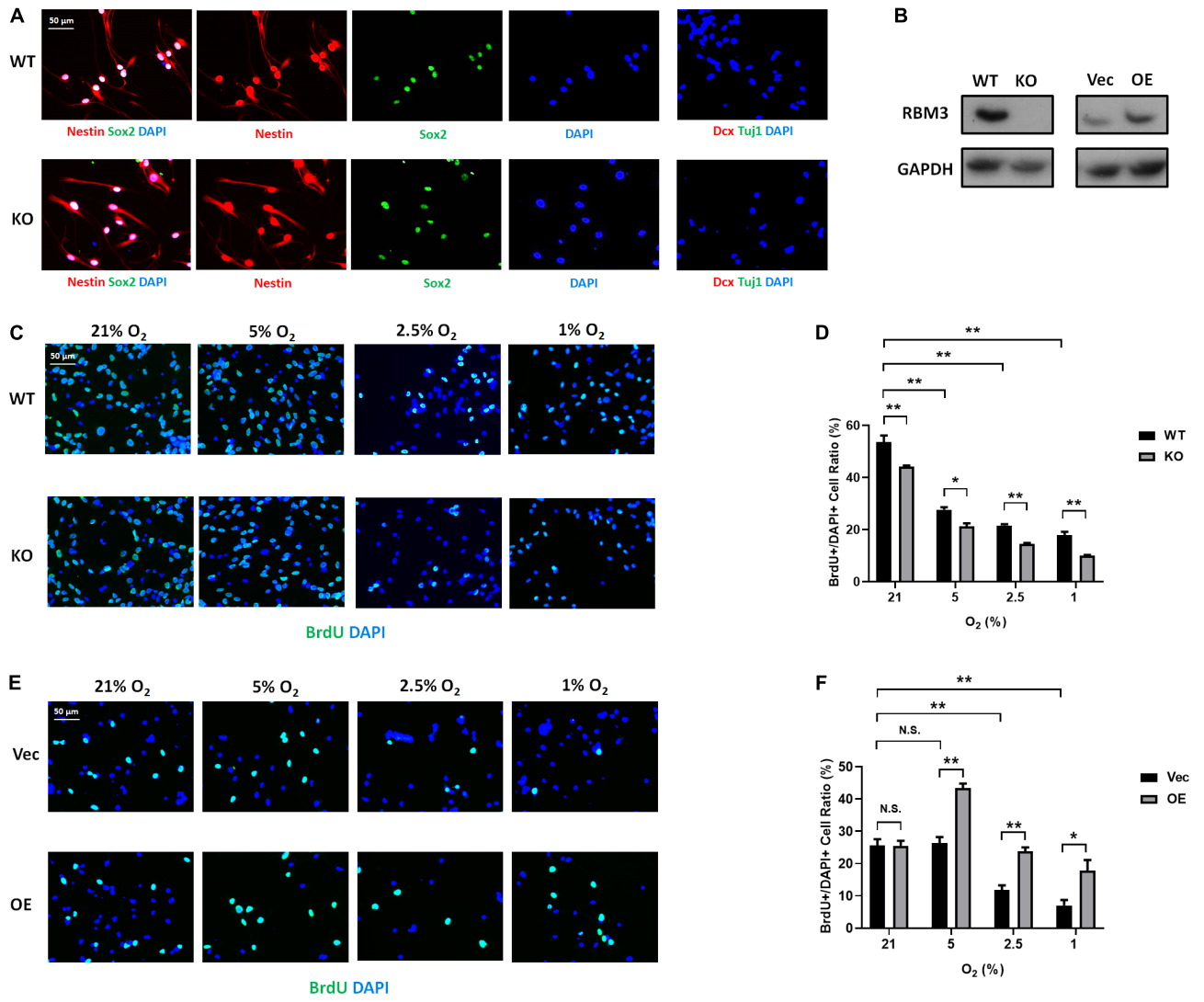

FIGURE 5 | RBM3 positively regulates proliferation in primary NSC from the SGZ of adult mice under hypoxia. **(A)** Representative Nestin/Sox2 and Dcx/Tuj1 double staining of primary RBM3 WT and KO NSCs from the SGZ of adult mice. Nuclei were counterstained with DAPI. **(B)** RBM3 protein expression in RBM3 WT and KO primary NSCs, and vector transfected WT NSCs from the SGZ of adult mice. Vec: empty vector; OE: RBM3-overexpressing vector. **(C)** Representative BrdU and DAPI staining of SGZ-derived adult WT or KO NSCs after 24 h 21, 5, 2.5, or 1% O_2 treatment. **(D)** Two-way ANOVA followed by Tukey's test was used for the comparisons in panel **(C)**. $^*p < 0.05$; $^{**}p < 0.01$. **(E)** Representative BrdU and DAPI staining of SGZ-derived adult WT NSCs transfected with empty or RBM3-overexpressing vector after 24 h 21, 5, 2.5, or 1% O_2 treatment. **(F)** Two-way ANOVA followed by Tukey's test was used for the comparisons in panel **(E)**. N.S., not significant; $^*p < 0.05$; $^{**}p < 0.01$.

involved in mediating neuro-inflammation (Rajayer et al., 2013; Zhou et al., 2014), instead, RBM3 tends to be a safer target in clinical use.

Ischemic stroke and global HI injury are the most common cerebral hypoxic injuries, which induce irreversible damage to the brain from infants to adults (Huang and Castillo, 2008; Ekker et al., 2018). Although NSCs normally reside in hypoxic niche in physiological conditions, they can also migrate to injured regions for neuro-regeneration in these pathological conditions with moderate to severe hypoxia. Our recent study provides evidence that RBM3 behaves as a potential target to maintain NSC pool in HI conditions (Zhu et al., 2019). In addition, as the endogenous migrating NSCs are usually not sufficient to replace lost neurons by neurogenesis, exogenous transplantation of NSC is required for improved recovery not only by cell replacement, but also by multiple by-stand mechanisms (Kalladka and Muir, 2014; Vishwakarma et al., 2014; Huang and Zhang, 2019). When preparing exogenous NSCs *in vitro*, physiologically hypoxic pre-conditioning may benefit to mimic *in vivo* environment (Wakai et al., 2016), but can also produce disadvantageous effects, as hypoxia is a complex process. As the promotion of proliferation is largely mediated by hypoxia-inducible factor-1α (HIF-1α) signaling (Mohyeldin et al., 2010; Li et al., 2014), RBM3 regulation is independent of HIF-1α (Wellmann et al., 2004).

Therefore, manipulating RBM3 expression opens a new avenue to increase viability, proliferation capacity, and multi-potency of cultured NSCs and probably other types of stem cells, which may improve therapeutic effects after transplantation.

DATA AVAILABILITY STATEMENT

All datasets generated for this study are available upon request to the corresponding author.

ETHICS STATEMENT

The animal experiment involved in this study was approved by the Cantonal Veterinary Office of Basel (License Number 2064). All the manipulations were executed according to the Ethical Principles and Guidelines for Experiments on Animals of the Swiss Academy of Medical Sciences and the Swiss Academy of Sciences.

AUTHOR CONTRIBUTIONS

XZ and SW designed the study, interpreted data, and wrote the manuscript. JY and TG performed all experiments in part assisted by AZ. RG and JK were involved in the interpretation and discussion of the results. All authors approved the manuscript.

FUNDING

This study was funded by the Swiss National Science Foundation (SNSF, 31003A_163305) and the China Scholarship Council (CSC, 201606170071).

ACKNOWLEDGMENTS

We sincerely thank Dr. Simone Keck and Janine Boegli (University of Basel, Switzerland) for the assistance of flow cytometry experiments.

SUPPLEMENTARY MATERIAL

The Supplementary Material for this article can be found online at: https://www.frontiersin.org/articles/10.3389/fcell.2019.00288/full#supplementary-material

TABLE S1 | Stability test of housekeeping genes under hypoxia for real-time PCR. The *Ct* values of six commonly used housekeeping genes, beta-actin (*actb*), glyceraldehyde 3-phosphate dehydrogenase (*gapdh*), ribosomal protein L13a (*rpl13a*), 45S pre-ribosomal RNA (*rn45s*), 28S ribosomal RNA (*rn28s1*) and alpha-tubulin-1 (*tuba1*), were measured by real-time PCR under 21, 5, 2.5, and 1% hypoxic conditions in C17.2 cells. Their stability was ranked by geNorm method (https://genorm.cmgg.be/). *Actb* shows the lowest *M* value, indicating its highest stability under hypoxic conditions and thereby selected as reference gene in real-time PCR experiments.

REFERENCES

Bond, A. M., Ming, G. L., and Song, H. (2015). Adult mammalian neural stem cells and neurogenesis: five decades later. *Cell Stem Cell* 17, 385–395. doi: 10.1016/j.stem.2015.09.003

Chen, P., Yue, X., Xiong, H., Lu, X., and Ji, Z. (2019). RBM3 upregulates ARPC2 by binding the 3'UTR and contributes to breast cancer progression. *Int. J. Oncol.* 54, 1387–1397. doi: 10.3892/ijo.2019.4698

Chip, S., Zelmer, A., Ogunshola, O. O., Felderhoff-Mueser, U., Nitsch, C., Buhrer, C., et al. (2011). The RNA-binding protein RBM3 is involved in hypothermia induced neuroprotection. *Neurobiol. Dis.* 43, 388–396. doi: 10.1016/j.nbd.2011.04.010

Clarke, L., and Van Der Kooy, D. (2009). Low oxygen enhances primitive and definitive neural stem cell colony formation by inhibiting distinct cell death pathways. *Stem Cells* 27, 1879–1886. doi: 10.1002/stem.96

Danno, S., Itoh, K., Matsuda, T., and Fujita, J. (2000). Decreased expression of mouse Rbm3, a cold-shock protein, in Sertoli cells of cryptorchid testis. *Am. J. Pathol.* 156, 1685–1692. doi: 10.1016/s0002-9440(10)65039-0

De Filippis, L., and Delia, D. (2011). Hypoxia in the regulation of neural stem cells. *Cell Mol. Life Sci.* 68, 2831–2844. doi: 10.1007/s00018-011-0723-5

Ekker, M. S., Boot, E. M., Singhal, A. B., Tan, K. S., Debette, S., Tuladhar, A. M., et al. (2018). Epidemiology, aetiology, and management of ischaemic stroke in young adults. *Lancet Neurol.* 17, 790–801. doi: 10.1016/S1474-4422(18)30233-3

Felfly, H., Zambon, A. C., Xue, J., Muotri, A., Zhou, D., Snyder, E. Y., et al. (2011). Severe Hypoxia: consequences to neural stem cells and neurons. *J. Neurol. Res.* 1:10.4021/jnr70w. doi: 10.4021/jnr70w

Francis, K. R., and Wei, L. (2010). Human embryonic stem cell neural differentiation and enhanced cell survival promoted by hypoxic preconditioning. *Cell Death Dis.* 1:e22. doi: 10.1038/cddis.2009.22

Fuentealba, L. C., Obernier, K., and Alvarez-Buylla, A. (2012). Adult neural stem cells bridge their niche. *Cell Stem Cell* 10, 698–708. doi: 10.1016/j.stem.2012.05.012

Gage, F. H., and Temple, S. (2013). Neural stem cells: generating and regenerating the brain. *Neuron* 80, 588–601. doi: 10.1016/j.neuron.2013.10.037

Huang, B. Y., and Castillo, M. (2008). Hypoxic-ischemic brain injury: imaging findings from birth to adulthood. *Radiographics* 28, 417–439. doi: 10.1148/rg.282075066

Huang, L., and Zhang, L. (2019). Neural stem cell therapies and hypoxic-ischemic brain injury. *Prog. Neurobiol.* 173, 1–17. doi: 10.1016/j.pneurobio.2018.05.004

Jackson, T. C., Manole, M. D., Kotermanski, S. E., Jackson, E. K., Clark, R. S., and Kochanek, P. M. (2015). Cold stress protein RBM3 responds to temperature change in an ultra-sensitive manner in young neurons. *Neuroscience* 305, 268–278. doi: 10.1016/j.neuroscience.2015.08.012

Kalladka, D., and Muir, K. W. (2014). Brain repair: cell therapy in stroke. *Stem Cells Cloning* 7, 31–44.

Lengronne, A., Pasero, P., Bensimon, A., and Schwob, E. (2001). Monitoring S phase progression globally and locally using BrdU incorporation in TK(+) yeast strains. *Nucleic Acids Res.* 29, 1433–1442. doi: 10.1093/nar/29.7.1433

Li, L., Candelario, K. M., Thomas, K., Wang, R., Wright, K., Messier, A., et al. (2014). Hypoxia inducible factor-1alpha (HIF-1alpha) is required for neural stem cell maintenance and vascular stability in the adult mouse SVZ. *J. Neurosci.* 34, 16713–16719. doi: 10.1523/JNEUROSCI.4590-13.2014

Ludwig, P. E., Thankam, F. G., Patil, A. A., Chamczuk, A. J., and Agrawal, D. K. (2018). Brain injury and neural stem cells. *Neural Regen. Res.* 13, 7–18. doi: 10.4103/1673-5374.224361

Mas-Bargues, C., Sanz-Ros, J., Roman-Dominguez, A., Ingles, M., Gimeno-Mallench, L., El Alami, M., et al. (2019). Relevance of oxygen concentration in stem cell culture for regenerative medicine. *Int. J. Mol. Sci.* 20:E1195. doi: 10.3390/ijms20051195

Matsuda, A., Ogawa, M., Yanai, H., Naka, D., Goto, A., Ao, T., et al. (2011). Generation of mice deficient in RNA-binding motif protein 3 (RBM3) and characterization of its role in innate immune responses and cell growth. *Biochem. Biophys. Res. Commun.* 411, 7–13. doi: 10.1016/j.bbrc.2011.06.038

Mohyeldin, A., Garzon-Muvdi, T., and Quinones-Hinojosa, A. (2010). Oxygen in stem cell biology: a critical component of the stem cell niche. *Cell Stem Cell* 7, 150–161. doi: 10.1016/j.stem.2010.07.007

Panchision, D. M. (2009). The role of oxygen in regulating neural stem cells in development and disease. *J. Cell Physiol.* 220, 562–568. doi: 10.1002/jcp.21812

Pilotte, J., Cunningham, B. A., Edelman, G. M., and Vanderklish, P. W. (2009). Developmentally regulated expression of the cold-inducible RNA-binding motif protein 3 in euthermic rat brain. *Brain Res.* 1258, 12–24. doi: 10.1016/j.brainres.2008.12.050

Rajayer, S. R., Jacob, A., Yang, W. L., Zhou, M., Chaung, W., and Wang, P. (2013). Cold-inducible RNA-binding protein is an important mediator of alcohol-induced brain inflammation. *PLoS One* 8:e79430. doi: 10.1371/journal.pone.0079430

Santilli, G., Lamorte, G., Carlessi, L., Ferrari, D., Rota Nodari, L., Binda, E., et al. (2010). Mild hypoxia enhances proliferation and multipotency of human neural stem cells. *PLoS One* 5:e8575. doi: 10.1371/journal.pone.0008575

Sureban, S. M., Ramalingam, S., Natarajan, G., May, R., Subramaniam, D., Bishnupuri, K. S., et al. (2008). Translation regulatory factor RBM3 is a proto-oncogene that prevents mitotic catastrophe. *Oncogene* 27, 4544–4556. doi: 10.1038/onc.2008.97

Ushio, A., and Eto, K. (2018). RBM3 expression is upregulated by NF-kappaB p65 activity, protecting cells from apoptosis, during mild hypothermia. *J. Cell Biochem.* 119, 5734–5749. doi: 10.1002/jcb.26757

Vieira, H. L., Alves, P. M., and Vercelli, A. (2011). Modulation of neuronal stem cell differentiation by hypoxia and reactive oxygen species. *Prog. Neurobiol.* 93, 444–455. doi: 10.1016/j.pneurobio.2011.01.007

Vishwakarma, S. K., Bardia, A., Tiwari, S. K., Paspala, S. A., and Khan, A. A. (2014). Current concept in neural regeneration research: NSCs isolation, characterization and transplantation in various neurodegenerative diseases and stroke: a review. *J. Adv. Res.* 5, 277–294. doi: 10.1016/j.jare.2013.04.005

Wakai, T., Narasimhan, P., Sakata, H., Wang, E., Yoshioka, H., Kinouchi, H., et al. (2016). Hypoxic preconditioning enhances neural stem cell transplantation therapy after intracerebral hemorrhage in mice. *J. Cereb. Blood Flow Metab.* 36, 2134–2145. doi: 10.1177/0271678x15613798

Wang, B., Jedlicka, S., and Cheng, X. (2014). Maintenance and neuronal cell differentiation of neural stem cells C17.2 correlated to medium availability sets design criteria in microfluidic systems. *PLoS One* 9:e109815. doi: 10.1371/journal.pone.0109815

Wellmann, S., Bettkober, M., Zelmer, A., Seeger, K., Faigle, M., Eltzschig, H. K., et al. (2008). Hypoxia upregulates the histone demethylase JMJD1A via HIF-1. *Biochem. Biophys. Res. Commun.* 372, 892–897. doi: 10.1016/j.bbrc.2008.05.150

Wellmann, S., Buhrer, C., Moderegger, E., Zelmer, A., Kirschner, R., Koehne, P., et al. (2004). Oxygen-regulated expression of the RNA-binding proteins RBM3 and CIRP by a HIF-1-independent mechanism. *J. Cell Sci.* 117, 1785–1794. doi: 10.1242/jcs.01026

Wellmann, S., Truss, M., Bruder, E., Tornillo, L., Zelmer, A., Seeger, K., et al. (2010). The RNA-binding protein RBM3 is required for cell proliferation and protects against serum deprivation-induced cell death. *Pediatr. Res.* 67, 35–41. doi: 10.1203/PDR.0b013e3181c13326

Xia, W., Su, L., and Jiao, J. (2018). Cold-induced protein RBM3 orchestrates neurogenesis via modulating Yap mRNA stability in cold stress. *J. Cell Biol.* 217, 3464–3479. doi: 10.1083/jcb.201801143

Yang, H. J., Ju, F., Guo, X. X., Ma, S. P., Wang, L., Cheng, B. F., et al. (2017). RNA-binding protein RBM3 prevents NO-induced apoptosis in human neuroblastoma cells by modulating p38 signaling and miR-143. *Sci. Rep.* 7:41738. doi: 10.1038/srep41738

Yuan, L. L., Guan, Y. J., Ma, D. D., and Du, H. M. (2015). Optimal concentration and time window for proliferation and differentiation of neural stem cells from embryonic cerebral cortex: 5% oxygen preconditioning for 72 hours. *Neural Regen. Res.* 10, 1516–1522. doi: 10.4103/1673-5374.165526

Zhang, Q., Wang, Y. Z., Zhang, W., Chen, X., Wang, J., Chen, J., et al. (2017). Involvement of cold inducible RNA-binding protein in severe hypoxia-induced growth arrest of neural stem cells in vitro. *Mol. Neurobiol.* 54, 2143–2153. doi: 10.1007/s12035-016-9761-1

Zhou, M., Yang, W. L., Ji, Y., Qiang, X., and Wang, P. (2014). Cold-inducible RNA-binding protein mediates neuroinflammation in cerebral ischemia. *Biochim. Biophys. Acta* 1840, 2253–2261. doi: 10.1016/j.bbagen.2014.02.027

Zhu, X., Buhrer, C., and Wellmann, S. (2016). Cold-inducible proteins CIRP and RBM3, a unique couple with activities far beyond the cold. *Cell Mol. Life Sci.* 73, 3839–3859. doi: 10.1007/s00018-016-2253-7

Zhu, X., Yan, J., Bregere, C., Zelmer, A., Goerne, T., Kapfhammer, J. P., et al. (2019). RBM3 promotes neurogenesis in a niche-dependent manner via IMP2-IGF2 signaling pathway after hypoxic-ischemic brain injury. *Nat. Commun.* 10:3983. doi: 10.1038/s41467-019-11870-x

Zhuang, R. J., Ma, J., Shi, X., Ju, F., Ma, S. P., Wang, L., et al. (2017). Cold-inducible protein RBM3 protects UV irradiation-induced apoptosis in neuroblastoma cells by affecting p38 and JNK pathways and Bcl2 family proteins. *J. Mol. Neurosci.* 63, 142–151. doi: 10.1007/s12031-017-0964-3

Conflict of Interest: The authors declare that the research was conducted in the absence of any commercial or financial relationships that could be construed as a potential conflict of interest.

1.50E+00

	9.31E-03	1.37E-02	5.50E-03	4.62E-01	6.38E-01	4.58E-03	
1.5	*actb*	*gapdh*	*rpl13a*	*rn45s*	*rn28s1*	*tuba1*	Normalisation Factor
21% O2	9.62E-03	1.38E-02	4.14E-03	3.39E-01	4.59E-01	5.27E-03	0.8834
5% O2	1.18E-02	1.21E-02	5.16E-03	6.06E-01	9.74E-01	4.81E-03	1.1409
2.5% O2	1.07E-02	1.93E-02	8.93E-03	7.89E-01	7.95E-01	5.79E-03	1.3861
1% O2	6.18E-03	1.09E-02	4.80E-03	2.81E-01	4.65E-01	3.01E-03	0.7158
M < 1.5	**0.377**	**0.394**	**0.436**	**0.435**	**0.445**	**0.387**	

2.3 Research Article III

The RNA-binding motif protein 3 is altered by neuroblastoma differentiation and promotes cell migration

Ongoing project, unpublished

2.3.1 Introduction

Neuroblastoma, a childhood sympathetic nervous system cancer that originates from neural crest cells [1, 2], is often described as enigmatic and unpredictable because it exhibits three distinct patterns of clinical behavior: life-threatening progression; maturation to ganglioneuroblastoma or ganglioneuroma; and spontaneous regression [3-5], the incidence of which is about 200-fold greater than that for any other human cancer, such as renal carcinoma or malignant melanoma [6]. The most convincing demonstration of spontaneous regression is when primary neuroblastoma and metastatic disease disappear without any treatment [4, 7-9]. This usually occurs when the disease is distributed in the liver and/or bone marrow and skin but not in cortical bone or distant nodes [10, 11].

A 1994 study suggested that the most likely explanation for spontaneous regression of neuroblastoma is delay in the developmental time-switch for apoptosis [12]. Recent genomic and biological studies have shed light on the clinical behavior of neuroblastoma which extends from spontaneous regression or differentiation in some patients to relentless disease progression in others. Several mechanisms of spontaneous regression have been suggested, including neurotrophin deprivation [13, 14], humoral or cellular immunity, loss of telomerase activity [15, 16], and altered epigenetic regulation [17-19]. Thus, future therapies may focus increasingly on specific genes and biological pathways that contribute to malignant transformation or progression.

Neuroblastoma cell lines are heterogeneous, comprising at least three distinct cell phenotypes: (1) neuroblastic N-type cells, which are immature nerve cells, precursors to the sympathoadrenal cell lineage of the neural crest [20, 21]; (2) non-neuronal substrate-adherent S-type cells, which are multipotent precursors to Schwann cells, melanocytes and glial cells, and can form the non-neuronal lineage of the neural crest [20, 22]; and (3) intermediate I-type cells, which are intermediate with respect to N- and S-type cells in terms of morphology and biochemical markers [20, 22, 23], and which may represent either a stem cell or an intermediate stage in the trans-differentiation between N- and S-type cells [22, 24]. I-type and N-type cells are more malignant than S-type cells [25-27].

RBM3 expression correlates with good prognosis in several cancers and causes cellular differentiation and apoptosis [28]. Interestingly, high RBM3 expression is found in poorly differentiated prostate tumor [29], whereas experimental down-regulation of RBM3 in prostate

cancer cells attenuates cell survival and enhances *in-vitro* chemosensitivity [30]. These observations are consistent with the role of RBM3 in promoting cell proliferation and survival but cannot explain the favorable prognosis, indicating the involvement of other mechanisms. If altered apoptosis is an important pathogenetic mechanism in different cell types, the degree of spontaneous apoptosis might differ from that seen in progression [31, 32]. Less known is the role of RBM3 in cell morphology and motility in neuronal precursor cells, specifically at the boundary with oncogenic development. Thus elucidating the role of RBM3 in neuronal precursor cell migration and neuroblastoma development may shed light on the spontaneous apoptosis and regression of neuroblastoma.

Both IMP1 and IMP3 have been reported to increase proliferation and invasion as oncofetal proteins in cancers of the pancreas, kidney, and lung. IMP1 is associated with lower overall patient survival and MYCN abundance [33, 34]. High expression of IMP1 is associated with tumor metastasis and poor overall prognosis. Furthermore, its paralog, IMP3, has been touted as a biomarker for a growing list of cancers, including neuroblastoma in one report [33]. A few studies have found IMP2 isoforms to be expressed in several tumor-derived and transformed cells [35, 36]. Moreover, the *IMP2* gene is amplified at a higher frequency in several solid tumors while IMP2 depletion inhibits the proliferation of human cancer cell lines [37]. Such evidence suggests a role for the IMP isoform family as biomarkers of cancer progression and metastasis and target molecules for cancer therapy.

2.3.2 Methods

Cell culture and reagents

NB cell lines SH-EP, SK-N-AS, LAN-1, SK-N-SH, and NB8 were provided by Dr. Mühlethaler-Mottet at the Institut Universitaire de Pathologie, Lausanne. SK-N-BE(2)C were provided by Dr. Hemmi, University of Zürich. SH-SY5Y cells were provided by Dr. Kohler, Department for Biomedicine, Basel. All NB cells were grown in Dulbecco's modified Eagle's medium supplemented with 2 mM-glutamine, 100 U/ml penicillin, 0.1 mg/ml streptomycin and 10 % of FCS. Cells were maintained at 37°C in a saturated humidity atmosphere containing 95% air and 5% CO_2.

Plasmid transient transfection

All plasmids expressing GFP-RBM3, full-length or truncated IMP2 were transiently transfected into NB cell lines with FuGENE HD Transfection Reagent (Promega) for 48 h; 2 μg of each plasmid was used to transfect 1×10^6 seeded cells.

Protein isolation and Western blot

Total proteins were extracted from cultured cells or homogenized rat brain with lysis buffer (1% Triton X-100, 50 mM Tris, 150 mM NaCl, 1× Roche Protease Inhibitor Cocktail, pH 8.0). Total protein concentrations in cleared cell lysates were determined with RC DC Protein Assay (Bio-Rad). Lysates were loaded onto Mini-Protean TGX pre-cast gels (Bio-rad) and transferred to PVDF membranes (Amersham/GE Healthcare Life Sciences). Membranes were incubated with primary antibodies overnight at 4°C and then with HRP-linked secondary antibodies for 1 h at room temperature (RT).

Primary and secondary antibodies:

Anti-mouse RBM3 (Proteintech, 14363-1-AP): rabbit polyclonal, diluted 1:750

Anti-mouse IMP2 (Abnova, H00010644-M01): mouse monoclonal, diluted 1:500

Anti-mouse GAPDH (Abcam, ab8245): mouse monoclonal, diluted 1:5000

HRP-linked anti-rabbit secondary antibody (Cell Signaling Technology, 7074S): diluted 1:5000

HRP-linked anti-mouse secondary antibody (Cell Signaling Technology, 7076S): diluted 1:5000

Neurosphere assay

Neurosphere assays were performed to test the self-renewal capacity of cultured NB cell lines. Pre-cultured NB cells were plated at a density of 5000 cells per 100 μL medium in each well of 96-well plates to form primary neurospheres. Cells were cultured in complete DMEM-F12 medium (Gibco) supplemented with 1× B27 supplement (Gibco), 2 mM L-glutamine (Gibco), 20 ng/mL EGF and 20 ng/mL FGF2 (PeproTech). Four replicates were included in each group. The culture medium was changed every second day. Neurosphere images were captured after 7 days culture.

Wound healing assay

NB cells were seeded at an initial density of 5×10^5 cells in 6-well culture plates for 24 hours. The cell monolayer was 'scratched' in a straight line using a P200 pipette tip. The debris was removed and the scratch edge smoothed by washing the cells once with 1 ml growth medium, replaced with 2 ml medium. Images were captured at different time points as indicated.

Differentiation assay

NB cells were seeded at an initial density of 10^5 cells in 6-well culture plates for 24 hours. Cultured cells were subjected to directed differentiation by incubation in medium containing 10 μM retinoic acid (RA) and grown for 7 days before harvest.

2.3.3 Results

1. RBM3 promotes neuroblastoma cell line proliferation

Established primary tumor-derived neuroblastoma cell lines display distinct morphologies that reflect their heterogeneous genetic make-up. For instance, the Kelly and BE(2)-M17 cell lines bearing *mycn* amplification are associated with NB aggressiveness (N-type). In contrast, the SH-EP cell line, subcloned from SK-N-SH [22], lacks *mycn* amplification and displays S-type morphology (Table 1).

Table 1: Human neuroblastoma cell line morphology

Cell line	Type	Stage	gender & age	MycN-amplification
Kelly	neuronal	4	0.1 year, Male	+
BE(2)-M17	neuronal	4	2.2 year, Male	+
LA-N-1	neuronal	4	2 year, Male	+
SK-N-SH	neuronal	4	4 years, Female	-
SH-SY5Y	neuronal	4	4 years, Female	-
SH-EP	substrate adherent	4	4 year, female	-
SK-N-AS	substrate adherent	4	8 year, Female	-
SK-N-BE(2)-C	intermediate subtype	4	4 years, Female	+

In order to evaluate its effect on neuronal-type cell line migration RBM3 was knocked down using si-RNA in SH-SY5Y cells. Wound healing assay was performed after 24 hours transfection. Wildtype RBM3 clearly promoted cell migration, with the cells closing the wound at 48 h, whereas si-RNA knock-down RBM3 significantly inhibited treated SH-SY5Y cell migration (Figure 1.1). The self-renewal ability of neuroblastoma cells was assessed by sphere-forming assay in SH-SY5Y cells. After 7 days culture, we found increased sphere number and

size when overexpressing RBM3 compared to the vector group. In contrast, silencing RBM3 reduced sphere number and size (Figure 1.2). The results demonstrated that RBM3 promotes SH-SY5Y migrating ability and self-renewal capacity.

2. RA-induced differentiation alters RBM3 and IMP2 expression

RA is used in the treatment protocol for high-risk neuroblastoma patients as it inhibits proliferation and induces cell differentiation [38, 39]. SH-SY5Y and Kelly, two neuronal-type neuroblastoma cell lines, were incubated with 10 μM RA to induce neuronal differentiation. After 5 days, cells progressively developed phenotypic changes compatible with neuronal-like morphology characterized by neurite outgrowth (Figure 2.1). RBM3 and IMP2 expression in the SH-SY5Y cell line decreased progressively over 3 days of RA treatment (Figure 2.2), while increasing in the Kelly line (Figure 2.2 A). We noticed that IMP2 molecular weight was different in Kelly and SH-SY5Y cells, indicating that various IMP2 isoforms are present in different cell types. No obvious change in CIRP was found in the whole cell lysates. In addition, cytoplasmic and nuclear protein fractions were isolated from RA-treated cells using a nuclear extraction kit according to the manufacturer's recommendations. Western blot detected no RBM3 in the nuclear extract, but gradually increasing levels were observed in the cytoplasmic extract of SH-SY5Y cells. In Kelly cells, RA-induced differentiation regulated IMP2 levels in the opposite direction. These results demonstrate that IMP2 could regulate, or be regulated in, differentiated neuroblastoma cell lines.

2.3.4 Discussion

Much remains to be done in elucidating the roles of RBM3 and IMP2 in neuroblastoma development. So far we have only confirmed that RBM3 promotes neuroblastoma cell line proliferation *in vitro*. However, we have not shown how RBM3 affects cell migration or sphere formation. Is there less apoptosis when RBM3 is overexpressed? Is general translation enhanced? Does RBM3 interact with other proteins in certain pathways and, if so, how? These remain open questions. Interestingly, RA-induced differentiation alters the levels of RBM3 expression. We also need to find out if RBM3 levels change when NB cell lines are induced by other reagents such as BrdU or ionomycin, and conversely whether RBM3 alters NB cell line differentiation.

In this project, we studied RBM3 and IMP2 separately as there is yet no case for combining them. Little is known about the structure and function of the IMP2 protein, and how its activity

may relate to cancer. One report has identified multiple transcription start sites of the human, mouse and rat *Imp2* genes in a highly conserved region only 50–90 nts upstream of the major translation start site; in addition, two isoforms, p58 and p62, are not generated by protease cleavage [35]. The first RRM domain of IMP2, which is absent in the p58 isoform, contains highly conserved RNP1 and RNP2 motifs important for RNA recognition, in contrast to the second RRM domain which has poor RNP signatures; in addition to binding to RNA, RRM domains can participate in protein-protein interaction and facilitate inter- or intra-molecular dimerization of RRM domain-containing protein [40, 41]. Thus loss of the RRM1 domain in the small isoform might affect its binding affinity and specificity to both RNA and protein partners, as well as its own structure, dimer formation, and stability as seen in other RRM-containing proteins. RRM domains in IMPs may function to modulate the RNA-binding activity of the KH domains. In order to find which isoforms can be altered after differentiation, we designed specific primers for each IMP2 domain to identify the changes. Moreover, we also overexpressed each isoform in all types of neuroblastoma cell line to determine whether any differentiated marker can be increased.

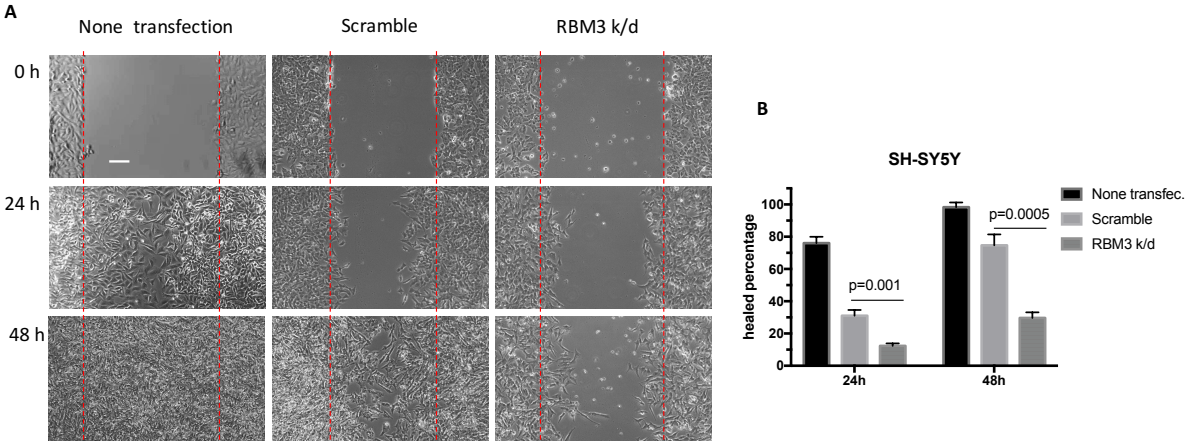

Figure 1.1 Wound healing assay. A, SH-SY5Y cells were transfected with RBM3 siRNA and scramble siRNA respectively. Movement of cells into wound was shown for each group at 0, 24h and 48 h post scratch (10×). The red dotted lines indicated the boundary lines of scratch. Cell migration was assessed by recover of the scratch. Scale bar: 100 μm. B, The area of the wound was measured at the two time points in every group, and % reduction of initial scratch area was compared. Three independent experiments were performed (n=3). Bars represent the means ± SEM. t-test was used for statistical analysis.

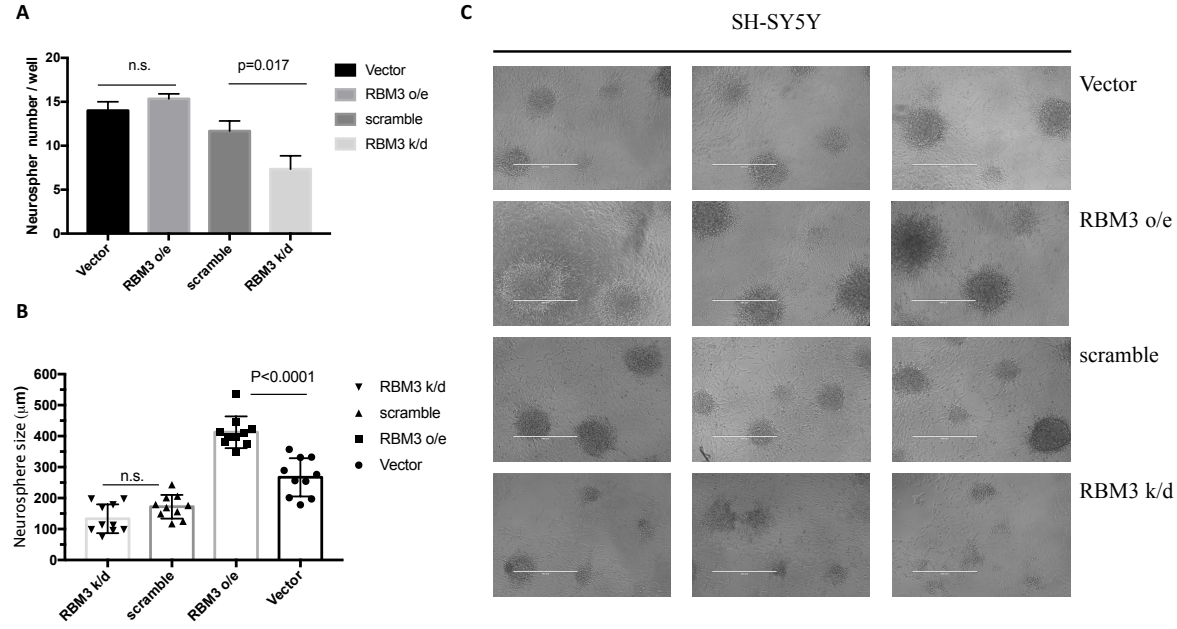

Figure 1.2 SH-SY5Y neurosphere assay. SH-SY5Y were transfected with plasmids or siRNA for 48 hours, then seeded into 96-well plates in equal amounts for 7 days. A, total amount of neurosphere in each well; B, neurosphere size after 7 days culture. Bars represent the means ± SEM. o/e, overexpression; k/d, knockdown; n.s., not significant. Three independent experiments were performed (n=3). t-test was used for statistical analysis. C, Representative of neurosphere on day 7. All neurospheres were measured with diameters. Scale bar: 400 μm.

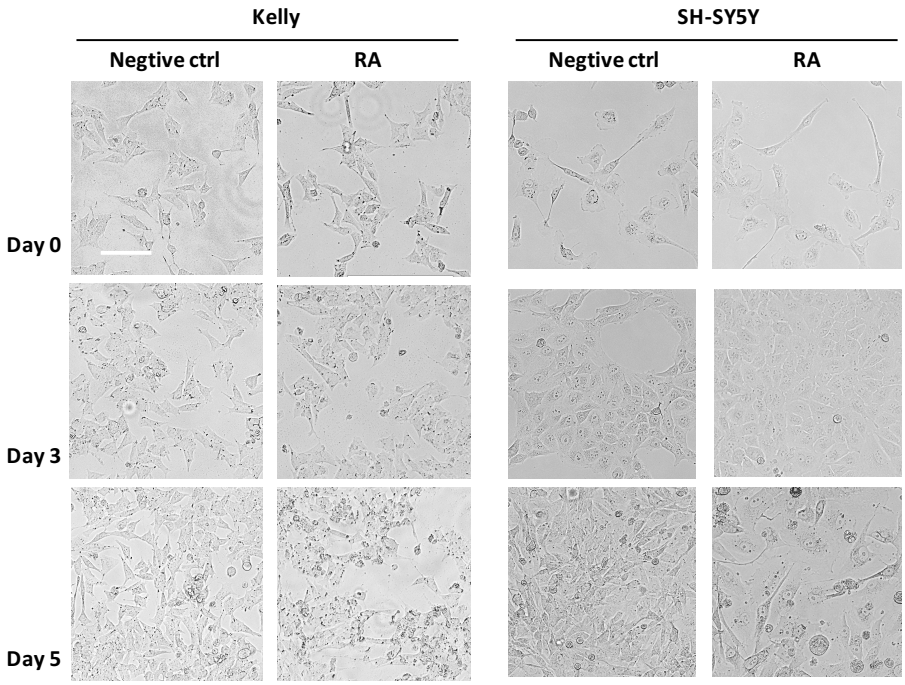

Figure 2.1 Morphological appearance of undifferentiated and differentiated neuroblastoma cell lines. SH-SY5Y and Kelly were treated with 10 μM retinoic acid (RA). Radom fields were chosen for representation on day 3 and day5. Scale bar: 200 μm.

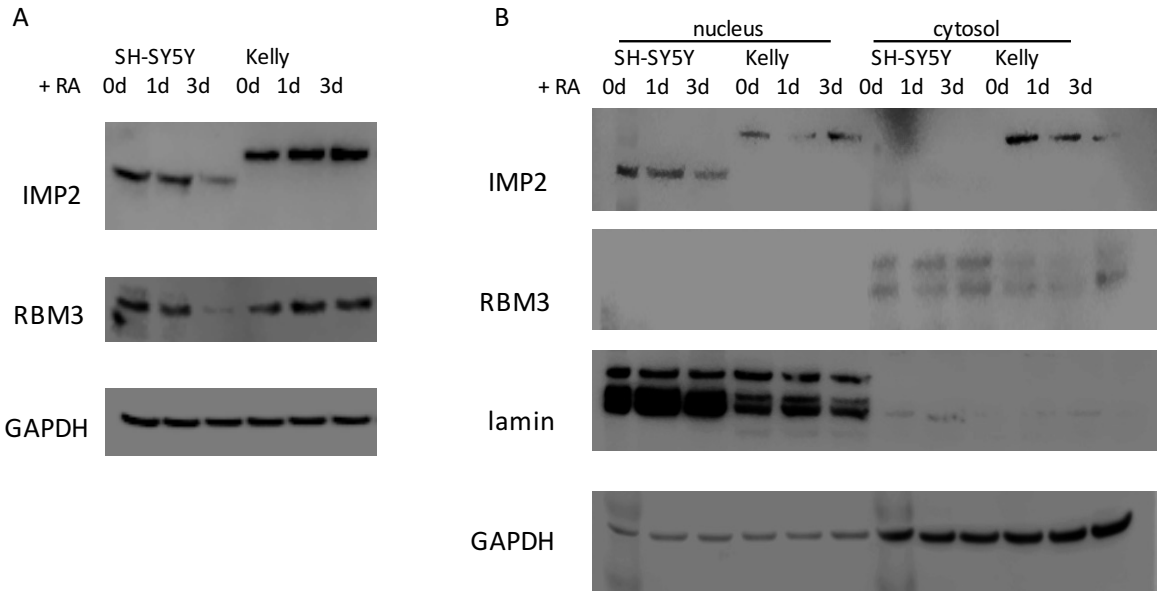

Figure 2.2 RBM3 expression in different neuroblastoma cell lines. Cells were treated with 10 μM retinoic acid (RA) for 1 or 3 days. Western blot was analyzed with RBM3 and IMP2 antibodies for the whole cell lysate, nucleus extraction, and cytosol extraction.

2.3.5 References

1. Maris, J.M., et al., *Neuroblastoma.* Lancet, 2007. **369**(9579): p. 2106-20.

2. Marshall, G.M., et al., The prenatal origins of cancer. Nat Rev Cancer, 2014. **14**(4): p. 277-89.

3. Smith, M.A., et al., Outcomes for children and adolescents with cancer: challenges for the twenty-first century. J Clin Oncol, 2010. **28**(15): p. 2625-34.

4. Diede, S.J., Spontaneous regression of metastatic cancer: learning from neuroblastoma. Nat Rev Cancer, 2014. **14**(2): p. 71-2.

5. Gatta, G., et al., Childhood cancer survival in Europe 1999-2007: results of EUROCARE-5--a population-based study. Lancet Oncol, 2014. **15**(1): p. 35-47.

6. Brodeur, G.M. and R. Bagatell, Mechanisms of neuroblastoma regression. Nat Rev Clin Oncol, 2014. **11**(12): p. 704-13.

7. Matthay, K.K., Stage 4S neuroblastoma: what makes it special? J Clin Oncol, 1998. **16**(6): p. 2003-6.

8. Nakagawara, A., Molecular basis of spontaneous regression of neuroblastoma: role of neurotrophic signals and genetic abnormalities. Hum Cell, 1998. **11**(3): p. 115-24.

9. Brodeur, G.M., Neuroblastoma: biological insights into a clinical enigma. Nat Rev Cancer, 2003. **3**(3): p. 203-16.

10. Kushner, B.H., et al., Survival from locally invasive or widespread neuroblastoma without cytotoxic therapy. J Clin Oncol, 1996. **14**(2): p. 373-81.

11. Sharp, S.E., M.J. Gelfand, and B.L. Shulkin, *Pediatrics: diagnosis of neuroblastoma.* Semin Nucl Med, 2011. **41**(5): p. 345-53.

12. Pritchard, J. and J.A. Hickman, Why does stage 4s neuroblastoma regress spontaneously? Lancet, 1994. **344**(8926): p. 869-70.

13. Tacconelli, A., et al., TrkA alternative splicing: a regulated tumor-promoting switch in human neuroblastoma. Cancer Cell, 2004. **6**(4): p. 347-60.

14. Tacconelli, A., et al., Alternative TrkAIII splicing: a potential regulated tumor-promoting switch and therapeutic target in neuroblastoma. Future Oncol, 2005. **1**(5): p. 689-98.

15. Hiyama, E., et al., Correlating telomerase activity levels with human neuroblastoma outcomes. Nat Med, 1995. **1**(3): p. 249-55.

16. Samy, M., et al., Loss of the malignant phenotype of human neuroblastoma cells by a catalytically inactive dominant-negative hTERT mutant. Mol Cancer Ther, 2012. **11**(11): p. 2384-93.

17. Astuti, D., et al., RASSF1A promoter region CpG island hypermethylation in phaeochromocytomas and neuroblastoma tumours. Oncogene, 2001. **20**(51): p. 7573-7.

18. Simoes-Costa, M. and M.E. Bronner, Insights into neural crest development and evolution from genomic analysis. Genome Res, 2013. **23**(7): p. 1069-80.

19. Batora, N.V., et al., Transitioning from genotypes to epigenotypes: why the time has come for medulloblastoma epigenomics. Neuroscience, 2014. **264**: p. 171-85.

20. Ross, R.A., et al., Human neuroblastoma I-type cells are malignant neural crest stem cells. Cell Growth Differ, 1995. **6**(4): p. 449-56.

21. Ross, R.A. and B.A. Spengler, *Human neuroblastoma stem cells.* Semin Cancer Biol, 2007. **17**(3): p. 241-7.

22. Ciccarone, V., et al., Phenotypic diversification in human neuroblastoma cells: expression of distinct neural crest lineages. Cancer Res, 1989. **49**(1): p. 219-25.

23. Walton, J.D., et al., Characteristics of stem cells from human neuroblastoma cell lines and in tumors. Neoplasia, 2004. **6**(6): p. 838-45.

24. Ross, R.A., B.A. Spengler, and J.L. Biedler, Coordinate morphological and biochemical interconversion of human neuroblastoma cells. J Natl Cancer Inst, 1983. **71**(4): p. 741-7.

25. Piacentini, M., et al., Differential growth of N- and S-type human neuroblastoma cells xenografted into scid mice. correlation with apoptosis. J Pathol, 1996. **180**(4): p. 415-22.

26. Spengler, B.A., et al., Cell lineage and differentiation state are primary determinants of MYCN gene expression and malignant potential in human neuroblastoma cells. Oncol Res, 1997. **9**(9): p. 467-76.

27. Ross, R.A., J.L. Biedler, and B.A. Spengler, A role for distinct cell types in determining malignancy in human neuroblastoma cell lines and tumors. Cancer Lett, 2003. **197**(1-2): p. 35-9.

28. Chatterji, P. and A.K. Rustgi, RNA Binding Proteins in Intestinal Epithelial Biology and Colorectal Cancer. Trends Mol Med, 2018. **24**(5): p. 490-506.

29. Shaikhibrahim, Z., et al., Epigenetics-related genes in prostate cancer: expression profile in prostate cancer tissues, androgen-sensitive and -insensitive cell lines. Int J Mol Med, 2013. **31**(1): p. 21-5.

30. Zeng, Y., et al., Down-regulating cold shock protein genes impairs cancer cell survival and enhances chemosensitivity. J Cell Biochem, 2009. **107**(1): p. 179-88.

31. Qing, G., et al., ATF4 regulates MYC-mediated neuroblastoma cell death upon glutamine deprivation. Cancer Cell, 2012. **22**(5): p. 631-44.

32. Ham, J., et al., Exploitation of the Apoptosis-Primed State of MYCN-Amplified Neuroblastoma to Develop a Potent and Specific Targeted Therapy Combination. Cancer Cell, 2016. **29**(2): p. 159-72.

33. Chen, S.T., et al., Insulin-like growth factor II mRNA-binding protein 3 expression predicts unfavorable prognosis in patients with neuroblastoma. Cancer Sci, 2011. **102**(12): p. 2191-8.

34. Bell, J.L., et al., IGF2BP1 harbors prognostic significance by gene gain and diverse expression in neuroblastoma. J Clin Oncol, 2015. **33**(11): p. 1285-93.

35. Le, H.T., A.M. Sorrell, and K. Siddle, Two isoforms of the mRNA binding protein IGF2BP2 are generated by alternative translational initiation. PLoS One, 2012. **7**(3): p. e33140.

36. Bell, J.L., et al., Insulin-like growth factor 2 mRNA-binding proteins (IGF2BPs): post-transcriptional drivers of cancer progression? Cell Mol Life Sci, 2013. **70**(15): p. 2657-75.

37. Dai, N., et al., IGF2 mRNA binding protein-2 is a tumor promoter that drives cancer proliferation through its client mRNAs IGF2 and HMGA1. Elife, 2017. **6**.

38. Sidell, N., Retinoic acid-induced growth inhibition and morphologic differentiation of human neuroblastoma cells in vitro. J Natl Cancer Inst, 1982. **68**(4): p. 589-96.

39. Matthay, K.K., et al., Treatment of high-risk neuroblastoma with intensive chemotherapy, radiotherapy, autologous bone marrow transplantation, and 13-cis-retinoic acid. Children's Cancer Group. N Engl J Med, 1999. **341**(16): p. 1165-73.

40. Maris, C., C. Dominguez, and F.H. Allain, The RNA recognition motif, a plastic RNA-binding platform to regulate post-transcriptional gene expression. FEBS J, 2005. **272**(9): p. 2118-31.

41. Clery, A., M. Blatter, and F.H. Allain, *RNA recognition motifs: boring? Not quite.* Curr Opin Struct Biol, 2008. **18**(3): p. 290-8.

Chapter 3. Discussion and outlook

3.1 Discussion

Therapeutic hypothermia has been described as the most potent neuroprotective strategy [1-3]. Although its benefits are well established in experimental models of stroke, there is limited evidence of its effectiveness in a clinical trial setting [4-7]. Most pre-clinical studies have used small rodent models in which target temperatures can be reached within minutes and maintained with reasonable control [8], to no obvious detrimental effect [8, 9]. This contrasts with the clinical trial setting in which several hours are required for cooling and rewarming [10-13]. Cooling presents substantial challenges and systemic side effects in humans [14], such as shivering [15], immunosuppression [16], pneumonia [17, 18], and cardiovascular events [11]. On the other hand, a potential advantage of therapeutic hypothermia over other neuroprotective agents is its ability to activate numerous pathways simultaneously by several mechanisms during the ischemic and reperfusion window, and to reduce damage beyond the neuron to include the entire neurovascular unit [19, 20]. More investigation is needed to better understand the underlying mechanisms of such intervention and to overcome the clinical barriers to the routine use of therapeutic hypothermia in stroke.

The effect of hypothermia on endogenous neurogenesis in injured brain is somewhat controversial [21-26]. It seems that mild hypothermia enables the differentiation of precursor cells while preventing apoptosis [25, 26], whereas cooling to below 30°C suppresses cell proliferation and induces phase-specific and nonspecific cell cycle arrest as a result of reduced energy supply [21, 24]. Therapeutic hypothermia is widely known to protect the brain from HI injury [3, 27] but there is limited and inconsistent information as to whether it promotes or inhibits injury-induced NSC proliferation and neuronal differentiation or if anti-apoptosis is the key mechanism [28]. Mammalian cells generally respond to cold temperatures by arresting the cell cycle and inhibiting protein translation and gene transcription [3]. Cold-inducible proteins, both RBM3 and cold inducible RNA-binding protein (CIRP), are specifically induced by mild hypothermia [29, 30]. RBM3 has recently been shown to orchestrate neurogenesis by modulating Yap mRNA stability in cold stress [31]. Our own work has found that cold inducible RBM3 is indispensable for neuroprotection and post-injury neuroregeneration. Although cooling promotes neurogenesis under certain conditions, it also reduces the metabolic rate, thus inhibiting NSC proliferation and neurogenesis. In such a complex process, cold-inducible proteins represent an ideal target for post-injury neurogenesis and could possibly replace therapeutic hypothermia.

As we have reported, RBM3-deficient mice do not exhibit an obvious phenotype under physiological conditions [32, 33]. Transcriptome changes are rare in RNA sequencing results when comparing RBM3 WT and KO mice. In an earlier study our group identified a family of RBM3-binding proteins of which more than half are involved in transcription and translation. Among the top-ranked interacting proteins, NF45 and NF90 are nuclear factors associated with dsRNA. RBM3 has been shown to prevent oxidative stress-induced cell apoptosis by inhibiting PERK phosphorylation with the assistance of NF90 [34]. IMP3 is an interactor with a higher score than IMP2, which itself is expressed in most adult tissues [35-37] (unlike oncofetal protein IMP3 [38]). Thus we focused more on IMP2-RBM3 interaction in the adult mice model.

We elevated RBM3 and IMP2 expression, thereby stimulating IGF2 release in SVZ but not SGZ NSCs. As the main downstream factor of IMP2, IGF2 is abundant in the proliferative regions of both embryonic and adult brain [39], similarly to the temporal and spatial expression pattern of IMP2 and RBM3. In recent years, IGF2 has been identified as a positive regulator of the proliferation of embryonic and neonatal NSCs [40, 41], and adult NSCs [42, 43]. Interestingly, SVZ-NSC responses to exogenous IGF2 follow a paracrine pattern, while SGZ-NSCs secrete IGF2 and regulate self-renewal in an autocrine manner [42, 43]. Our results support the hypothesis that RBM3 upregulates IGF2 expression and secretion in SGZ-NSCs but not SVZ-NSCs, explaining why only SGZ-NSC proliferation is affected by RBM3 expression level after HI injury. The choroid plexus produces CSF including IGF2 [43, 44]. However, as we tested in part one, RBM3 is not expressed in choroid plexus in adult WT mice. RBM3 is unlikely to regulate IGF2 levels in CSF, which may explain why SVZ-NSC proliferation was unaffected in RBM3 KO mice. Actually, the IGF2 response in SVZ-NSC is niche-dependent but not intrinsic to these cells as they react with the IGF2 produced in CSF but not with IGF2 secreted by itself [42, 43]. We found that RBM3 not only protects NSCs from HI-induced apoptosis, it also stimulates NSC proliferation and neuronal differentiation. Our studies indicate that RBM3 behaves as a potential target for maintaining the NSC pool in hypoxia-ischemia conditions. As the promotion of proliferation is largely mediated by hypoxia-inducible factor-1α (HIF-1α) signaling [45, 46], RBM3 regulation is independent of HIF-1α [47]. Therefore, manipulating RBM3 expression opens a new avenue for increasing viability, proliferation capacity and pluripotency in cultured NSCs and probably in other types of stem cell, which may improve therapeutic effects after NSC transplantation.

The only known homologous protein of RBM3 in mammals, CIRP [48], has attracted several studies [49-52]. Current understanding of the biological function of intracellular RBM3 and CIRP suggests they stabilize specific mRNAs and facilitate translation for survival advantage when cells are stressed [53]. In our study we found that RBM3 is induced not only by hypothermia, but also to comparable levels by mild (8%) and severe (1%) hypoxia via a mechanism involving neither HIF nor mitochondria *in vitro* [47]. We also found that overexpressed RBM3 relieved hypoxia-induced cell cycle arrest in G0/G1 phase and increased cell transit into S phase. CIRP has been reported to promote G1/S transition in the cell cycle of NSCs exposed to hypoxia [54]. Such actions suggest that intracellular RBM3 and CIRP might both be preventive in hypoxia-induced brain injury. There is also evidence that extracellular CIRP is a damage-associated molecular pattern (DAMP) molecule [50]. Especially when cells are exposed to hypoxic stress or LPS, CIRP translocates from the nucleus to the cytoplasm and is actively released from macrophages. Its role in hypoxia-ischemia brain injury remains controversial. Qiang *et al* suggested that recombinant CIRP proteins induce TNF-α release from macrophages *in vitro,* stimulate inflammatory responses and cause tissue injury in animals; they identified extracellular CIRP as a *bona fide* proinflammatory mediator [50]. CIRP is also involved in mediating neuro-inflammation [55, 56]. Extracellular CIRP levels increase in ischemic stroke models, causing massive neuronal damage [56]. On the other hand, overexpression of CIRP reduces H_2O_2-induced apoptosis, indicating a neuroprotective role [57]. In contrast, as an intracellular protein, RBM3 has no such deleterious effect, and cannot in principal be released into the circulation, although high levels were found in human serum after cardiac arrest (CA), possibly due to ischemic cell necrosis [58]. Therefore, RBM3 tends to be a safer target modulator of post-injury neurogenesis than CIRP.

Besides playing a neuroprotective role after injury, high RBM3 expression increases tumor sensitivity to chemotherapy and is associated with better prognosis [59], being an independent prognostic marker and treatment predictive marker in several cancers [60-63]. Oxygen-regulated expression of RBM3 is dose-dependent and subject to cell vulnerability, and developmental or pathological changes, such as hypoxia-ischemia, carcinogenesis, and inflammation [48]. Embryonic fibroblasts from RBM3-deficient mice show a marked increase in the number of G2-phase cells [33], confirming that RBM3 is essential for cells to divide through mitosis. This may explain why tumors with high RBM3 expression show increased sensitivity to chemotherapy and are associated with better prognosis than RBM3-low or even RBM3-negative tumors [59]. RBM3 inhibits staurosporine-induced apoptosis in neuron-like

PC12 cells by repressing PARP cleavage [64]. The induction of Bcl-2 and suppression of caspase expression may also be involved in RBM3-mediated survival [34, 65]. In the third part of study, we found that RBM3 promotes neuroblastoma cell line proliferation and that RA-induced differentiation alters the levels at which it is expressed in various cell types. However, its role in neuroblastoma progression is unclear and the specific mechanisms are still unknown: how RBM3 expression changes at different neuroblastoma stages, or whether it regulates neuroblastoma cell apoptosis by interacting with other proteins, and if so, by which pathways, are questions that remain unelucidated.

Several studies have suggested that RBM3 prevents apoptosis in human neuroblastoma cells by modulating p38 signaling and miR-143 [66-68]. Pritchard and Hickman suggested that the most likely explanation for spontaneous regression of neuroblastoma is delay in the developmental time-switch for apoptosis [69].

Little is known about the structure and function of the IMP2 protein, and how its activity may relate to cancer. One report has identified multiple transcription start sites of the human, mouse and rat *Imp2* genes in a highly conserved region only 50–90 nts upstream of the major translation start site; in addition, two isoforms, p58 and p62, are not generated by protease cleavage [70]. The first RRM domain of IMP2, which is absent in the p58 isoform, contains highly conserved RNP1 and RNP2 motifs important for RNA recognition, in contrast to the second RRM domain which has poor RNP signatures; in addition to binding to RNA, RRM domains can participate in protein-protein interaction and facilitate inter- or intra-molecular dimerization of RRM domain-containing protein [71, 72]. Thus loss of the RRM1 domain in the small isoform might affect its binding affinity and specificity to both RNA and protein partners, as well as its own structure, dimer formation, and stability as seen in other RRM-containing proteins. RRM domains in IMPs may function to modulate the RNA-binding activity of the KH domains [70]. In order to find which isoforms can be altered after differentiation, we designed specific primers for each IMP2 domain to identify the changes. Moreover, we also overexpressed each isoform in all types of neuroblastoma cell line to determine whether any differentiated marker can be increased.

3.2 Outlook

RBM3 not only protects NSCs from HI-induced apoptosis, it also stimulates NSC proliferation and neuronal differentiation. RBM3 is indispensable for neuroprotection and post-injury

neuroregeneration. RBM3-targeted therapy could be safe to administer in brain disorders. Manipulating RBM3 expression opens a new avenue to increase viability, proliferation capacity, and multi-potency of NSCs and probably other types of stem cells.

References

1. Lyden, P.D., et al., Therapeutic hypothermia for acute stroke. Int J Stroke, 2006. **1**(1): p. 9-19.

2. Choi, H.A., N. Badjatia, and S.A. Mayer, Hypothermia for acute brain injury--mechanisms and practical aspects. Nat Rev Neurol, 2012. **8**(4): p. 214-22.

3. Yenari, M.A. and H.S. Han, Neuroprotective mechanisms of hypothermia in brain ischaemia. Nat Rev Neurosci, 2012. **13**(4): p. 267-78.

4. Schwab, S., et al., Feasibility and safety of moderate hypothermia after massive hemispheric infarction. Stroke, 2001. **32**(9): p. 2033-5.

5. Richard Green, A., T. Odergren, and T. Ashwood, Animal models of stroke: do they have value for discovering neuroprotective agents? Trends Pharmacol Sci, 2003. **24**(8): p. 402-8.

6. Clifton, G.L., et al., Very early hypothermia induction in patients with severe brain injury (the National Acute Brain Injury Study: Hypothermia II): a randomised trial. Lancet Neurol, 2011. **10**(2): p. 131-9.

7. Chamorro, A., et al., Neuroprotection in acute stroke: targeting excitotoxicity, oxidative and nitrosative stress, and inflammation. Lancet Neurol, 2016. **15**(8): p. 869-881.

8. van der Worp, H.B., et al., Hypothermia in animal models of acute ischaemic stroke: a systematic review and meta-analysis. Brain, 2007. **130**(Pt 12): p. 3063-74.

9. Lamb, J.A., P.S. Rajput, and P.D. Lyden, Novel method for inducing rapid, controllable therapeutic hypothermia in rats using a perivascular implanted closed-loop cooling circuit. J Neurosci Methods, 2016. **267**: p. 55-61.

10. Kammersgaard, L.P., et al., Feasibility and safety of inducing modest hypothermia in awake patients with acute stroke through surface cooling: A case-control study: the Copenhagen Stroke Study. Stroke, 2000. **31**(9): p. 2251-6.

11. De Georgia, M.A., et al., Cooling for Acute Ischemic Brain Damage (COOL AID): a feasibility trial of endovascular cooling. Neurology, 2004. **63**(2): p. 312-7.

12. Hemmen, T.M., et al., Intravenous thrombolysis plus hypothermia for acute treatment of ischemic stroke (ICTuS-L): final results. Stroke, 2010. **41**(10): p. 2265-70.

13. Ovesen, C., et al., Feasibility of endovascular and surface cooling strategies in acute stroke. Acta Neurol Scand, 2013. **127**(6): p. 399-405.

14. van der Worp, H.B., et al., EuroHYP-1: European multicenter, randomized, phase III clinical trial of therapeutic hypothermia plus best medical treatment vs. best medical treatment alone for acute ischemic stroke. Int J Stroke, 2014. **9**(5): p. 642-5.

15. Wu, T.C. and J.C. Grotta, Hypothermia for acute ischaemic stroke. Lancet Neurol, 2013. **12**(3): p. 275-84.

16. Liu, K., et al., Pharmacological hypothermia: a potential for future stroke therapy? Neurol Res, 2016. **38**(6): p. 478-90.

17. Lyden, P.D., et al., Intravascular Cooling in the Treatment of Stroke (ICTuS): early clinical experience. J Stroke Cerebrovasc Dis, 2005. **14**(3): p. 107-14.

18. Lyden, P., et al., Results of the ICTuS 2 Trial (Intravascular Cooling in the Treatment of Stroke 2). Stroke, 2016. **47**(12): p. 2888-2895.

19. Zhao, H., G.K. Steinberg, and R.M. Sapolsky, General versus specific actions of mild-moderate hypothermia in attenuating cerebral ischemic damage. J Cereb Blood Flow Metab, 2007. **27**(12): p. 1879-94.

20. Lampe, J.W. and L.B. Becker, State of the art in therapeutic hypothermia. Annu Rev Med, 2011. **62**: p. 79-93.

21. Kanagawa, T., et al., A decrease of cell proliferation by hypothermia in the hippocampus of the neonatal rat. Brain Res, 2006. **1111**(1): p. 36-40.

22. Lasarzik, I., et al., Assessment of postischemic neurogenesis in rats with cerebral ischemia and propofol anesthesia. Anesthesiology, 2009. **110**(3): p. 529-37.

23. Imada, S., et al., Hypothermia-induced increase of oligodendrocyte precursor cells: Possible involvement of plasmalemmal voltage-dependent anion channel 1. J Neurosci Res, 2010. **88**(16): p. 3457-66.

24. Saito, K., et al., Moderate low temperature preserves the stemness of neural stem cells and suppresses apoptosis of the cells via activation of the cold-inducible RNA binding protein. Brain Res, 2010. **1358**: p. 20-9.

25. Silasi, G. and F. Colbourne, Therapeutic hypothermia influences cell genesis and survival in the rat hippocampus following global ischemia. J Cereb Blood Flow Metab, 2011. **31**(8): p. 1725-35.

26. Xiong, M., et al., Post-ischemic hypothermia promotes generation of neural cells and reduces apoptosis by Bcl-2 in the striatum of neonatal rat brain. Neurochem Int, 2011. **58**(6): p. 625-33.

27. Kurisu, K. and M.A. Yenari, Therapeutic hypothermia for ischemic stroke; pathophysiology and future promise. Neuropharmacology, 2018. **134**(Pt B): p. 302-309.

28. Yenari, M.A. and H.S. Han, Influence of therapeutic hypothermia on regeneration after cerebral ischemia. Front Neurol Neurosci, 2013. **32**: p. 122-8.

29. Pilotte, J., et al., Developmentally regulated expression of the cold-inducible RNA-binding motif protein 3 in euthermic rat brain. Brain Res, 2009. **1258**: p. 12-24.

30. Liao, Y., et al., The role of cold-inducible RNA binding protein in cell stress response. Int J Cancer, 2017. **141**(11): p. 2164-2173.

31. Xia, W., L. Su, and J. Jiao, Cold-induced protein RBM3 orchestrates neurogenesis via modulating Yap mRNA stability in cold stress. J Cell Biol, 2018. **217**(10): p. 3464-3479.

32. Chappell, S.A. and V.P. Mauro, The internal ribosome entry site (IRES) contained within the RNA-binding motif protein 3 (Rbm3) mRNA is composed of functionally distinct elements. J Biol Chem, 2003. **278**(36): p. 33793-800.

33. Matsuda, A., et al., Generation of mice deficient in RNA-binding motif protein 3 (RBM3) and characterization of its role in innate immune responses and cell growth. Biochem Biophys Res Commun, 2011. **411**(1): p. 7-13.

34. Zhu, X., et al., Cold-inducible RBM3 inhibits PERK phosphorylation through cooperation with NF90 to protect cells from endoplasmic reticulum stress. FASEB J, 2016. **30**(2): p. 624-34.

35. Yaniv, K. and J.K. Yisraeli, The involvement of a conserved family of RNA binding proteins in embryonic development and carcinogenesis. Gene, 2002. **287**(1-2): p. 49-54.

36. Yisraeli, J.K., VICKZ proteins: a multi-talented family of regulatory RNA-binding proteins. Biol Cell, 2005. **97**(1): p. 87-96.

37. Christiansen, J., et al., IGF2 mRNA-binding protein 2: biological function and putative role in type 2 diabetes. J Mol Endocrinol, 2009. **43**(5): p. 187-95.

38. Bell, J.L., et al., Insulin-like growth factor 2 mRNA-binding proteins (IGF2BPs): post-transcriptional drivers of cancer progression? Cell Mol Life Sci, 2013. **70**(15): p. 2657-75.

39. Fernandez, A.M. and I. Torres-Aleman, The many faces of insulin-like peptide signalling in the brain. Nat Rev Neurosci, 2012. **13**(4): p. 225-39.

40. Lehtinen, M.K., et al., The cerebrospinal fluid provides a proliferative niche for neural progenitor cells. Neuron, 2011. **69**(5): p. 893-905.

41. Ziegler, A.N., et al., IGF-II promotes stemness of neural restricted precursors. Stem Cells, 2012. **30**(6): p. 1265-76.

42. Bracko, O., et al., Gene expression profiling of neural stem cells and their neuronal progeny reveals IGF2 as a regulator of adult hippocampal neurogenesis. J Neurosci, 2012. **32**(10): p. 3376-87.

43. Ferron, S.R., et al., Differential genomic imprinting regulates paracrine and autocrine roles of IGF2 in mouse adult neurogenesis. Nat Commun, 2015. **6**: p. 8265.

44. Terauchi, A., et al., Retrograde fibroblast growth factor 22 (FGF22) signaling regulates insulin-like growth factor 2 (IGF2) expression for activity-dependent synapse stabilization in the mammalian brain. Elife, 2016. **5**.

45. Mohyeldin, A., T. Garzon-Muvdi, and A. Quinones-Hinojosa, Oxygen in stem cell biology: a critical component of the stem cell niche. Cell Stem Cell, 2010. **7**(2): p. 150-61.

46. Li, L., et al., Hypoxia inducible factor-1alpha (HIF-1alpha) is required for neural stem cell maintenance and vascular stability in the adult mouse SVZ. J Neurosci, 2014. **34**(50): p. 16713-9.

47. Wellmann, S., et al., Oxygen-regulated expression of the RNA-binding proteins RBM3 and CIRP by a HIF-1-independent mechanism. Journal of Cell Science, 2004. **117**(9): p. 1785-1794.

48. Zhu, X., C. Buhrer, and S. Wellmann, Cold-inducible proteins CIRP and RBM3, a unique couple with activities far beyond the cold. Cell Mol Life Sci, 2016. **73**(20): p. 3839-59.

49. Morf, J., et al., Cold-inducible RNA-binding protein modulates circadian gene expression posttranscriptionally. Science, 2012. **338**(6105): p. 379-83.

50. Qiang, X., et al., Cold-inducible RNA-binding protein (CIRP) triggers inflammatory responses in hemorrhagic shock and sepsis. Nat Med, 2013. **19**(11): p. 1489-1495.

51. Ward, P.A., An endogenous factor mediates shock-induced injury. Nat Med, 2013. **19**(11): p. 1368-9.

52. Li, J., et al., Cold-Inducible RNA-Binding Protein Regulates Cardiac Repolarization by Targeting Transient Outward Potassium Channels. Circ Res, 2015. **116**(10): p. 1655-9.

53. Cekanaviciute, E., et al., Gut bacteria from multiple sclerosis patients modulate human T cells and exacerbate symptoms in mouse models. Proc Natl Acad Sci U S A, 2017. **114**(40): p. 10713-10718.

54. Zhang, Q., et al., Involvement of Cold Inducible RNA-Binding Protein in Severe Hypoxia-Induced Growth Arrest of Neural Stem Cells In Vitro. Mol Neurobiol, 2017. **54**(3): p. 2143-2153.

55. Rajayer, S.R., et al., Cold-inducible RNA-binding protein is an important mediator of alcohol-induced brain inflammation. PLoS One, 2013. **8**(11): p. e79430.

56. Zhou, M., et al., Cold-inducible RNA-binding protein mediates neuroinflammation in cerebral ischemia. Biochim Biophys Acta, 2014. **1840**(7): p. 2253-61.

57. Li, S., et al., Cold-inducible RNA binding protein inhibits H(2)O(2)-induced apoptosis in rat cortical neurons. Brain Res, 2012. **1441**: p. 47-52.

58. Rosenthal, L.M., et al., RBM3 and CIRP expressions in targeted temperature management treated cardiac arrest patients-A prospective single center study. PLoS One, 2019. **14**(12): p. e0226005.

59. Ehlen, A., et al., RBM3-regulated genes promote DNA integrity and affect clinical outcome in epithelial ovarian cancer. Transl Oncol, 2011. **4**(4): p. 212-21.

60. Jogi, A., et al., Nuclear expression of the RNA-binding protein RBM3 is associated with an improved clinical outcome in breast cancer. Mod Pathol, 2009. **22**(12): p. 1564-74.

61. Ehlen, A., et al., Expression of the RNA-binding protein RBM3 is associated with a favourable prognosis and cisplatin sensitivity in epithelial ovarian cancer. J Transl Med, 2010. **8**: p. 78.

62. Jonsson, L., et al., Low RBM3 protein expression correlates with tumour progression and poor prognosis in malignant melanoma: an analysis of 215 cases from the Malmo Diet and Cancer Study. J Transl Med, 2011. **9**: p. 114.

63. Grupp, K., et al., High RNA-binding motif protein 3 expression is an independent prognostic marker in operated prostate cancer and tightly linked to ERG activation and PTEN deletions. Eur J Cancer, 2014. **50**(4): p. 852-61.

64. Chip, S., et al., The RNA-binding protein RBM3 is involved in hypothermia induced neuroprotection. Neurobiol Dis, 2011. **43**(2): p. 388-96.

65. Ferry, A.L., P.W. Vanderklish, and E.E. Dupont-Versteegden, Enhanced survival of skeletal muscle myoblasts in response to overexpression of cold shock protein RBM3. Am J Physiol Cell Physiol, 2011. **301**(2): p. C392-402.

66. Yang, H.J., et al., RNA-binding protein RBM3 prevents NO-induced apoptosis in human neuroblastoma cells by modulating p38 signaling and miR-143. Sci Rep, 2017. **7**: p. 41738.

67. Zhuang, R.J., et al., Cold-Inducible Protein RBM3 Protects UV Irradiation-Induced Apoptosis in Neuroblastoma Cells by Affecting p38 and JNK Pathways and Bcl2 Family Proteins. J Mol Neurosci, 2017. **63**(2): p. 142-151.

68. Yang, H.J., et al., Cold-inducible protein RBM3 mediates hypothermic neuroprotection against neurotoxin rotenone via inhibition on MAPK signalling. J Cell Mol Med, 2019. **23**(10): p. 7010-7020.

69. Pritchard, J. and J.A. Hickman, Why does stage 4s neuroblastoma regress spontaneously? Lancet, 1994. **344**(8926): p. 869-70.

70. Le, H.T., A.M. Sorrell, and K. Siddle, Two isoforms of the mRNA binding protein IGF2BP2 are generated by alternative translational initiation. PLoS One, 2012. **7**(3): p. e33140.

71. Maris, C., C. Dominguez, and F.H. Allain, The RNA recognition motif, a plastic RNA-binding platform to regulate post-transcriptional gene expression. FEBS J, 2005. **272**(9): p. 2118-31.

72. Clery, A., M. Blatter, and F.H. Allain, *RNA recognition motifs: boring? Not quite.* Curr Opin Struct Biol, 2008. **18**(3): p. 290-8..

Abbreviations

AMPA: Aminomethyl Phosphonic Acid

BrdU: Bromodeoxyuridine

CA: Cardiac Arrest

CIRP: Cold-Inducible RNA-Binding Protein

CoIP: Co-Immunoprecipitation

CSF: Cerebrospinal Fluid

DAMP: Damage-Associated Molecular Pattern

DEGs: Differentially Expressed Genes

DG: Dentate Gyrus

EGF: Epidermal Growth Factor

EGL: External Germinal Layer

ELISA: Enzyme-Linked Immunosorbent Assay

ER: Endoplasmic Reticular

FGF2: Fibroblast Growth Factor 2

GFAP: Glial Fibrillary Acidic Protein

GSEA: Gene Set Enrichment Analysis

HI: Hypoxia-Ischemia

HIE: Hypoxia-Ischemia Encephalopathy

HIF-1 α: Hypoxia-Inducible Factor-1α

Iba1: Ionized Calcium-Binding Adapter Molecule 1

IGF2: Insulin-Like Growth Factor-2

IMPs: IGF2 mRNA-Binding Proteins

KH: K Homology

KO: Knockout

MAP2: Microtubule-Associated Protein 2

NSCs: Neural Stem Cells

OE: Overexpression

OGD: Oxygen-Glucose Deprivation

Oligo2: Oligodendrocyte Transcription Factor 2

OPCs: Oligodendrocyte Precursor Cells

ABBREVIATIONS

P0: Postnatal Day 0

PARP: Poly-ADP-Ribose Polymerase

PLA: Proximity Ligation Assay

RA: Retinoic Acid

RBM3: RNA-Binding Motif

RBP: RNA-Binding Protein

RIP: RNA-Immunoprecipitation

RMS: Rostral Migratory Stream

ROS: Reactive Oxygen Species

RRM: RNA Recognition Motif

RTN3: Reticulon-3

SGZ: Subgranular Zone

Sox2: Sex Determining Region Y-Box 2

SVZ: Subventricular Zone

Tuj1: Neuron-Specific Class III B-Tubulin

TUNEL: Transferase dUTP Nick End Labeling

Vec: Empty Vector

WT: Wild-Type

Acknowledgement

I would like to express my special appreciation and thanks to my supervisor, Dr. Sven Wellmann, for your unfailing support of my PhD and related research, for your patience, motivation, and immense knowledge. I could not have imagined having a better supervisor. Your advice on both my work and career has been priceless.

I would also like to thank Prof. Dr. Marek Basler and Dr. Francisco Campos for serving as my committee members. Prof. Dr. Basler's input on my projects has been especially valuable, as has been his career advice at the yearly PAC meetings.

My sincere thanks also go to Dr. Zhu Xinzhou, who provided me with the opportunity to join this group, and who helped me throughout both the research and the writing of the thesis. Without his precious support neither would have been possible.

I would also like to thank Prof. Dr. Josef Kapfhammer and Prof. Raphael Guzman. I'm most grateful for your support and advice.

I'm deeply grateful to Andrea Zelmer, the lab technician at UKBB, for all her willing and expert help with my bench work.

Thanks too to MD student Tessa Goerne for your scientific discussions and project support. I very much enjoyed working with you.

I am deeply indebted to the China Scholarship Council for the funding I received for my research and a truly amazing study experience.

Last but not least, I would like to thank my parents and my husband for your continuing support, beyond all expectation. This venture would have been impossible without it.